Non-perturbative collective properties of trapped ultracold atomic gases

by

Vitaliy Kaurov

A dissertation submitted to the Graduate Faculty in Physics in partial fulfillment of the requirements for the degree of Doctor of Philosophy

The City University of New York

2006

UMI Number: 3232028

ProQuest Information and Learning Company
300 North Zeeb Road
P.O. Box 1346
Ann Arbor, MI 48106-1346

This manuscript has been read and accepted for the Graduate Faculty in Physics in satisfaction of the dissertation requirement for the degree of Doctor of Philosophy.

	A. Kuklov
Date	Chair of Examining Committee
	S. Catto
Date	Executive Officer
	G. Aizin
	A. Levine
	T. Schaefer
	D. Schmeltzer
	W. Schreiber
	Supervisory Committee

THE CITY UNIVERSITY OF NEW YORK

Abstract

Non-perturbative collective properties of trapped ultracold atomic gases

by Vitaliy Kaurov

Thesis supervisor: Prof. Dr. Anatoly Kuklov

In this thesis two problems in the field of ultracold atomic gases are investigated: 1) Atomic Josephson vortex in quasi-1D double-waveguide containing one-component atomic superfluid; 2) Drag effect in strongly interacting two-component superfluid in optical lattice.

In the first problem quasi-one-dimensional long Bose-Josephson junction is considered. It consists of two parallel waveguides containing single-component atomic Bose-Einstein condensates coupled by tunneling. It is shown that such system supports atomic Josephson vortex (JV) - a soliton characterized by circulating atomic supercurrent. Exact stationary solution is found within mean field approach. Dynamics of the long Bose-Josephson junction is analyzed variationally and numerically. It is shown that upon increasing the Josephson coupling, the JV transforms spontaneously into a dark soliton and vice versa. This *reversible* interconversion has no analogy in higher spatial dimensions. Atomic JV can be controllably manipulated by imposing a tunneling bias current created by a difference of chemical potentials on the waveguides. This effect, which has its origin in the Berry phase structure of

a vortex, is very robust in the whole range of the parameters where the JV exists. Acceleration of the JV up to a certain threshold speed, determined by the strength of the Josephson coupling, results in the phase slip causing switching of the vorticity. It is shown how the JV can be created by the phase imprinting technique and can be identified by a specific tangential feature in the interference picture produced by expanding clouds released from the waveguides. It is proposed that the JV can be utilized for controlled and coherent transfer of Bose-Einstein condensates and as a possible mobile qubit.

The second problem is devoted to investigating the mutual drag – non-dissipative coherent transfer of momentum from one component to another – in strongly interacting two-component superfluids in optical lattice (OL). While being analogous to the Andreev-Bashkin (AB) effect in the Galilean-invariant superfluid Helium, the drag in OL is shown to be drastically different due to breaking of the Galilean symmetry by OL. The combination of strong interaction and OL violates the AB relation of the drag coefficient to the effective mass of quasi-particles. In particular, this coefficient can change sign. Two competing drag mechanisms in OL are shown to be: the vacancy-assisted motion and proximity to a quasi-molecular state. Strong drag can radically change the structure of lowest energy topological excitation — vortex or persistent current. In contrast to the standard situation in a single-component superfluid, a vortex can become a composite object in which singular circulation of one component binds several circulation quanta of the other component. In the SQUID-type geometry, the circulation can become fractional. The analytical (within the Mean Field approach) and numerical (by the Monte Carlo Worm-Algorithm) results are presented. It is found that the Mean Field does not adequately describes all aspects of the drag effect in OL.

Contents

List of Figures

Chapter 1

Introduction

1.1 Historical insight

The physics of dilute ultracold atomic gases started its turbulent development just a decade ago, in 1995, when JILA and MIT groups performed milestone experiments producing Bose-Einstein Condensate (BEC) of alkali metal atoms. The JILA group reported condensation of rubidium atoms in the July 14, 1995 issue of *Science* [4]. Shortly after that the MIT group published their result about BEC of sodium atoms in November 27, 1995 issue of *Physical Review Letters* [28]. Since then, this field of research was an active and growing part of theoretical and experimental physics constantly delivering new results. Nevertheless, despite its modernity, the roots of BEC go back into 1924 when the first ideas about BEC were formulated by Bose and Einstein. Our understanding of BEC was formed over the span of 8 decades and still continues to develop. The history of the ideas and experimental discoveries that led to the modern BEC science is quite remarkable and deserves at least a brief recounting of the most important facts. The short account given below is rather incomplete and for further reading we refer to the great reviews by Griffin [52], Balibar [9, 10] and

Leggett [72].

In the early 1920s, then little known Indian scientist Satyendra Nath Bose found it impossible to publish his work in any European journal because editors were plainly rejecting his paper. In that paper Bose employed a new kind of statistics to derive Plank's radiation formula from Einstein's idea of photons. This statistics featured novel ideas of indistinguishability of massless photons and ability of any quantum state to accommodate any amount of particles. Being rejected by publishers, Bose sent his article to Einstein in 1924, who gladly embraced Bose's ideas, translated the paper to German and arranged its publication in the leading German physics journal [16]. Later Einstein generalized Bose statistics to the case of an ideal atomic gas and predicted that at sufficiently low temperature atoms would mostly occupy the single lowest quantum state forming what now is called a Bose-Einstein condensate [35, 36]. An astonishing fact is that Einstein made his prediction in the very early stages of quantum mechanics development, when the fundamental difference between bosons and fermions was not realized yet [52].

After publishing his seminal paper Einstein never returned to the topic of BEC again, at least in official publications. There was some setback in further research due to mostly accepted criticism of the Einstein paper by Uhlenbeck [113]. By one or another reason Einstein's idea was not taken seriously and there were no theoretical developments till 1938. At the same time experimental research started to gain momentum. In 1908 Kamerlingh Onnes liquefied ^{4}He cooling it down to the temperature of $4.215K$ at normal pressure. In the first half of 30s, when the Einstein idea was already forgotten, various sources (e.g. see ref.[79]) reported "strange" behavior and singularities of some Helium thermodynamic functions when it was chilled down through the temperature of $2.17K$. Most known is probably the lambda point of the ^{4}He heat capacitance dependence on temperature. In 1938 Kapitza [77] and inde-

pendently Allen and Misener [2] published their work concerning the *superfluidity* (a term coined by Kapitza) of ^{4}He in the same issue of *Nature*. Superfluidity is defined through a complex of phenomena. A superfluid (SF) can flow frictionlessly through narrow channels and pores that are impermeable to conventional liquids. If a narrow tube is placed in a bath of SF helium and the tube is heated, the helium will flow upwards through the tube and escape through the top (fountain effect). If it is placed in an open container SF helium will climb the walls of the container and flow over the top forming a thin Helium film a single atom thick. Some other effects can continue this list. By the end of the 1930s there was a body of experimental evidence demanding theoretical explanation. Interestingly enough, the same year Kapitza, Allen and Misener published their work, Uhlenbeck withdrew his objections of the Einstein BEC theory realizing that in the proper thermodynamic limit BEC is well defined [75]. Uhlenbeck's reevaluation of the BEC hypothesis and experiments with ^{4}He set proper stage for the ideas of London, Tisza and Landau.

London had heard about the strange behavior of ^{4}He at low temperatures and that Uhlenbeck revoke his critique of the Einstein's work and conjectured that there is a connection between the phenomena of BEC and experiments on liquid Helium. He noted that ^{4}He was a boson and the critical temperature of ideal BEC predicted by Einstein is close to the lambda-point temperature, and that the heat capacitance of an ideal BEC has a peak at the critical temperature, which was in a way similar to experimental data. London discussed his ideas in a short letter in *Nature* in April 1938 [86]. Shortly after he shared his views with Tisza. Both of them published further articles on the topic, but only Tisza was able to come up with a model, which could actually explain the experiments with liquid Helium. As London, Tisza explicitly associated SF phenomena with existence of BEC, namely, he suggested that the ground state of atoms – BEC – does not participate in dissipative process and behaves

as a new type of *frictionless* fluid. He viewed liquid Helium as a mixture of SF and *normal* (consisting of excited atoms) components. In two detailed papers [112] Tisza developed two-fluid hydrodynamics of such a mixture and was able to explain current experimental results and make a few correct predictions including the existence of so called *second sound* (transmission of heat by thermal waves rather then by diffusion where normal and superfluid components move out of phase). Nevertheless, it is well known now that the two-fluid picture cannot be derived by associating SF and normal components *directly* with condensed and excited atoms. In fact, only $\sim 10\%$ of ^{4}He atoms form BEC as temperature approaches zero, yet almost all atoms constitute the SF component. Another drawback of the Tisza model was the use of the *ideal* Bose gas, while liquid Helium is a strongly interacting system. More correct approach to the two-fluid model was independently developed by Landau in his seminal works [81, 82]. The concept of BEC was not used in the papers at all. Instead of atomic states Landau considered states of liquid. The Landau paper [81] was a milestone in theoretical condensed matter physics, because it changed the way the many-body problem was approached in general. The key idea was introduction of *quasiparticles* as means of description of excitations in a many-body system. Another incisive idea of Landau was the celebrated form of the quasiparticle excitation spectrum [82], which started as phonon branch, smoothly passed through a maximum and then a minimum (see FIG.1.1). Excitations described by the part of the spectrum around the minimum were called rotons. In this way normal component of the liquid corresponded to the phonons and rotons and the SF component corresponded to the liquid's ground state.

With the simple arguments of conservation energy and momentum Landau was able to show that if the flow of liquid ^{4}He through a narrow rigid tube is below some critical velocity, then the flow will not create excitations and will be *superfluid* (flow with no resistance). He also deduced that if the energy spectrum is given by $E(p)$

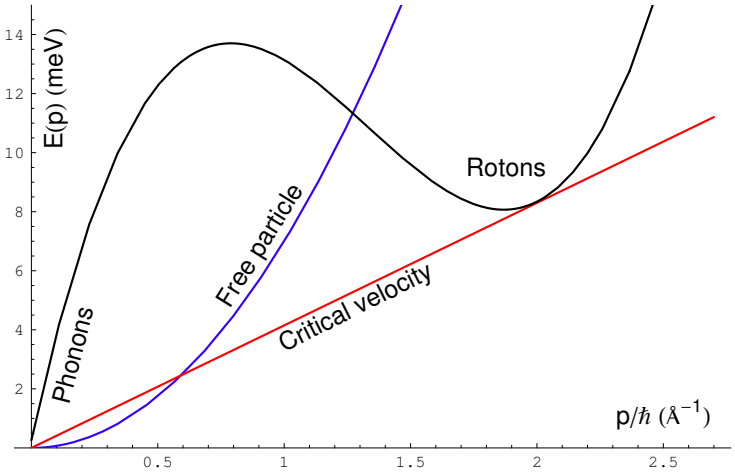

Figure 1.1: Schematic representation of excitation spectrum in ^{4}He.

where $p = \hbar k$ is the momentum and k is the wave vector of quasiparticles, then the critical velocity is $\sim min[E(p)/p]$. This can be interpreted geometrically as the slope of line tangential to $E(k)$ from below (red color on FIG.1.1). It is obvious now that the role of interaction is crucial for superfluidity: the parabolic spectrum of free particles (blue color on FIG.1.1) yields zero critical velocity. It is also clear that the roton part of the spectrum is responsible for the value of critical velocity much less than the speed of sound (the slope of the phonon branch). The Landau spectrum was a purely phenomenological supposition, nevertheless it was correct and allowed *qualitative* calculations of thermodynamic properties of ^{4}He, critical SF velocity and the second sound. Experiments with neutron scattering confirmed the Landau spectrum. Landau's theory yielded much more precise results than the London-Tisza theory and now is considered a standard phenomenological approach to SF ^{4}He. Nevertheless it was not based on the concept of BEC and, moreover, Landau was very critical about the London-Tisza approach, as so was London about Landau's theory. A historical look at this bitter controversy can be found in discussions by Balibar [9, 10] and Griffin [52]. Now, when a credit they deserve is given to both outstanding scientists

we can quote Balibar from his London prize lecture [10]:

> *Both London and Landau probably died too early to admit that they both had part of the truth.*

Remarkably, six years after the death of London, Landau received *The Fritz London Memorial Prize*.

The next major breakthrough can be attributed to Bogoliubov and his work [15]. Basically that paper introduced the technique of second quantization in condensed matter physics. Bogoliubov considered a weakly interacting Bose gas and showed that BEC was not significantly affected by interaction, yet the excitation spectrum changed remarkably in the long-wave limit (small quasiparticle momentum). Instead of the usual parabolic spectrum of free Bose gas, Bogoliubov obtained a phonon branch, which confirmed phenomenological prediction of Landau. Next came works by Feynman [39, 39, 41] where he applies his path integral formalism to ^{4}He and explains the phonon-roton spectrum (which was postulated phenomenologically by Landau) from a microscopic point of view. Penrose and Onsager [97] in 1956 introduced definition of BEC for an *interacting* system through the concept of *off-diagonal long-range order* (ODLRO). They were able to estimate BEC fraction in ^{4}He to be $\sim$ 8%. After that interest in *interacting* BEC remarkably increased and the great body of work published in 1950s - 1960s forms the foundation of modern BEC physics. One of the most important contributions of that period was done by Pitaevskii who developed the idea of nonuniform time-dependent order parameter or macroscopic BEC wave function. He [99] and independently Gross [53, 54] derived the now famous Gross-Pitaevskii equation which, in 1995, became "reborn" as an essential tool for description of realistic BECs in dilute atomic gases.

State of the art experimental techniques, such as magnetic and optical trapping of

atoms, evaporative and laser cooling, were developed through the period from 1968 to 1995 and included outstanding works by V.S. Letokhov, A. Ashkin, T.W. Hansch, A.L. Schawlow, V.L. Balykin, W.D. Phillips, S. Chu, J. Dalibard, D.E. Pritchard, C. Cohen-Tannoudji. In 1997 W.D. Phillips, S. Chu, and C. Cohen-Tannoudji were awarded the Nobel Prize "for development of methods to cool and trap atoms with laser light". It was the very combination of theses techniques that served as the final stroke to achieve the long sought goal of BEC creation. First BECs were created at JILA in 1995 [4] and MIT [28]. These remarkable works were awarded 2001 Nobel Prize to Eric A. Cornell, Wolfgang Ketterle and Carl E. Wieman (for the achievement of Bose-Einstein condensation in dilute gases of alkali atoms, and for early fundamental studies of the properties of the condensates). What followed was an explosion of experimental and theoretical work concentrating around a wide variety of phenomena such as matter-wave interferometry, vortices and vortex lattices, solitons and other topological formations, bosonic Josephson effect, Feshbach resonances, spinor and multicomponent BECs, low-dimensional BEC, quantum phase transitions (QPT), optical lattices, etc. The experimental field continued developing rapidly bringing such versatile techniques as imaging of vortex cores, non-destructive imaging, trapping BEC on microchips in magnetic waveguides and in optical waveguides made of hollow laser beams, transport of BEC with magnetic conveyor belts and optical tweezers [56].

In conclusion I cannot resist to mention a story that, despite being absolutely accidental, seems to posses some symbolic significance. The history of science is full of unexpected turns and strange coincidences and this was once again demonstrated at the beginning of last year. The year 2005 marked the 10th anniversary of experimental realization of BEC in dilute atomic gases and was also the year declared by the United Nations as The World Year of Physics, honoring the 100th anniversary of

pioneering contributions by Albert Einstein in 1905. It was quite a twist of fate that exactly this year an original handwritten manuscript by Einstein dated 1924 and named "Quantentheorie des einatomigen idealen Gases" (Quantum theory of the monatomic ideal gas) was accidentally discovered by a student at a university in the Netherlands. The manuscript contains the first documented prediction of Bose-Einstein condensation and is considered the last great breakthrough of Einstein's genius. *The Instituut-Lorentz for Theoretical Physics* Leiden, Netherlands, has an excellent online exhibition where the manuscript can be accessed and fully viewed [84]. That paper hides a few other historical gems. For instance in 1923 de Broglie formulated the idea of matter waves in his PhD thesis [19]. Among all great physicists of that time Einstein was first to use and refer to the de Broglies idea in his BEC paper [35], arguing that due to the wave nature of particles they must obey photon statistics [52]. Once again it speaks a great deal for the perceptiveness and acuteness of Einsteins mind.

1.2 Definitions of Bose-Einstein condensation

Even though the BEC of an ideal uniform Bose gas became long ago a standard textbook topic, the problem in general has some pitfalls and subtleties and can be considered within a few quite different approaches. To define BEC on a qualitative level we need to consider the phase-space density $n\lambda_{dB}^3$, where $\lambda_{dB} = \sqrt{2\pi\hbar^2/mk_BT}$ is the thermal de Broglie wavelength and n is the atomic density. The rough criterion of BEC is $n\lambda_{dB}^3 \sim 1$, which means that the atomic de Broglie wavelength exceeds inter-atomic spacing and atom wave packets overlap. The reason that this criterion works is that the overlap of wave packets allows quantum indistinguishability of Bosons to play a decisive role. This indistinguishability is reflected in the form of the Bosonic wave function: different configurations due to the exchange of positions of atoms (permutations) do not change the system. In other words, the Bosonic wave function is *symmetric* under such permutations. This symmetry is the most fundamental cause of BEC.

A common textbook approach is to associate BEC with macroscopic population of atoms in the single lowest quantum state deriving it from Bose-Einstein distribution function. Clear connection between the symmetry of the wave function under permutations and macroscopic population of a single quantum state is rarely discussed despite the fact that it gives deep insight into the physics of BEC [91]. In general, definitions of BEC can be given using three formally different approaches, which are summarized in the following subsections. The choice of a particular approach depends on the goals one pursues (pedagogical purposes, analytical calculations, numerical simulations, etc.) and system-specific factors. Whether and how BEC occurs (i.e. behavior of thermodynamic functions at the transition) depends on such aspects of the system as dimensionality, size (amount of particles), geometry (structure of

external confinement) and the type of interaction between bosons. Variation of these and other conditions lead to a vast variety of BEC systems with, sometimes, radically different properties. We start from a brief account of BEC definitions.

1.2.1 Conventional approach to an ideal Bose gas

This approach associates BEC with macroscopic population of the single lowest quantum state deriving it directly from Bose-Einstein statistics. Given first by Einstein [35] it is the original approach and the most popular among textbooks. Having disadvantage of being applicable to only *ideal* Bose gas, it is probably the most straightforward and easy to introduce definition of BEC. In this and subsequent sections we will mostly follow works [26, 91].

Because most of the traps confining BEC atoms are approximately parabolic, the external potential is chosen in the form

$$V_{\text{ext}}(\mathbf{r}) = \frac{m}{2}(\omega_x^2 x^2 + \omega_y^2 y^2 + \omega_z^2 z^2) \ . \tag{1.1}$$

Due to the absence of interaction the many-particle problem is reduced to a problem of a single particle in 3D harmonic oscillator potential. Eigenvalues are given by

$$\varepsilon_{n_x n_y n_z} = \sum_k \hbar\omega_k \left(n_k + \frac{1}{2}\right) \tag{1.2}$$

where the summation index runs over spatial dimensions: $k = x, y, z$. The ground state of the many-particle system consists of all particles collected in the lowest single-particle state ($n_x = n_y = n_z = 0$). For an ideal gas of N noninteracting bosons the

ground state wave function is

$$\phi(\mathbf{r}_1, .., \mathbf{r}_N) = \prod_i \varphi_0(\mathbf{r}_i), \tag{1.3}$$

where $\varphi_0(\mathbf{r})$ is the harmonic oscillator ground state wave function of a single atom with mass m

$$\varphi_0(\mathbf{r}) = \left(\frac{m\omega_{\rm ho}}{\pi\hbar}\right)^{3/4} \exp\left[-\frac{m}{2\hbar}(\omega_x x^2 + \omega_y y^2 + \omega_z z^2)\right] \ , \tag{1.4}$$

where

$$\omega_{\rm ho} = (\omega_x\omega_y\omega_z)^{1/3} \ , \tag{1.5}$$

is the geometric average of the oscillator frequencies. It is connected to the oscillator length

$$a_{\rm ho} = \left(\frac{\hbar}{m\omega_{\rm ho}}\right)^{1/2} \ , \tag{1.6}$$

defining the size of the atomic cloud, which is an important system length scale. The atomic density distribution is given by

$$n(\mathbf{r}) = N|\varphi_0(\mathbf{r})|^2 \ , \tag{1.7}$$

which means that the atomic cloud spatial size is independent of the amount of atoms N. At finite temperature only part of the atoms is condensed in the ground state, the rest forming a thermal cloud and being spread over excited levels according to the Boltzmann distribution. It can be easily shown [26] that the radius of the thermal cloud is greater than a_{ho}. The same is true for the distributions of the thermal and BEC clouds in momentum space. Thus in harmonic traps emergence of BEC can be associated with the appearance of a sharp peak above the broader (thermal) distribu-

tion in both spatial and momentum coordinates. This fact was verified experimentally and now it is a standard experimental criterion for BEC detection.

The critical temperature of BEC transition and all thermodynamic functions for an ideal Bose gas can be found by considering the grand-canonical ensemble. The total amount of atoms N and total energy E are obtained via summations with statistical weights given by the Bose-Einstein distribution:

$$N = \sum_{n_x,n_y,n_z} \left\{\exp[\beta(\varepsilon_{n_x n_y n_z} - \mu)] - 1\right\}^{-1} , \tag{1.8}$$

$$E = \sum_{n_x,n_y,n_z} \varepsilon_{n_x n_y n_z} \left\{\exp[\beta(\varepsilon_{n_x n_y n_z} - \mu)] - 1\right\}^{-1} , \tag{1.9}$$

where μ is the chemical potential and $\beta = (k_B T)^{-1}$. The usual textbook definition is: *BEC occurs when below some critical temperature T_c the lowest quantum state becomes macroscopically occupied.* The key to understanding BEC is the behavior of the chemical potential μ at low temperatures. In general the value of μ must be lower than the energy of the ground state, because occupation numbers cannot be negative. Then, in order to have macroscopic ($\sim N$) population of the ground state, as temperature $T \to 0$ the chemical potential must approach the ground state energy $\mu_c = 3\hbar\bar{\omega}/2$, where $\bar{\omega} = (\omega_x + \omega_y + \omega_z)/3$. The next step is to go from discrete summation in (1.8) to continuous integration over occupation numbers n_x, n_y, n_z. Such a replacement is an approximation and despite being justified for $N \to \infty$ (energy level spacing $\to 0$) it miscounts part of atoms N_0 belonging to the BEC [91]. Introducing it artificially as a separate term we obtain

$$N - N_0 = \sum_{n_x,n_y,n_z \neq 0} \frac{1}{\exp[\beta\hbar(\omega_x n_x + \omega_y n_y + \omega_z n_z)] - 1} , \tag{1.10}$$

$$N - N_0 = \int_0^\infty \frac{dn_x dn_y dn_z}{\exp[\beta\hbar(\omega_x n_x + \omega_y n_y + \omega_z n_z)] - 1} \,. \tag{1.11}$$

where we substituted the explicit value μ_c in the sum over *excited* states. The integral in (1.11) can be expressed through the Riemann ζ-function

$$N - N_0 = \zeta(3)\left(\frac{k_B T}{\hbar\omega_{\rm ho}}\right)^3 \,. \tag{1.12}$$

To find the critical temperature T_c of BEC transition we assume that right at the transition point the amount of BEC atoms N_0 is still ~ 0. Then from (1.12) one obtains

$$k_B T_c = \hbar\omega_{\rm ho}\left(\frac{N}{\zeta(3)}\right)^{1/3} = 0.94\ \hbar\omega_{\rm ho}\ N^{1/3} \,. \tag{1.13}$$

Substituting this value back into (1.12) we obtain the temperature dependence of the fraction of condensed atoms for $T < T_c$ (see FIG.1.2)

$$\frac{N_0}{N} = 1 - \left(\frac{T}{T_c}\right)^3 \,. \tag{1.14}$$

The total energy (1.9) of the system is found in a similar manner

$$\frac{E}{N k_B T_c} = \frac{3\zeta(4)}{\zeta(3)}\left(\frac{T}{T_c}\right)^4 \,. \tag{1.15}$$

In realistic systems the amount of atoms in a trap can reach millions and, according to (1.13), $k_B T$ can be hundreds times greater than the interlevel energy spacing $\hbar\omega_{\rm ho}$.

A uniform system has different temperature dependence of condensed atomic fraction $N_0/N = 1 - (T/T_c)^{3/2}$ (see FIG.1.2), where $k_B T_c = (2\pi\hbar^2/m)[n/\zeta(3/2)]^{2/3}$. This shows how a system-specific feature, in this particular case geometry of confinement, can influence characteristics of BEC transition. The reason is that the energy spectrum of a harmonic oscillator is different from that of a particle confined in a box.

The harmonic oscillator energy depends linearly on quantum numbers, which inter-

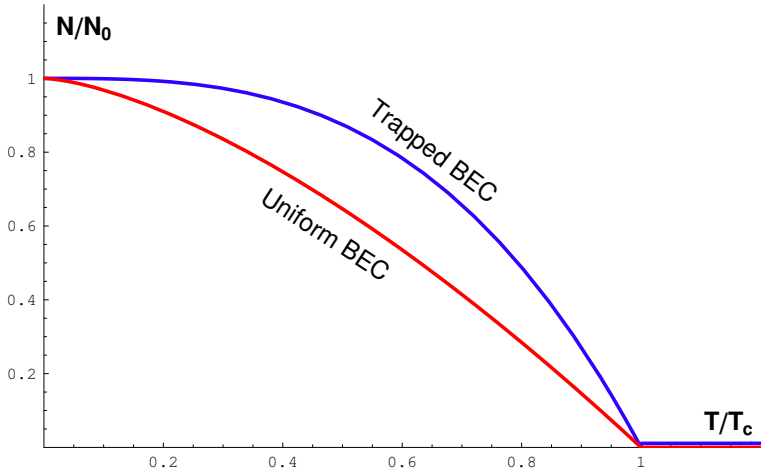

Figure 1.2: Temperature dependence of BEC fraction for uniform and harmonically trapped Bose gases

estingly enough allows one to obtain some closed analytical expressions not derivable in the uniform case. Indeed the summation in (1.8) can be evaluated explicitly. For simplicity let us consider the isotropic case $\omega_x = \omega_y = \omega_z = \omega$. Then expression (1.8) takes form

$$N = \sum_{n_x,n_y,n_z} \frac{1}{e^{\beta[\hbar\omega(n_x+n_y+n_z+\frac{3}{2})-\mu]} - 1} \tag{1.16}$$

The first step is to represent the fraction under summation through a geometric progression

$$N = \sum_{n_x,n_y,n_z} \sum_{l=1}^{\infty} e^{-l\beta\hbar\omega(n_x+n_y+n_z)-l\alpha} \tag{1.17}$$

where

$$\alpha = \frac{3}{2}\beta\hbar\omega - \beta\mu \ . \tag{1.18}$$

When the order of summations is interchanged and the summation over quantum

numbers n_k is evaluated we obtain

$$N = \sum_{l=1}^{\infty} \frac{e^{-\alpha l}}{(1 - e^{-l\beta\hbar\omega})^3} \ . \tag{1.19}$$

To connect this expression to the approximate results obtained earlier one realizes that in the thermodynamic limit $\omega \sim 1/N^{1/3}$ is very small and so is the power of the exponent in (1.19) for $l < N^{1/3}$. Expanding in powers of the exponents argument and keeping the first term only we obtain

$$N' = \sum_{l=1}^{\infty} \frac{e^{-\alpha l}}{(l\beta\hbar\omega)^3} = \left(\frac{k_B T}{\hbar\omega}\right)^3 \zeta(3) \tag{1.20}$$

where we set $\alpha = 0$. This is identical to (1.12) besides the BEC fraction N_0, which we again did not account for and need to introduce artificially. Thus this approximation and the original one with replacement of sums with integration have the same cause leading to the disappearance of BEC fraction N_0. However the last example is much easier to analyze. Indeed from the full expression (1.16) one finds that the occupation of the ground state for $T < T_c$ is

$$n_0 = \frac{1}{e^{\alpha} - 1} = \sum_{l=1}^{\infty} e^{-\alpha l} \cong \frac{1}{\alpha} \tag{1.21}$$

which means that α is of the order of $1/N$ and in the summation terms up to order of N must be considered. On the other hand deriving (1.20) we considered only $l < N^{1/3}$ terms and thus neglected the condensate. If omission of the terms with large l leads to the loss of BEC fraction, then what is the physical meaning of these terms? The answer to this question is given in the frame of the so called "loop-gas" approach. Complete derivations are somewhat tedious and we refer interested readers to a very instructive work [91], which we rather briefly summarize in the section 1.2.3.

1.2.2 Density matrix approach

Density matrix is probably most useful quantity in description of BEC. Several criteria it offers for BEC occurrence [47, 96, 97] are applicable even for interacting Bose systems. Once again let us consider symmetric under permutations many-body wave function $\Psi(\mathbf{r}_1\mathbf{r}_2...\mathbf{r}_N, t)$. One-particle reduced density matrix is defined through a mutually orthogonal set of many-body states Ψ_s contributing to a statistical mixture with probability p_s:

$$\rho(\mathbf{r}, \mathbf{r}', t) \equiv N \sum_s p_s \int d\mathbf{r}_2...d\mathbf{r}_N \Psi_s^*(\mathbf{r}\mathbf{r}_2...\mathbf{r}_N, t)\Psi_s(\mathbf{r}'\mathbf{r}_2...\mathbf{r}_N, t) \tag{1.22}$$

It can be also defined through bosonic field operators

$$\rho(\mathbf{r}, \mathbf{r}', t) \equiv \left\langle \hat{\psi}^\dagger(\mathbf{r}, t)\hat{\psi}(\mathbf{r}', t) \right\rangle \tag{1.23}$$

where averages denoted by triangular brackets are taken with respect to the statistical mixture and quantum distributions. When coordinates $\mathbf{r}$, $\mathbf{r}'$ are regarded as indexes, it is obvious from definition (1.22) that matrix function $\rho(\mathbf{r}, \mathbf{r}', t)$ is Hermitian. It can be diagonalized with a complete orthonormal basis of single-particle eigenfunctions $\chi_i(\mathbf{r}, t)$:

$$\rho(\mathbf{r}, \mathbf{r}', t) = \sum_i n_i(t)\chi_i^*(\mathbf{r}, t)\chi_i(\mathbf{r}', t) \ . \tag{1.24}$$

Real quantities $n_i(t)$ are expectation values of the operators $a_i^\dagger(t)a_i(t)$ formed with creation and annihilation operators defined as

$$a_i(t) = \int \hat{\psi}(\mathbf{r}, t)\chi_i^*(\mathbf{r}, t)d\mathbf{r} \tag{1.25}$$

$$\hat{\psi}(\mathbf{r},t) = \sum_i \chi_i(\mathbf{r},t) a_i(t) \tag{1.26}$$

Decomposition (1.24) means that $\chi_i(\mathbf{r},t)$ are eigenfunctions of the operator $\rho(\mathbf{r},\mathbf{r}',t)$ with eigenvalues $n_i(t)$

$$\int \rho(\mathbf{r},\mathbf{r}',t)\chi_i(\mathbf{r}',t)d\mathbf{r}' = n_i(t)\chi_i(\mathbf{r},t) \ . \tag{1.27}$$

In the simplest case the Bose-Einstein condensation sets in when some single eigenvalue becomes of the order of total macroscopic number of bosons in the system $n_i(t) = N_0(t) \sim N$ (the choice of zero index is arbitrary) while the ratio N_0/N remains finite in the thermodynamic limit $N \to \infty$. The single particle eigenstate $\chi_0(\mathbf{r},t)$ is called condensate wave function and its eigenvalue $N_0(t)$ represents mean value of the bosons in the condensate. If several sates accrue macroscopic eigenvalues the BEC is called fragmented.

This definition of Bose-Einstein condensation is extremely powerful, because it is also true for the interacting case. To demonstrate its usefulness let us compare condensation of an ideal Bose gas and a strongly interacting system such as superfluid Helium ^{4}He. For an ideal Bose gas at zero temperature the one-particle density matrix (1.22) can be easily evaluated analytically from effective reduction to one-particle problem:

$$\rho\left(\mathbf{r}-\mathbf{r}'\right) = \frac{N}{V} = n \ , \tag{1.28}$$

independently of the distance $|\mathbf{r}-\mathbf{r}'|$ (V is the volume of the system). We cannot deduce the density matrix analytically for ^{4}He, because of strong interactions, yet experiments show that ^{4}He does contain BEC fraction below the critical temperature. With help of quantum Monte Carlo (QMC) simulations, the density matrix can be calculated numerically [24]. Results are schematically shown on the FIG.1.3 While

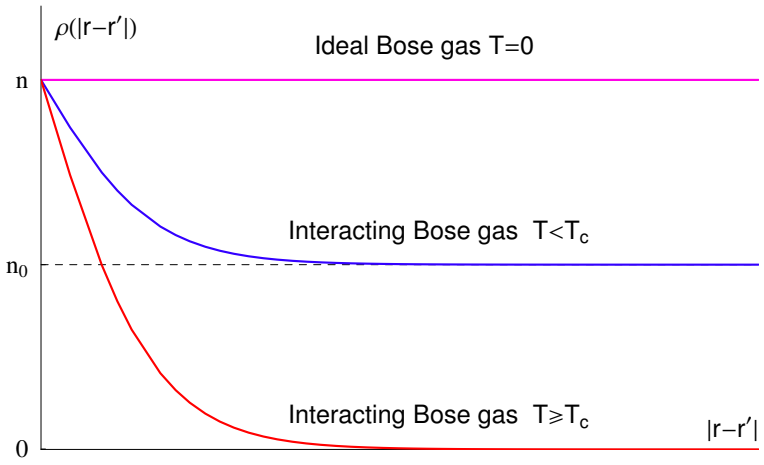

Figure 1.3: One-particle density matrix for an ideal and interacting Bose gases

the density matrix depends on the distance $|\mathbf{r}-\mathbf{r}'|$ for ^{4}He, it is still tends to a constant $n_0 < n$ as distance grows for temperatures below critical. Above the critical temperature the density matrix vanishes at large distances. The constant n_0 gives measure of the BEC density in an interacting system. Thus a general rigorous criterion of Bose-Einstein condensation can be written as following

$$\lim_{|\mathbf{r}-\mathbf{r}'|\to\infty} \left\langle \hat{\psi}^\dagger(\mathbf{r})\hat{\psi}(\mathbf{r}') \right\rangle = \left\{ \begin{array}{cc} n_0(T), & T < T_c \\ 0 & T \geqslant T \end{array} \right\} \tag{1.29}$$

This is the definition of ODLRO introduced in refs.[47, 96, 97]. To give an instructive physical meaning to this definition let us imagine a boson annihilated from an excited state and created in the condensate at point $\mathbf{r}$, while another boson is removed from the condensate at point $\mathbf{r}'$. In BEC such process has nonvanishing quantum amplitude and phase at *any* separation $|\mathbf{r}-\mathbf{r}'|$ no matter how large it is. This is a demonstration of *macroscopic quantum coherence*. The fact that the density matrix is constant for arbitrarily large distances $|\mathbf{r}-\mathbf{r}'|$ suggests possibility of *independent* statistical

averaging in (1.23):

$$\lim_{|\mathbf{r}-\mathbf{r}'|\to\infty} \left\langle \hat{\psi}^\dagger(\mathbf{r})\hat{\psi}(\mathbf{r}') \right\rangle = \left\langle \hat{\psi}^\dagger(\mathbf{r}) \right\rangle \left\langle \hat{\psi}(\mathbf{r}') \right\rangle \tag{1.30}$$

If we calculate these separated averages in the Fock-state representation of *definite* number of particles, we obtain zero expectation values, because a bosonic field operator maps a Fock state $|N\rangle$ on an orthogonal state $|N \pm 1\rangle$. Nevertheless if we use so called *coherent states* representation of *definite* phase, then expectation values will not vanish. Thus we defined *macroscopic wave function* or *order parameter* of BEC as

$$\Phi(\mathbf{r}, t) = \left\langle \hat{\psi}(\mathbf{r}, t) \right\rangle \ , \tag{1.31}$$

which is a complex number. Thus BEC possess a well defined phase

$$\Phi(\mathbf{r}, t) = \sqrt{n_0\left(\mathbf{r}, t\right)} e^{i\theta(\mathbf{r},t)} \tag{1.32}$$

associated with the concept of so-called "spontaneously broken gauge symmetry". The single particle density matrix in terms of the BEC wave function is

$$\lim_{|\mathbf{r}-\mathbf{r}'|\to\infty} \rho(\mathbf{r}, \mathbf{r}', t) = \Phi^*(\mathbf{r}', t)\Phi(\mathbf{r}, t) \tag{1.33}$$

Strictly speaking conceptions of broken gauge symmetry and off-diagonal long-range order are not applicable in the finite size systems, yet function $\Phi(\mathbf{r}, t)$ retains its significance.

1.2.3 Loop-gas approach

Above we mentioned that most fundamentally BEC occurs as a result of the symmetry of the bosonic wave function under permutations (exchange) of two or more particles. Due to the indistinguishability of bosons different arrangements obtained from such permutations still correspond to the same configuration of the system. Because of this property the statistical distribution for the ideal Bose gas allows macroscopic population of the ground state at low temperatures. But if the symmetry under permutations is so important, can one derive BEC directly from this symmetry? This question was first approached by Matsubara [88] and Feynman [42] who developed a classification scheme and statistics for permutations. An excellent discussion of the method can be found in the work of Mullin [91], which we briefly summarize below. All the following calculations are for an ideal Bose gas.

Let us introduce *symmetrized* N-particle bosonic density matrix [42, 91]

$$\rho\left(\mathbf{R}_N, \mathbf{R}_N{}'\right) = \frac{1}{N!}\sum_P \sum_j e^{-\beta E_j} \psi_j^*\left(P\left[\mathbf{R}_N\right]\right) \psi_j\left(\mathbf{R}_N{}'\right) \tag{1.34}$$

where $\mathbf{R}_N = \{\mathbf{r}_1 ... \mathbf{r}_N\}$ are positions of N bosons, and summations over P and j are the summations over all possible permutations and states correspondingly. The partition function is given then by the trace of the density matrix

$$Z_N = \frac{1}{N!}\sum_P \int d\mathbf{R}_N \left\langle P\left[\mathbf{R}_N\right] \left| e^{-\beta H} \right| \mathbf{R}_N{}' \right\rangle \tag{1.35}$$

Notation $P[\mathbf{R}_N]$ means permutations of particles' coordinates. If, for example,

$$P = \begin{pmatrix} 1 & 2 & 3 & 4 & 5 \\ \downarrow & \downarrow & \downarrow & \downarrow & \downarrow \\ 3 & 1 & 2 & 4 & 6 \end{pmatrix} \tag{1.36}$$

then $P\mathbf{r}_1 = \mathbf{r}_3$. The "identity" permutation (singlet) is a trivial exchange of a particle with itself and has size 1, because it contains one particle. First nontrivial permutation is an exchange of two bosons and it has size 2. Generally a permutation has size l, if l bosons participate in permutation. It is reminiscent of a "loop", because such exchange of particles is "closed", i.e. whatever particle is last, it takes the place of the first one. For example we can have the following loop of size three: $1 \to 6,\ 6 \to 3,\ 3 \to 1$. Any possible permutation can be constructed out of singlets (unchanged bosons) and loops of different sizes, which is clear from the following example:

$$\underbrace{\begin{pmatrix} 1 & 2 & 3 & 4 & 5 & 6 \\ \downarrow & \downarrow & \downarrow & \downarrow & \downarrow & \downarrow \\ 2 & 1 & 3 & 6 & 4 & 5 \end{pmatrix}}_{l=6} = \underbrace{\begin{pmatrix} 3 \\ \downarrow \\ 3 \end{pmatrix}}_{\text{singlet}} \underbrace{\begin{pmatrix} 1 & 2 \\ \downarrow & \downarrow \\ 2 & 1 \end{pmatrix}}_{\text{doublet}} \underbrace{\begin{pmatrix} 4 & 5 & 6 \\ \downarrow & \downarrow & \downarrow \\ 6 & 4 & 5 \end{pmatrix}}_{\text{triplet}} \tag{1.37}$$

Consider a permutation P consisting of q_l loops with length l. Then necessarily

$$N = \sum_l l C_l \tag{1.38}$$

It can be shown that the number of permutations consisting of q_1 loops with length $l = 1$, q_2 loops with length $l = 2$, etc. is given by [42, 91]

$$C(q_1, q_2, ...) = \frac{N!}{\prod_l l^{q_l} q_l!} \tag{1.39}$$

Thus we can rewrite the partition function in terms of the *loops*

$$Z_N = \frac{1}{N!} \sum_{\{q_1, q_2, \ldots\}} C\left(q_1, q_2, \ldots\right) \prod_l Z\left(l\right)^{q_l} \tag{1.40}$$

where

$$Z(l) = \int d\mathbf{r}_1 \ldots d\mathbf{r}_l \left\langle P\left[\mathbf{R}_l\right] \left| e^{-\beta H} \right| \mathbf{R}_l{}' \right\rangle \tag{1.41}$$

It is hard to perform further summation, because of the constrained (1.38). Instead we can consider a system with variable number of bosons N and apply statistic of the grand canonical ensemble, which will allow to perform summation over q_l independently. The grand canonical partition function is

$$\mathbb{Z} = \sum_N e^{\beta\mu N} Z_N = \prod_l \sum_{q_l} \frac{1}{q_l!} \left(\frac{Z\left(l\right) e^{\beta\mu l}}{l} \right)^{q_l} = \prod_l \exp\left(\frac{Z\left(l\right) e^{\beta\mu l}}{l} \right) \tag{1.42}$$

where μ is chemical potential. The average number of particles then is

$$\langle N \rangle = k_B T \frac{\partial}{\partial \mu} \ln \mathbb{Z} = \sum_l Z\left(l\right) e^{\beta\mu l} \tag{1.43}$$

and because

$$\langle N \rangle = \sum_l l \left\langle q_l \right\rangle \tag{1.44}$$

we obtain

$$\left\langle q_l \right\rangle = \frac{Z\left(l\right) e^{\beta\mu l}}{l} \tag{1.45}$$

In ideal gas partition function of l particles can be replaced by a product of single-particle partition functions. Our single-particle problem corresponds to a harmonic oscillator. It is easy to perform integration over all particle coordinates in (1.41) and

with help of simple geometric progression obtain:

$$Z\left(l\right)=\frac{e^{-3\beta\mu l\hbar\omega/2}}{\left(1-e^{-3\beta\mu l\hbar\omega}\right)^{3}} \tag{1.46}$$

Substituting this expression into (1.43) we finally reinstate the result (1.19)

$$\langle N\rangle=\sum_{l=1}^{\infty}\frac{e^{-\alpha l}}{\left(1-e^{-l\beta\hbar\omega}\right)^{3}}\ .$$

It is intuitively clear that in ideal Bose gas short loops are facilitated by spatial proximity of particles (e.g. one may expect a triplet permutation when 3 bosons are close to each other). If interparticle separation is greater than particle de Broglie wave length, long loops are suppressed, because quantum overlap of many particles simultaneously is a rare event. Thus it is exactly at the onset of BEC when macroscopic amount of bosons becomes engaged in long permutations. This picture is rather different from standard one with collapse of macroscopic number of bosons in the ground state, yet it is more illustrative. The connection between these approaches can be established with help of expression (1.19). The summation in (1.19) runs over all possible loop sizes l. Thus index l is not a mere consequence of a mathematical trick, but is number of bosons participating in a closed permutation. At the onset of BEC smaller loops suddenly join to form macroscopically large loops so that loops of all sizes contribute to BEC fraction. This is why BEC fraction was lost in previous calculations when we neglected large $l\sim N$. The presence of all particles in the ground state at absolute zero corresponds to equal probability of finding loops with any possible size. Size of the loops strongly fluctuates with macroscopic loops constantly forming and breaking. In this picture emergence of BEC is associated with sudden appearance of macroscopically large loops with the size $l\sim N$ below critical

temperature T_c.

1.3 Mean-field description of BEC

1.3.1 Gross-Pitaevskii equation

Consider a general system of N interacting bosons of mass m in external potential $V_{ext}(\mathbf{r})$. The single-particle Hamiltonian is

$$H_0 = -\frac{\hbar^2}{2m}\nabla^2 + V_{ext}(\mathbf{r}) \ . \tag{1.47}$$

If two-body interatomic potential is $V(\mathbf{r}-\mathbf{r}')$ and $\hat{\psi}(\mathbf{r})$, $\hat{\psi}^\dagger(\mathbf{r})$ are bosonic field operators with bosonic field commutation relations

$$[\hat{\psi}(\mathbf{r}), \hat{\psi}(\mathbf{r})] = 0 \ , \quad [\hat{\psi}^\dagger(\mathbf{r}), \hat{\psi}^\dagger(\mathbf{r})] = 0 \ , \quad [\hat{\psi}(\mathbf{r}), \hat{\psi}^\dagger(\mathbf{r}')] = \delta(\mathbf{r}-\mathbf{r}') \ , \tag{1.48}$$

then in second quantization many-body Hamiltonian takes form

$$\hat{H} = \int d\mathbf{r}\hat{\psi}^\dagger(\mathbf{r})H_0\hat{\psi}(\mathbf{r}) + \\ + \frac{1}{2}\int d\mathbf{r}\int d\mathbf{r}'\hat{\psi}^\dagger(\mathbf{r})\hat{\psi}^\dagger(\mathbf{r}')V(\mathbf{r}-\mathbf{r}')\hat{\psi}(\mathbf{r}')\hat{\psi}(\mathbf{r}) \ . \tag{1.49}$$

In the Heisenberg picture the dynamics of the bosonic fields is described by the Heisenberg equation of motion

$$i\hbar\frac{d}{dt}\hat{\psi}(\mathbf{r},t) = [\hat{\psi}, \hat{H}] \tag{1.50}$$

which, if we use (1.48), becomes

$$i\hbar\frac{d}{dt}\hat{\psi}(\mathbf{r},t) = \left\{H_0 + \int d\mathbf{r}'\hat{\psi}^\dagger(\mathbf{r}',t)V(\mathbf{r}-\mathbf{r}')\hat{\psi}(\mathbf{r}',t)\right\}\hat{\psi}(\mathbf{r}',t) \ . \tag{1.51}$$

The interatomic interaction $V(\mathbf{r}-\mathbf{r}')$ plays an essential role in a realistic many body system and generally is described by rather complex interaction potential. Solving many body problem by taking in account all peculiarities of interatomic potential is impossible. Nevertheless current BEC experiments are carried out in the regimes which allow for great simplification of the problem. A few experimental facts must be mentioned to understand the nature of this simplification. First of all an atomic gas is not thermodynamically stable under the general conditions of BEC formation. In nonideal gaseous system the part of interatomic interaction responsible for formation molecules and liquid or solid states is always present. It means that being cooled to extremely low temperatures BEC does not approach the ground state, but some metastable exited state. The life time of BEC in such state is determined by the atomic collision process. Though to form a simple diatomic molecule it is enough to collide just two atoms, such formation is extremely slow, if no third atom is present to carry away excess of energy and momentum. The dominant recombination process is three-body one and it can be significantly suppressed (made improbable) by making BEC dilute enhancing thus its metastability. Usual BEC life time ranges from several to hundreds of seconds. Second, at very low temperatures de Broglie wavelengths of atoms are much greater than the range of interatomic potential. Third, atoms are rarely approaching each other closely due to extremely low energy and density. This weak interaction suggests that only s-wave scattering is dominant. In this case the scattering amplitude is independent of angle (insensitive to the details of the potential) and is characterized by a single parameter: the *s-wave scattering length* a. Thus we could replace the real potential by an effective one with the same scattering properties. The potential that suits the purpose is

$$V(\mathbf{r}-\mathbf{r}') = g\delta(\mathbf{r}-\mathbf{r}') = \frac{4\pi\hbar^2 a}{m}\delta(\mathbf{r}-\mathbf{r}') \tag{1.52}$$

The effective interaction is repulsive (attractive), if a is positive (negative). Implying existence of ODLRO let us represent the bosonic field operators as a sum of the BEC order parameter (a complex number) and small operator perturbation

$$\hat{\psi}(\mathbf{r},t) = \Phi(\mathbf{r},t) + \delta\hat{\psi}(\mathbf{r},t) \tag{1.53}$$

Substituting (1.53) and (1.52) into (1.51) and keeping only lowest order terms we obtain dynamical equation for the BEC wave function

$$i\hbar\frac{\partial}{\partial t}\Phi(\mathbf{r},t) = \left(-\frac{\hbar^2\nabla^2}{2m} + V_{ext}(\mathbf{r}) + g\left|\Phi(\mathbf{r},t)\right|^2\right)\Phi(\mathbf{r},t)\ . \tag{1.54}$$

It is called Gross-Pitaevskii (GP) equation and was obtained independently by Pitaevskii [99] and Gross [53, 54]. GP equation is valid when the s-wave scattering length is much smaller than average interatomic separation and when number of BEC atoms is much lager than 1. We can introduce dimensionless quantity equal to the amount of atoms in a "scattering volume" na^3, where n is average atom density. The gas is dilute when $na^3 \ll 1$. In current experiments typical values of the gas parameter are always less than 10^{-3}. Because we neglected quantum fluctuations $\delta\hat{\psi}(\mathbf{r},t)$, GP equation describes BEC at zero temperature with the condensate containing all atoms.

1.3.2 One dimensional BEC

First problem of this thesis considers one-dimensional (1D) system, namely 1D long Bose-Josephson junction. Because all calculations are done in the mean-filed approximation it is important to clarify when the mean-filed regime is valid for 1D case. The physics of 1D BEC is quite counterintuitive and can be drastically different from

2D and 3D cases. Though significant advance on the problem was already done in 1960s, only recently 1D Bose gas was realized experimentally. It is achieved by making transverse confinement of the usual 3D atomic trap several orders stronger than axial, creating thus highly anisotropic elongated traps. Because it is even possible to produce 1D traps of a circular or more complex geometries and transport BEC along them on considerable distances, these traps are also called atomic waveguides (from "guiding matter waves" in analogy to the optical waveguides).

We may say that the BEC is effectively 1D, if the following condition is satisfied

$$l_0 \ll l_c \Leftrightarrow \mu \ll \hbar\omega_0 \tag{1.55}$$

where $l_0 = \sqrt{\hbar/m\omega_0}$ and ω_0 are the oscillator length and frequency of the transverse harmonic confinement respectively, $l_c = \hbar/\sqrt{m\mu}$ is the correlation (healing) length, and μ is the chemical potential.

Among remarkable aspects of 1D Bose gas is exact solvability for the case of spinless bosons interacting via delta-function potential as was shown by Lieb and Liniger [73, 73]. Surprisingly they found that the repulsive 1D Bose gas becomes less ideal with *decreasing* density. As 1D density n falls and interatomic separation $1/n$ increases the role of interaction becomes very important. If healing length becomes significantly smaller than the interatomic separation $nl_c \ll 1$, then 1D Bose gas enters Tonks-Girardeau (TG) regime of the impenetrable bosons [49, 50]. Due to strong repulsion and 1D confinement atoms cannot interchange their positions and acquire a sort of fermionic properties. As was shown by Girardeau [49, 50] such system can be mapped on the gas of free fermions. In the opposite limit $nl_c \gg 1$ the gas is weakly interacting and can be described by the GP equation. Reduction of 3D GP equation to the 1D case is done by renormalization of the interaction constant g (1.52) in the

GP cubic term

$$g_{1D} = \frac{2\hbar^2 a}{m l_0^2} \tag{1.56}$$

This result can obtained in the limit $a \ll l_0$ by solving scattering problem in the presence of transverse confinement [93] or simply by integrating out the transverse degrees of freedom of 3D problem. The crossover between the TG and GP regimes is driven by phase fluctuations. They become stronger with decreasing density (increasing interaction). When system is deep in the TG regime phase fluctuations completely destroy coherence of the Bose gas and mean-filed approach is inapplicable [98].

1.4 Solitons

One of the phenomena considered in this thesis, atomic Josephson vortex, is a particular *soliton* solution to the system of nonlinear differential equations. The research on solitons is tremendously broad field. In what follows brief history of solitons, their basic concepts and some applications to BEC are summarized mainly according to references [78, 102, 29].

1.4.1 A brief introduction to solitons

In recent years the field of nonlinear waves underwent rapid development mostly due to utilization of solitons in the fiber optics applications. Proponents of the technological use of solitons believe that it could become one of the fundamental technical innovations in the transport of information, claiming a place in the ongoing communications revolution. The discovery of the soliton reaches back to almost two centuries ago, into an era that is known as the industrial revolution. The solitary wave in water was first described by a Scottish engineer named Scott Russel in 1834. He was observing the movement of boats on a canal as he was interested in creating a more efficient hull design for canal boats. When the rope pulling one of the boats accidentally snapped, Russel saw a large, rounded mass of water, a smooth solitary wave gather around the prow of the boat, detach itself from the barge, and proceed without change of shape, or diminution of speed down the canal. He followed the wave for a few miles, and to his surprise the wave held its shape and diminished in height very gradually. He was so astonished by his observation that he built a 10-meter wave tank in his back yard to be able to further investigate the phenomenon. Ten years later he officially reported his observations of "waves of translation" to the British Association of the Advancement of Science. Russels discovery was refuted by

the scientific community of his times, as it was "common knowledge" that waves do not behave in the way described by Russel.

Almost half a century passed until Russels discovery was justified mathematically. Two independent groups were studying the propagation of shallow water waves at that time. They were theoretically described in 1872 by Boussinesqs equation, and in 1895 by the Korteweg de Vries equation. Both equations describe the evolution of the wave height, and have a localized solution, but the simpler of the two is the Korteweg de Vries equation. Almost three quarters of a century will have passed until the findings of Korteweg and de Vries were reinvestigated by a seemingly unrelated discovery. In 1955 E. Fermi, J. Pasta and S. Ulam were studying heat transfer in solids. They modeled a one-dimensional solid lattice by equal masses connected by nonlinear springs. They assumed that in the chain of atoms with nonlinear interactions between the masses the initial energy of a perturbation will be equally shared by all the degrees of freedom of the chain. Much to their surprise, their system did not reach energy equipartition, but returned almost periodically to the originally excited mode. The unexpected result motivated M. Kruskal and N. Zabusky to investigate the Korteweg de Vries equation numerically in 1965. They found that nonlinear solitary waves can occur naturally under the right conditions. The surprising result obtained by Kruskal and Zabusky was that despite the strong interaction between two solitary waves propagating at different speeds, the interaction is only temporary. The colliding waves recover their original shapes and speeds shortly after the interaction. Because the elastic nature of the interaction between the two waves was so similar to the elastic collision of elementary particles, Kruskal and Zabulsky called the waves "solitons".

It is important to point out that prior to Zabusky and Kruskals numerical investigations, analytical expressions describing collision events between solitary wave

solutions of an equation, now called the Sine-Gordon equation, were found by Seeger, Donth and Kochendorfer in 1953.

Kruskal and Zabulskys results have initiated a flurry of activity in the applied mathematics community. In 1967 the team of Gardner, Greene, Kruskal, and Miura found the exact solution of the Kortweg de Vries equation. Their powerful method is known as the inverse scattering transform. Based on it, a number of closed-form exact analytic solutions were obtained. These solutions explicitly demonstrate the elastic collisions observed by Zabulsky and Kruskal.

Gardner's group's findings were supported by Zakharov and Shabat, who were able to solve the nonlinear Schrodinger equation (NLS) describing the evolution of a general wave packets envelope. Subsequently even more complicated nonlinear equations were solved by using a systematic method developed by Ablowitz, Kaup, Newell, and Segur, which is known as the AKNS method. The remarkable advances in the past 40 years stirred interest in soliton research not only in the mathematics community, but in various fields from particle physics to cosmology. The vanguard of recent soliton research is however in the study of optical solitons, where the ultimate goal is to use these nonlinear "humps" to carry information in optical fiber networks.

Currently mathematical apparatus is well developed for solitons propagating in 1D and 2D media ($1+1$ and $2+1$ solitons, which means "space + time" dimensions). Higher-dimensional cases are far from complete understanding.

With experimental realization of BEC and turbulent development of the field of atomic optics, the solitons in BECs became the subject of great theoretical and experimental interest. They describe various topological formations in the macroscopic BEC wave function and may become useful in future applications such as, for example, matter-wave lasers and quantum computers.

One of the accepted definitions of *solitary wave* and *soliton* are the following. If

a solitary wave propagating with velocity v is described by a function $f(x,t)$, then $f(x,t) = f(x-vt)$, $f(x,t)$ is nonsingular, localized and has finite energy. Solitons are solitary waves that retain their shape and velocity asymptotically as time goes to infinity after collision with other solitons. This is why solitons are assigned particle-like properties. Real solitons are influenced by effects such as driving forces, or perturbations such as defects and frictional loss and are therefore metastable. The soliton concept for physicist can therefore best be defined in terms of a specific form of energy propagation [105]: "...localized, finite energy states which are fundamentally nonlinear objects and so cannot be reached by perturbation theory from any linear state..." In other terms, solitons are defined by physicist as representing a balance between dispersion (or dissipation) and nonlinearity.

1.4.2 Dark soliton

We consider repulsive ($a > 0$) GP equation in one spatial dimension and without trapping potential. In this case GP equation reduces to the defocusing NLS equation well known from optics

$$i\hbar\frac{\partial}{\partial t}\Phi(\mathbf{r},t) = \left(-\frac{\hbar^2\nabla^2}{2m} + g\left|\Phi(\mathbf{r},t)\right|^2\right)\Phi(\mathbf{r},t) \tag{1.57}$$

where g is given by (1.56). In context of dilute atomic gases this equation models quasi-1D BEC in a straight infinite waveguide. The ground state is uniform constant solution with density n. It was shown by Zakharov and Shabat [114] that (1.57) is integrable by the means of inverse scattering technique. Besides the trivial uniform

solution it also possesses solitonic solution

$$\Phi_{DS} = \sqrt{n}\left\{ i\frac{v}{c_s} + \sqrt{1-\frac{v^2}{c_s^2}}\tanh\left[\sqrt{1-\frac{v^2}{c_s^2}}\frac{x-vt}{\sqrt{2}l_c}\right]\right\} e^{-ignt/\hbar} \tag{1.58}$$

called dark soliton (DS). The word "dark" comes from the context of fiber optics and originates from the fact that the DS produces density depletion – a "dark spot" on the uniform background. Here $l_c = \hbar/\sqrt{mgn}$ is coherence (healing) length, $c_s = \sqrt{gn/m}$ is speed of sound and v is the DS velocity of propagation along the waveguide. When the DS is stationary ($v = 0$) density minimum in the DS center passes through zero and phase of the BEC wave function abruptly jumps by π (see FIG.1.4). The faster DS moves, the shallower density depletion and the smoother the phase with the jump less than π. Upon reaching the speed of sound $v = c_s$, DS becomes indistinguishable from background. The energy of the DS can be easily found by substitution of (1.58)

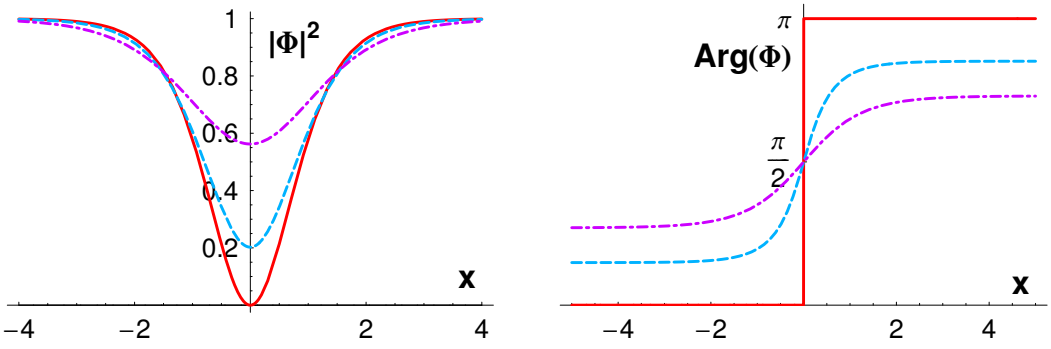

Figure 1.4: The density and phase of the DS solution at $t = 0$ for values of velocity $v = 0$ (red ——), $v = 0.45c_s$ (blue − − −), $v = 0.75c_s$ (violet − · − · −). The unit of the length is the healing length l_c, and the unit of density is n.

in the BEC Hamiltonian density and integrating over x. Relative to the energy of

the uniform background the DS energy is

$$E_{DS} = \frac{4\hbar m}{3g} (c_s - v)^{3/2} \tag{1.59}$$

Several teams reported experimental observation of DSs in ultracold atomic gases [21, 31, 5, 34] where DSs were created with phase imprinting technique and detected by absorption imaging. For a DS to be dynamically stable the BEC must be in quasi-1D regime according to (1.55). In dimensions higher than 1D so called "snake instability" develops (the deformation of the DS transverse plane due to excitations of the transverse modes) and the DS decays into vortices [92, 38, 5, 34].

Even highly anisotropic elongated BEC clouds are axially confined. Thus the DS solution (1.58) to a *uniform* problem is just an approximation to a true DS in a realistic BEC. The dynamics of a DS in a nonuniform system was considered by many authors (see reference [95] and references therein). In a BEC cloud with typical harmonic confinement a DS behaves like a particle-like object oscillating in a potential well (axially along the trap). Because the DS energy (1.59) is maximum for the stationary DS and monotonically falls to zero as DS speed approaches the speed of sound, the DS effectively behaves as a particle with negative mass and negative kinetic energy. It leads to the instability of the DS to acceleration in a dissipative system. This so called *antidamping* effect [21, 22] results from interaction of DS with thermal cloud.

1.4.3 Sine-Gordon kink: topological vs. nontopological solitons

The Sine-Gordon (SG) equation is used to describe wide variety of physics phenomena among which are dislocations in solids [45], domain walls in quasi-1D ferromagnets [37], mechanical chain of coupled pendula [104, 102], liquid crystals [85], hydrodynamics [46], etc.

For this work the most important application of the SG model is description of fluxons in a long superconducting Josephson junction [12]. It will be shown that though the SG model is well established for superconductors, it is insufficient for the description of the long bosonic Josephson junction. For this another generalized model must be employed, which in the limit of weak Josephson coupling will reduce to the SG model.

In 1D SG equation has the following form

$$\frac{\partial^2\theta}{\partial t^2} - c^2\frac{\partial^2\theta}{\partial x^2} + \omega^2 \sin(\theta) = 0 \tag{1.60}$$

The *kink* soliton solution of the equation (1.60) is given by

$$\theta = 4\arctan\left[\exp\left(\pm\frac{\omega}{c}\frac{x-vt}{\sqrt{1-(v/c)^2}}\right)\right] \tag{1.61}$$

where the choice of sign $\pm$ yields kink or anti-kink. Kink (anti-kink) starts at 0 (2π)at $x = -\infty$ and goes to 2π (0)at $x = +\infty$ (see FIG.1.5).

The SG equation can be derived from the following Lagrangian

$$L = \int dx \left[\frac{1}{2}\left(\frac{\partial\theta}{\partial t}\right)^2 - \frac{c^2}{2}\left(\frac{\partial\theta}{\partial x}\right)^2 - \omega^2(1-\cos(\theta))\right] \tag{1.62}$$

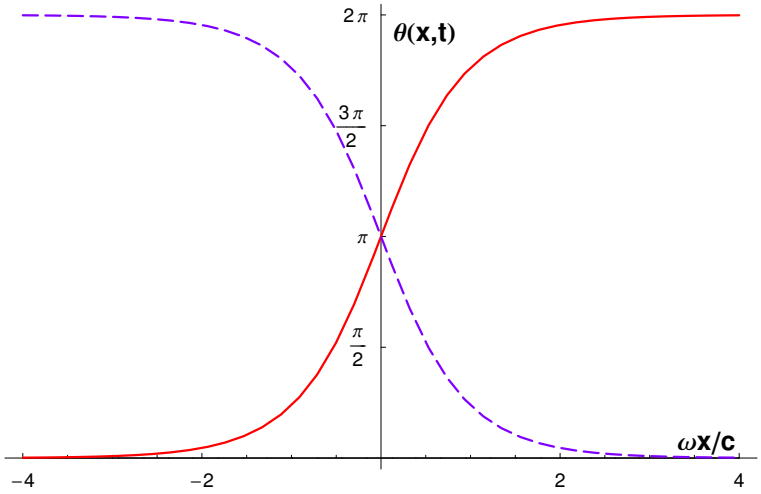

Figure 1.5: The SG kink (red ——) and anti-kink (blue − − −) given by (1.61) at $t = 0$ for the value of velocity $v = 0.8c$.

The SG energy can be found to be

$$E_{SG} = \frac{mc^2}{\sqrt{1-(v/c)^2}} \tag{1.63}$$

where $m = 8\omega/c$ is the "rest mass" of the kink. The kink behaves as relativistic particle with energy E_{SG}. With increasing speed the kink becomes narrower, which is relativistic Lorentz contraction. The kink solution is a *topological soliton*, because at $x = \pm\infty$ it asymptotically approaches different values and thus possesses *topological charge*

$$\frac{1}{2\pi}\int_{-\infty}^{\infty}\frac{\partial\theta}{\partial x}dx = \frac{1}{2\pi}\left(\theta\left(\infty\right)-\theta\left(-\infty\right)\right) = \pm 1 \tag{1.64}$$

where different sign corresponds to kink or anti-kink. The topological charge is a *conserved* quantity independent of the kink velocity and mass. The SG kink solution

originates in the form of "solitonic potential"

$$V(\theta) = \omega^2 (1 - \cos(\theta)) \tag{1.65}$$

which in SG case has infinitely many minima also called degenerate vacuum. A topological soliton $f(x,t)$ connects minima of the degenerate vacuum asymptotically at $x = \pm\infty$ with, *necessarily*, the following boundary conditions: $f(x = -\infty, t) \neq f(x = \infty, t)$ (in contrast to a nontopological soliton with $f(x = -\infty, t) = f(x = \infty, t)$). Thus the nature of a topological soliton lies not in its local structure, but in the boundary conditions. Illustratively a topological soliton can be imagined as a twist of an infinite flat belt. It is stable, because to "undo" the twist one needs to rotate an infinitely long system, which requires infinite energy.

1.5 Josephson effect

Josephson effect is a consequence of macroscopic quantum coherence and its observation in a particular system is a direct evidence of ODLRO. Predicted in 1962 [62] the effect was observed in superconductors, superfluid Helium ^{4}He and ^{3}He and most recently in ultracold atomic gases [1]. Besides the significance of effect for fundamental quantum physics it is also found numerous technological applications (e.g. metrological unit of voltage, measuring of weak magnetic fields). The superconducting Josephson junction serves as a powerful experimental tool for testing the behavior of solitons in realistic system. It is also one of the most promising candidates for storage and processing of quantum information.

Below we briefly discuss basics of the Josephson effect and its specifics for ultracold atomic gases following mostly [108, 109]. For detailed review of the Josephson effect see reference [12].

1.5.1 Superconducting Josephson effect

When the gauge symmetry of a macroscopic quantum system is spontaneously broken, the systems ground state is characterized by on order parameter, which is a complex number and has a definite phase. In a superconductor due to specific interaction of electrons with crystal lattice a fraction of electrons forms Cooper pairs. These pairs can condense in a single quantum state, because a pair consists of two electrons with opposite spin and is a boson. FIG.1.6 shows a layer of an insulator sandwiched between two superconductors. The layer is thick enough for Cooper pair condensates in each superconductor to be described by independent order parameters

$$\Psi_1 = \sqrt{\rho_1} e^{i\varphi_1} \quad , \quad \Psi_2 = \sqrt{\rho_2} e^{i\varphi_2} \tag{1.66}$$

where ρ_k stays for the Cooper pair density and φ_k for their coherent macroscopic phase. Though the layer is macroscopically thick it is still thin enough to allow tun-

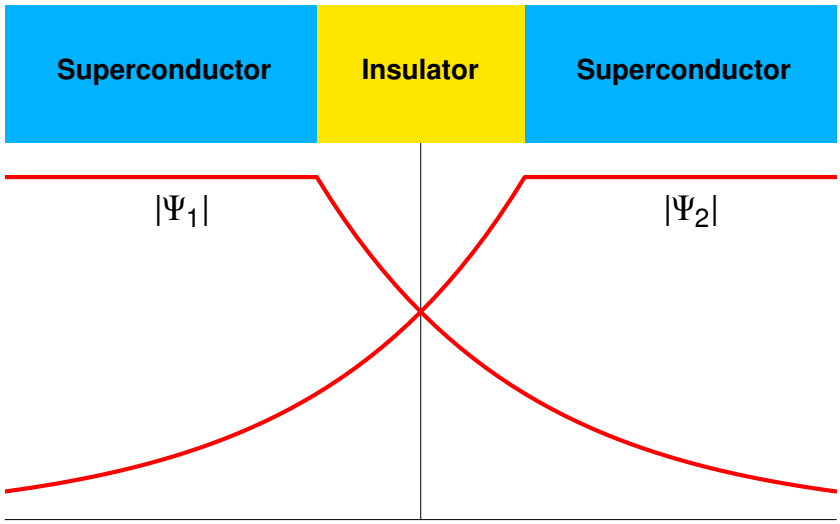

Figure 1.6: Schematic representation of superconducting Josephson junction. Each superconductor is described by a separate order parameter Ψ_k. Order parameters decay inside the insulator, which is thin enough for the order parameters to overlap.

neling of the electrons between the superconductors. If the layer ~ 100Å only single electrons can tunnel, but if the layer width is reduced to ~ 30Å, then Cooper pairs can be coherently exchanged between the superconductors, which is the Josephson effect. As was predicted by Josephson [62] *nondissipative* current of Cooper pairs satisfies the following equations:

$$\begin{aligned} I(\varphi) &= I_c \sin(\varphi) \\ \dot{\varphi} &= -\mu/\hbar \end{aligned} \tag{1.67}$$

where I_c is the critical current, $\varphi = \varphi_1 - \varphi_2$ is the relative phase and $\mu = \mu_1 - \mu_2$ is the relative chemical potential (produced by applied voltage $V = \mu/2e$). The Josephson

equations (1.67) can be derived from a generic *rigid* pendulum Hamiltonian

$$H(\varphi, N) = E_J(1 - \cos(\varphi)) + \frac{1}{2}E_C N^2 \tag{1.68}$$

where $N = N_1 - N_2$ is the number of tunneled particles, $E_J = \hbar I_c$ is the Josephson coupling energy, and $E_C = \partial\mu/\partial N$ is so called capacitive energy. When $E_J \gg E_C$ and $E_J \gg k_B T$ then the system is in the regime of small oscillations and (1.68) can approximated by the harmonic oscillator Hamiltonian

$$H(\varphi, N) \approx \frac{1}{2}E_J\varphi^2 + \frac{1}{2}E_C N^2 \tag{1.69}$$

with the so called *Josephson plasma* frequency

$$\omega_{JP} = \sqrt{E_J E_C}\Big/\hbar\ . \tag{1.70}$$

1.5.2 Bose Josephson junction

Recent experiments [23, 1] demonstrated that the described above Josephson effect takes place in ultracold atomic gases as well. Authors of reference [108, 101] consider a double well trapping potential containing BECs in each well (see FIG.1.7). They argued that a two-state model can be employed to describe the system

$$\begin{aligned} i\hbar\dot{\psi}_1 &= \left(E_1^0 + U_1 N_1\right)\psi_1 - K\psi_2 \\ i\hbar\dot{\psi}_2 &= \left(E_2^0 + U_2 N_2\right)\psi_2 - K\psi_1 \end{aligned} \tag{1.71}$$

with

$$\psi_{1,2} = \sqrt{N_{1,2}}\exp(i\varphi_{1,2})\ . \tag{1.72}$$

where $N_{1,2}$ and $\varphi_{1,2}$ are the number of particles and phases in the first and second

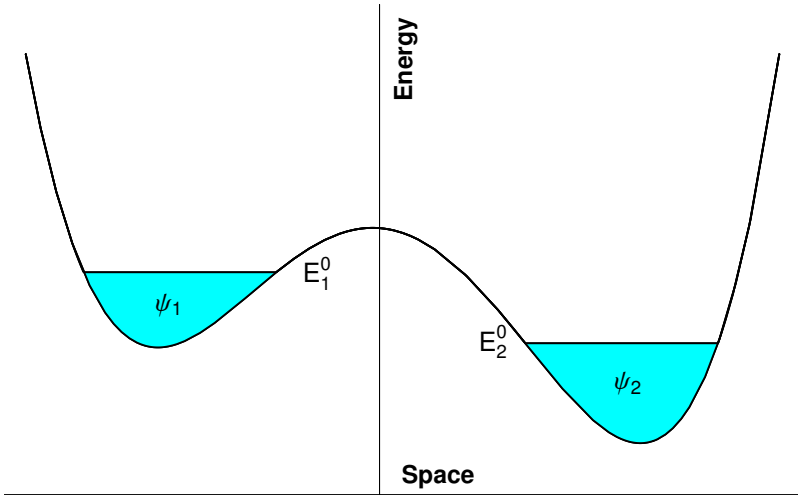

Figure 1.7: Schematic representation of the short BJJ.

wells. Complex amplitudes (1.72) introduced as

$$\Psi = \psi_1(t)\Phi_1(t) + \psi_2(t)\Phi_2(t) \tag{1.73}$$

with Ψ being an approximate solution of the complete GP equation describing two wells and $\Phi_{1,2}$ are the ground state solutions for isolated wells. Substituting ansatz (1.73) into the GP equation one can express the constants $E^0_{1,2}$, $U_{1,2}$ and K through the corresponding overlap integrals [108, 101]. The decomposition (1.73) is a good approximation, because inside the interwell barrier BEC wave function decays exponentially.

Introducing new variables of relative phase θ and fractional population misbalance $-1 < z < 1$

$$\begin{aligned} \theta &= \varphi_2 - \varphi_1 \\ z &= \frac{N_1 - N_2}{N_T} \end{aligned} \tag{1.74}$$

where $N_T = N_1 + N_2$ is conserved total number of atoms, one can obtain the following

system of equations

$$\begin{aligned} \dot{z} &= -\sqrt{1-z^2}\sin(\theta) \\ \dot{\theta} &= \Lambda z + \frac{z}{\sqrt{1-z^2}}\cos(\theta) + \Delta E \end{aligned} \tag{1.75}$$

Above the time was rescaled as $2Kt \to t$ and the following constants introduced

$$\begin{aligned} \Delta E &= \frac{E_1^0 - E_2^0}{2K} + \frac{(U_1 - U_2)\,N_T}{4K} \\ \Lambda &= \frac{(U_1 + U_2)\,N_T}{4K} \end{aligned} \tag{1.76}$$

Because system (1.75) is invariant under the following symmetry transformation

$$\Lambda \to -\Lambda\,,\ \theta \to -\theta + \pi\,,\ \Delta E \to -\Delta E\ , \tag{1.77}$$

solutions for negative ($\Lambda < 0$) and positive ($\Lambda > 0$) scattering length can be mapped onto each other. The system (1.75) can be interpreted mechanically as equations describing dynamics of *momentum shortened pendulum* (in contrast to the SJJ where the analogy is the rigid pendulum). Variables z and θ are canonically conjugate with the Hamiltonian

$$H = \frac{\Lambda}{2}z^2 - \sqrt{1-z^2}\cos(\theta) + z\Delta E \tag{1.78}$$

The pendulum has slant angle θ and length proportional to $\sqrt{1-z^2}$ decreasing with *angular momentum* z. According to equations (1.75) the conventional Josephson current (1.67) is now generalized as

$$\begin{aligned} I &= \frac{\dot{z}N_T}{2} = I_c\sqrt{1-z^2}\sin(\theta) \\ I_c &= KN_T \end{aligned} \tag{1.79}$$

Solutions of the system (1.75) can be obtained analytically in terms of the Jacobi

elliptic functions ([101]). One of the most important consequences of nonlinear nonrigidity of the pendulum is effect of *macroscopic quantum self-trapping* (MQST) when relative population oscillates with nonzero average $\langle z \rangle \neq 0$ [108, 101]. If one starts with initial condition $\theta(0) = 0$ then for the case of symmetric trap ($\Delta E = 0$) critical MQST parameter is

$$z_c = 2\sqrt{1-\Lambda}\Big/\Lambda \ . \tag{1.80}$$

If $z(0) > z_c$ then the oscillations are self-trapped [108, 101]. MQST was recently observed experimentally [1]. For a linearized system the frequency of small oscillations is given by

$$\omega_{JP} = \sqrt{2K\left(UN_T + 2K\right)} \tag{1.81}$$

Generally oscillations of z and θ have quite complex phase space. For a symmetric trap ($\Delta E = 0$) they can be classified into the following domains [23, 1]:

1. **Rabi oscillations**. When the interatomic interaction is absent ($\Lambda = 0$) one obtains sinusoidal dynamics with frequency $\omega_R = 2k/\hbar$. This is not the Josephson dynamics, but rather the usual Rabi dynamics of a two-level atom;

2. **Zero phase modes**. Oscillations for which time averages $\langle z(t) \rangle = \langle \theta(t) \rangle = 0$;

3. **MQST modes**. General oscillations with $\langle z(t) \rangle \neq 0$;

4. **π-phase modes**. General oscillations with $\langle \theta(t) \rangle = \pi$.

In a realistic system we could expect existence of the damping effects. To fully take it in account we need to generalize the above description to nonzero temperatures. Nevertheless simple phenomenological approach is also possible. Attributing dissipative losses to the exchange of normal atoms between the wells one can write

the Ohmic current as [115]

$$I_n = -G\Delta\mu \tag{1.82}$$

where $\Delta\mu$ is relative chemical potential and G is so called dc conductance. The system (1.75) then becomes [87]

$$\begin{aligned} \dot{z} &= -\sqrt{1-z^2}\sin(\theta) - \eta\dot{\theta} \\ \dot{\theta} &= \Lambda z + \frac{z}{\sqrt{1-z^2}}\cos(\theta) + \Delta E \\ \eta &= 2\hbar G/N_T \end{aligned} \tag{1.83}$$

1.5.3 Experimental realization of the long Bose-Josephson Junction

In the considered above Josephson effect the dependence of relative phase and population on spatial coordinate was not explicit and dynamical, but rather indirect through the constants depending on spatial overlap integrals. This situation is associated with so called *short* JJ where the system size does not have a significant spatial extent. In the contrast *long* JJ can have one or two extended spatial dimensions for which spatial coordinate must explicitly enter systems equations of motion. Long SJJ is very well studied (for a review see reference [12]) and conventionally described in the frame of SG model. Physical interpretation of SG kink soliton solution is *Josephson vortex* (JV) or *fluxon* consisting of circulating supercurrent. The JV is a 1D topological object and does not have core (in contrast to a 2D rotational vortices in quantum fluids). The JVs can propagate along the SJJ as particle-like objects. Their experimental observation is in good agreement with the perturbed SG model where effects of external forces such as drive and friction are taken in account.

The first problem of this thesis considers bosonic analog of a long SJJ, – long

BJJ. It shown that the SG model is insufficient for the description of long BJJ. The description requires a generalization, similar to the generalization for short BJJ form rigid to a non-rigid pendulum. The Josephson effect in a short BJJ was just recently observed experimentally [23, 1] with spectacular demonstration of the MQST [1]. Long BJJ may become the object of the following experiments in the closest future. The purpose of this section is to introduce experimental systems which are the most probable candidates for realization of long BJJ.

A long quasi-1D BJJ can be formed with two atomic waveguides placed parallel to each other in such proximity that Josephson tunneling takes place. BEC in an atomic waveguide was successfully realized with optical, magnetic and combined atomic traps. Schematic picture of the parallel atomic waveguides can be seen on the FIG.2.1. Below a few experimental systems of parallel waveguides will be discussed.

First system we mention was created by MIT group [80]. The trap was formed by orthogonally polarized $1064nm$ laser beam. Initially confinement was highly elongated single potential well – an atomic waveguide. The authors of [80] were able to split this single waveguide into two parallel ones *coherently*. The coherence was demonstrated by observation of interference fringes of expanding and overlapping BECs release from the waveguides. The distance between the waveguides was $13\mu m$.

Another system where 1D geometry can be readily realized is a BEC micro chip with purely magnetic confinement designed with help of miniature lithographically produced current carrying wires. A German group at *Physikalisches Institut der Universitt Tbingen* produced micro-fabricated chip with a set of parallel current carrying wires and flexibility to split a waveguide into two and then merge them back [94]. Another German team at *Max-Planck-Institut* manufactured a similar device and was actually able to split BEC from a single wave guide into two [57]. Separation between the wells was $135\mu m$. Finally MIT group made a step forward by *coherently* splitting

BEC in a single waveguide to a system of parallel waveguides [106]. Once again coherence was demonstrated by interference fringes of released BEC clouds. Separation between the wells was $15\mu m$.

The last system we discuss is similar to the previous one with the difference that magnetic confinement is produced by *permanent-magnet* atomic chip build on the base of magnetized videotape. United Kingdom team at *Imperial College* was able to manufacture a system of parallel atomic waveguides on a *permanent-magnet* microchip and load BEC into one of them [107].

1.6 Ultracold atoms in optical lattices

The field of solid state physics is tremendously rich and continues to produce new results and push technology forward. Nevertheless even in this splendid research area there are some limitations. For instance, crystal lattice of a solid body is pretty much invariable and fixed by the conditions under which this lattice forms. If periodic potential confining strongly interacting many-body system became experimentally adjustable, it would certainly generate some new ideas and put some old ones to test. Partially this process has begun with creation of artificial crystals formed by light: optical lattices (OLs). These lattices are produced by lasers, which are versatile tools to handle manipulations of atoms. Interaction of electromagnetic field with atoms has both conservative and dissipative aspects, which are employed for different purposes in experimental physics. The dissipative aspect is due to inelastic scattering, when absorption of a photon is followed by its spontaneous emission. Momentum transfer from the reemitted photon produces dissipative force, which is used for laser cooling and magneto-optical trapping [118]. The conservative aspect comes from the interaction between light and light-induced atom dipole moment, which produces so called ac-Stark shift in the potential energy. Spontaneous emission can be avoided by detuning laser frequency ω far from the transition frequency of the atom ω_0, in which case conservative optical potential can be formed [119]. Laser field can be then spatially modulated with help of counterpropagating laser beams producing standing light waves to form a necessary profile of potential energy. The sign of the detuning $\Delta = \omega - \omega_0$ defines whether the formed potential is repulsive (blue detuning $\omega > \omega_0$) or attractive (red detuning $\omega < \omega_0$).

1.6.1 Optical lattice potentials

The simplest OL is 1D and formed by just two counterpropagating laser beams. Resulting 1D standing light wave produces potential of the form

$$V(x) = V_0 \cos^2(kx) \tag{1.84}$$

where $k = 2\pi/\lambda$, λ is the wavelength of the laser field and V_0 is lattice depth. By imposing such potential on a cloud of ultracold atoms we confine them in disc-shaped domains placed parallel to each other with period $a = \lambda/2$ (see FIG.1.8). Further

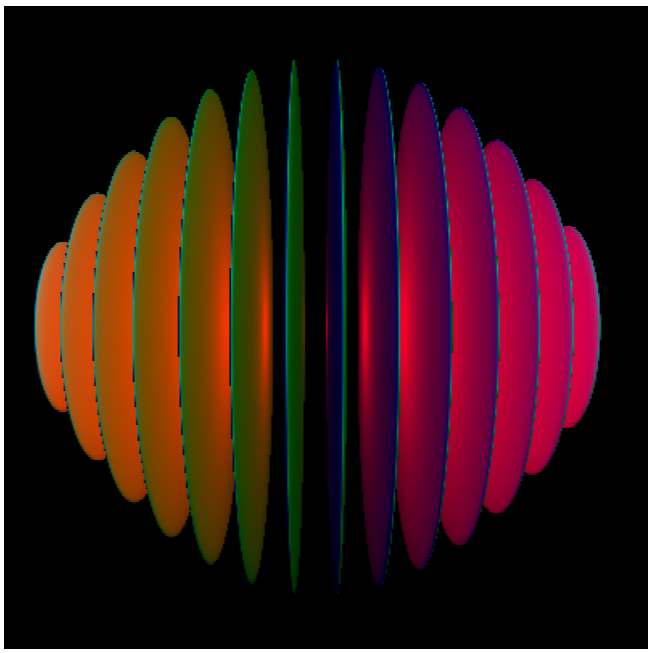

Figure 1.8: Schematic representation of BEC clouds confined in 1D OL. Two other dimensions are not affected by the lattice. The overall spherical shape of the BEC cloud results from additional harmonic confinement superimposed on OL.

implementation of the same idea leads to formation 2D and 3D OL by adding second and correspondingly third standing light waves in additional orthogonal spatial dimensions (see FIG.1.9 and FIG.1.10). The 3D OL can be represented by the following

potential

$$V(x) = V_{0x}\cos^2(kx) + V_{0y}\cos^2(kx) + V_{0z}\cos^2(kx) \tag{1.85}$$

The depth of this lattice for a particular spatial dimension V_{0k} $(k = x, y, z)$ depends on the intensity of corresponding counterpropagating laser beams and can be easily controlled in an experiment.

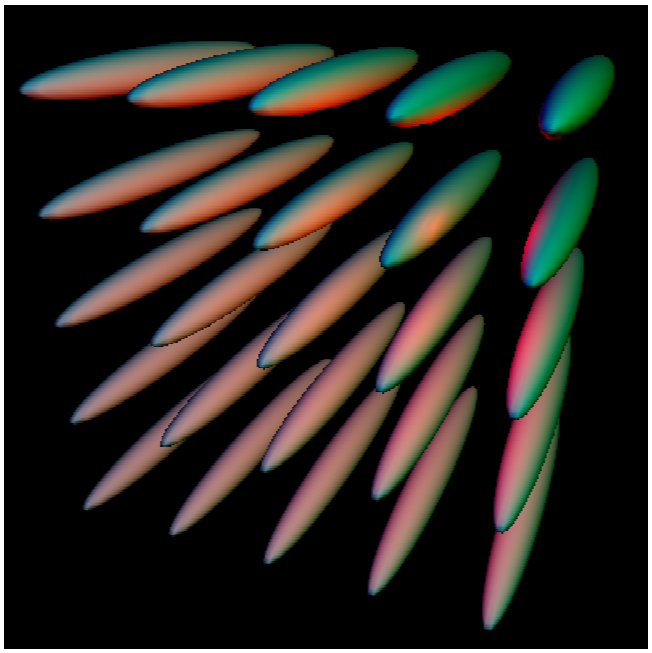

Figure 1.9: Additional counterpropagating laser beams in the orthogonal spatial dimension form 2D OL, with the remaining dimension being not confined by the lattice.

1.6.2 Bloch and Wannier functions

Felix Bloch, one of the founders of modern solid state physics, recollects the following in his article in the 1976 issue of *Physics Today*: "This was so simple that I couldn't think it could be much of a discovery, but when I showed it to Heisenberg he said right away: "That's it!" [13]. This quotation concerns his work about conduction of electrons in crystalline solids, in particular, a statement that later became known

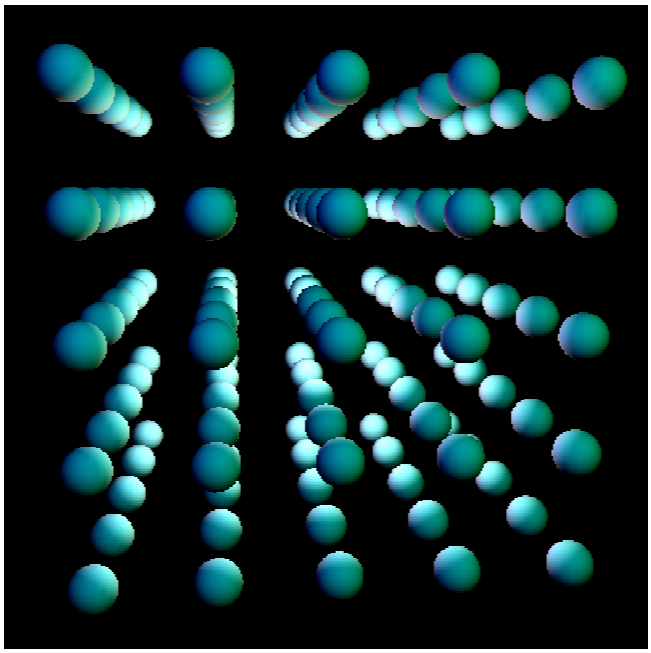

Figure 1.10: Three mutually orthogonal counterpropagating laser beams create 3D OL, with all three dimensions confined by the lattice.

as Bloch theorem, one of the most important theorems in solid state physics. The basic idea is that the periodic symmetry of crystal lattice must be reflected in the wave functions of electrons moving in the periodic potential imposed by the lattice. The case of atoms in periodic optical lattices requires imposition of the same logic to derive a correct quantum model.

For simplicity we consider motion in one dimension only. A particle of mass m moving in periodic potential $V(x) = V(x + a)$ is described by the Hamiltonian

$$H = \frac{p^2}{2m} + V(x) \tag{1.86}$$

According to the Bloch theorem general form of the wave function is a plane wave with the amplitude modulated by a periodic function $u_{q,n}(x)$ with the period equal

to the lattice period

$$\phi_{q,n}(x) = u_{q,n}(x)e^{iqx} \quad , \quad u_{q,n}(x) = u_{q,n}(x+a) \tag{1.87}$$

Substitution of (1.87) into Schrodinger equation

$$H\phi_{q,n}(x) = E_{q,n}\phi_{q,n}(x) \tag{1.88}$$

yields differential equation for the function $u_{q,n}(x)$

$$\left(\frac{(p+\hbar q)^2}{2m} + V(x)\right) u_{q,n}(x) = E_{q,n}u_{q,n}(x) \tag{1.89}$$

Quantity $\hbar q$ is called quasimomentum and q serves as a quantum number reflecting on translational symmetry of the periodic potential. Due to periodicity all information can be derived from so called first Brillouin zone $-\pi/a < q < \pi/a$. Dependence eigenvalues $E_{q,n}$ on q and n produces so called energy band structure, where n enumerates the bands. As the depth of potential lattice V_0 growth the gap between the bands increases and the width a of the bands decreases. Already for the OL depth $V_0 \sim 10E_R$, where $E_R = \hbar^2k^2/(2m)$ is recoil energy, the first energy gap is much larger than the width of the first and second energy bands. In the limit of infinitely deep OL ($V_0 \to \infty$) we obtain degenerate in q spectrum of a particle completely localized at a lattice cite. Index n then labels usual energies of a particle confined to a limited space.

When the lattice depth V_0 is sufficient enough to localize particles in potential

minima, a convenient choice of complete orthonormal basis is Wannier functions

$$w_n(x - x_i) = \frac{1}{\sqrt{M}} \sum_q e^{-iqx_i} \phi_{q,n}(x) \tag{1.90}$$

where M is total number of lattice sites located at x_i. As $V_0 \to \infty$, the Wannier function w_n approaches the harmonic oscillator wave function of nth state.

1.6.3 Bose-Hubbard model

As was shown by Jaksch and coauthors [59] gas of bosons in an OL can be described by Bose-Hubbard (BH) model. This model can be derived starting from the usual many-body Hamiltonian of a bosonic system (1.49) with interaction (1.52)

$$\hat{H} = \int d\mathbf{r} \hat{\psi}^\dagger(\mathbf{r}) H_0 \hat{\psi}(\mathbf{r}) + \frac{g}{2} \int d\mathbf{r} \hat{\psi}^\dagger(\mathbf{r}) \hat{\psi}^\dagger(\mathbf{r}) \hat{\psi}(\mathbf{r}) \hat{\psi}(\mathbf{r}) \tag{1.91}$$

where

$$H_0 = -\frac{\hbar^2}{2m} \nabla^2 + V_{lat}(\mathbf{r}) + V_{tra}(\mathbf{r}) \tag{1.92}$$

The OL potential $V_{lat}(\mathbf{r})$ is superimposed on the usual slowly varying trapping potential $V_{tra}(\mathbf{r})$. The main assumption leading to BH model is that the energies of atoms are much smaller than the first energy gap between the bands. Thus all atoms are restricted to the first band of the OL. One can expand bosonic operators in the Wannier basis and keep only lowest vibrational states

$$\hat{\psi}(\mathbf{r}) = \sum_i \hat{a}_i w(\mathbf{r} - \mathbf{r}_i) \tag{1.93}$$

which reduces (1.91) to

$$\hat{H} = -J \sum_{\langle i,j \rangle} \hat{a}_i^\dagger \hat{a}_j + \frac{U}{2} \sum_i \hat{a}_i^\dagger \hat{a}_i^\dagger \hat{a}_i \hat{a}_i + \sum_i \varepsilon_i \hat{a}_i^\dagger \hat{a}_i \tag{1.94}$$

with

$$J = \int d\mathbf{r} w^* (\mathbf{r} - \mathbf{r}_i) \left[-\frac{\hbar^2}{2m} \nabla^2 + V_{lat} (\mathbf{r}) \right] w (\mathbf{r} - \mathbf{r}_j) \tag{1.95}$$

$$\varepsilon_i = \int d\mathbf{r} V_{tra} (\mathbf{r}) \left| w (\mathbf{r} - \mathbf{r}_j) \right|^2 \approx V_{tra} (\mathbf{r}_i) \tag{1.96}$$

$$U = g \int d\mathbf{r} \left| w (\mathbf{r}) \right|^4 \tag{1.97}$$

In the BH Hamiltonian (1.94) $\hat{a}_i$ and $\hat{a}_i^\dagger$ are operators annihilating and creating (respectively) a boson on a OL site $\mathbf{r}_i$. They satisfy canonical commutation relations

$$\left[\hat{a}_i, \hat{a}_j^\dagger \right] = \delta_{ij} \tag{1.98}$$

Number operator counting amount of bosons on a OL site $\mathbf{r}_i$ is defined as $\hat{n}_i = \hat{a}_i^\dagger \hat{a}_i$. The summation $\langle i, j \rangle$ runs over the nearest neighbors. The constant J represents nearest neighbors tunneling matrix element and is responsible for the dynamical hopping of bosons from one OL site to another. During a jump between two neighboring sites a boson gains energy J. The constant U is the strength of the onsite repulsive interaction of bosons. Adding a boson to already occupied site costs energy U. We neglected contribution of the tunneling matrix elements to the sites other than the nearest neighbors and also offsite repulsive interaction, which is a good approximation for a deep enough OL ($V_0 > 5E_R$) [60]. Energy offset ε_i results from additional (besides the OL) confinement $V_{tra} (\mathbf{r})$. In the uniform case $\varepsilon_i = 0$.

1.6.4 Superfluid – Mott insulator transition

The great importance of the introduced above BH comes from the fact that despite being one of the simplest models for strongly interacting quantum systems it captures rich physics of quantum phase transitions (QPT). In contrast to the classical phase transitions driven by thermal fluctuations at temperatures $T > 0$, QPT occurs at $T = 0$ due to quantum fluctuations. One of such QPTs — SF-Mott insulator (MI) transition — was recently demonstrated experimentally [51] in ultracold atomic gases trapped in an OL. SF-MI transition can be derived from the BH Hamiltonian (1.94). In this section for simplicity we consider only uniform case $\varepsilon_i = 0$:

$$\hat{H} = -J \sum_{\langle i,j \rangle} \hat{a}_i^\dagger \hat{a}_j + \frac{U}{2} \sum_i \hat{a}_i^\dagger \hat{a}_i^\dagger \hat{a}_i \hat{a}_i \tag{1.99}$$

BH model possesses two distinct ground states corresponding to the cases when one of the terms in (1.99) is strongly dominant. In the SF regime $U/J \ll 1$ the tunneling term dominates. Boson are not localized at particular OL sites but rather smeared over the whole lattice. The many-body ground state can be represented as a product of identical single-particle Bloch waves. If a lattice of M contains N particles one has

$$|\Psi_{SF}\rangle_{U/J \approx 0} \propto \left(\sum_{i=1}^{M} \hat{a}_i^\dagger \right)^N |0\rangle \approx \prod_{i=1}^{M} |\phi_i\rangle \tag{1.100}$$

Each lattice site i is described by the many-body state $|\phi\rangle_i$ almost equivalent to a coherent state. Each coherent site-state is a superposition of different boson number states, describing amount of bosons on a particular site. The number of bosons on a lattice site is undetermined and follows Poissonian distribution as shown on FIG.1.11

and FIG.1.12. The nonvanishing quantity

$$\psi_j = \langle \phi_j | \, \hat{a}_j \, | \phi_j \rangle = \sqrt{\bar{n}_j} e^{\mathrm{i}\varphi_j} \tag{1.101}$$

describes matter wave on a site j and is characterized by definite phase φ_j and average number of atoms $\bar{n}_j$. The real part of expectation value of the hopping term on a

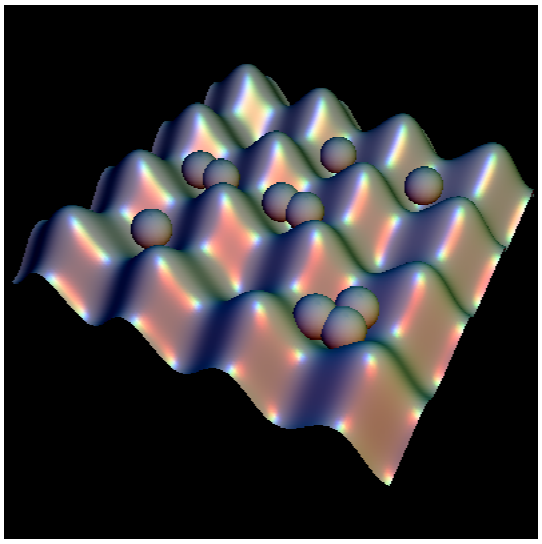

Figure 1.11: Schematic representation of an OL in SF regime. The number of atoms on a site fluctuates according to Poissonian distribution. Each site possesses definite phase and atoms behave coherently forming a macroscopic matter wave spread over the whole lattice.

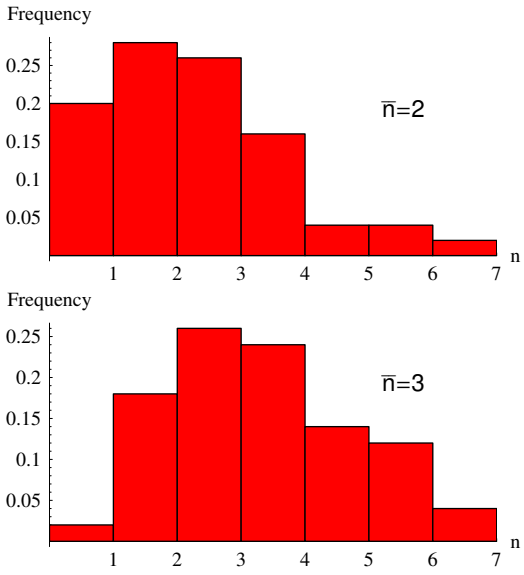

Figure 1.12: The histograms describe how frequently a particular amount of bosons can be found on a site if the average number of bosons is $\bar{n} = 2$ (top) and $\bar{n} = 3$ (bottom). The histograms represent Poissonian distribution.

particular lattice site can be interpreted as Josephson tunneling energy

$$\mathrm{Re}\left[\left\langle -J\hat{a}_i^\dagger \hat{a}_j \right\rangle\right] = \mathrm{Re}\left[\psi_i^* \psi_j\right] = -J\sqrt{\bar{n}_i \bar{n}_j}\cos\left(\varphi_i - \varphi_j\right) \tag{1.102}$$

Consequently neighboring sites having the same phase (coherence) lower the energy of the system.

In the opposite limit $U/J \gg 1$ the onsite interaction dominates, which makes fluctuations of atom number on a lattice site energetically costly. In this limit bosons become localized on OL sites and the many-body ground state is given by the product of local Fock states. For commensurate filling of n atoms per lattice site one can write the ground state as

$$|\Psi_{MI}\rangle_{J\approx 0} \propto \prod_{i=1}^{M} \left(\hat{a}_i^{\dagger}\right)^n |0\rangle \tag{1.103}$$

This ground state describes the MI regime. FIG.1.13 and FIG.1.14 schematically show formation of MI phase for the commensurate filling of one and two atoms per

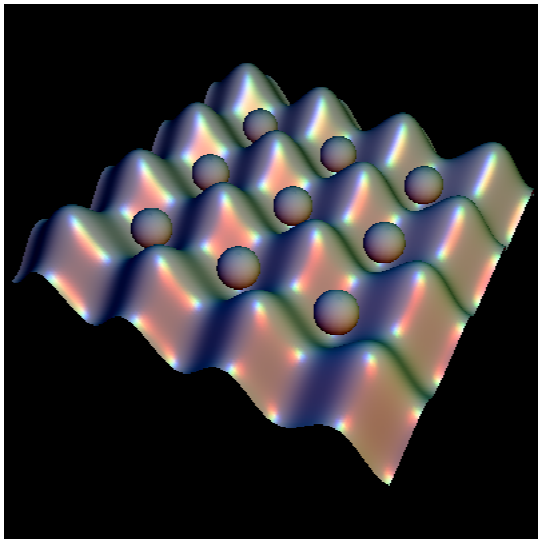

Figure 1.13: Mott insulator with commensurate filling of one atom per OL site.

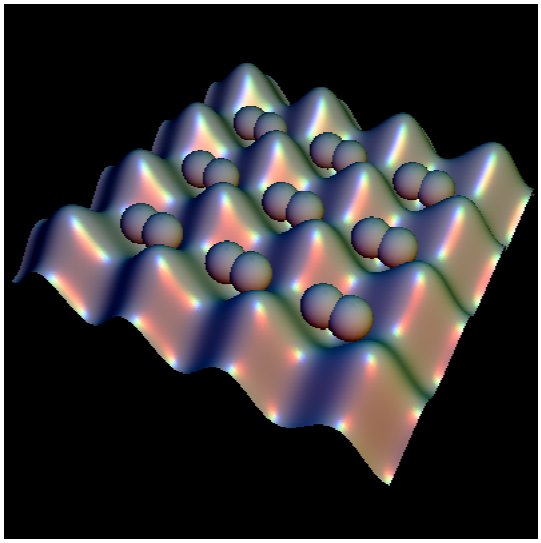

Figure 1.14: Mott insulator with commensurate filling of two atoms per OL site.

site respectively. With atom number fluctuations on a lattice site suppressed, the phase on this site becomes undetermined. Thus macroscopic coherence in the system is lost and

$$\psi_j = \langle \phi_j | \, \hat{a}_j \, | \phi_j \rangle = 0 \tag{1.104}$$

In the MI the phase interactions between the atoms determine system properties.

The interaction term minimizes the energy, if instead of coherent sates the Fock states realize.

Increase of OL depth V_0 decreases J and increases U [59]. Thus by varying V_0 it is possible to bring the system from SF to MI regime and vice versa. In practice parameter U/J can be varied from ~ 0 to ~ 2000 [14]. The transition occurs at $U/J = 5.8z$, where z is the number of nearest neighbors of a lattice site [59, 51]. SF and MI regimes are experimentally detected from the absorption image of expanding atomic cloud released from the OL confinement. If SF state was realized then matter waves from different sites will interfere due to global macroscopic coherence of the system. Absorption images then show formation of specific interference patterns with sharp spikes arranged in the order reflecting the OL symmetry. In the MI phase the macroscopic coherence is destroyed and interference patterns do not form.

1.6.5 Multicomponent quantum mixtures on optical lattices

The considered in the previous section *single*-component BH model is the simplest case of strongly interacting quantum system on a lattice. Flexibility of experimental setups for ultracold atoms in OL and actual experimental realization of SF-MI transition [51] stimulated many proposals for novel states in quantum *mixtures* [63, 67, 27, 90, 68, 69, 70, 58, 65, 11]. Single-component atoms in an OL have only two phases – SF and MI, while multi-component systems offers very reach nontrivial phase diagrams. To demonstrate the complexity of possible states let us consider a BH Hamiltonian of a commensurate two-component bosonic system [70]

$$H = -\sum_{\langle i,j\rangle\sigma}\left(t_\sigma \hat{a}^\dagger_{i\sigma}\hat{a}_{j\sigma} + H.c.\right) + \frac{1}{2}\sum_{i,\sigma,\sigma'} U_{\sigma\sigma'}\hat{n}_{i\sigma}\hat{n}_{i\sigma'} \qquad (1.105)$$

Index $\sigma = A, B$ labels different components A and B. Operator $\hat{a}^\dagger_{i\sigma}$ ($\hat{a}_{i\sigma}$) creates (annihilates) a boson of kind σ at OL site i. Number operators defined as $\hat{n}_{i\sigma} = \hat{a}^\dagger_{i\sigma}\hat{a}_{i\sigma}$ and summation $\langle i, j\rangle$ runs over nearest neighbors. Below we follow reference [70] and consider only equal fillings factors of the components $n_A = n_B = n$, where n is an integer.

The system described by Hamiltonian (1.105) can demonstrate interesting novel quantum phases. To characterize them it is useful to introduce order parameters ψ_A and ψ_B associated with species A and B respectively. Authors of reference [70] find the following five stable SF and MI phases of the Hamiltonian (1.105):

1. **MI** — Both A and B components are in MI phase and no SF current exists in the system. $\langle\psi_A\rangle = \langle\psi_B\rangle = \langle\psi_A\psi_B\rangle = 0$.

2. $\mathbf{MI}_A + \mathbf{SF}_B$ — MI of component A and SF of component B, or, similarly, the same state with components A and B interchanged. $\langle\psi_A\rangle = 0$, $\langle\psi_B\rangle \neq 0$ or $\langle\psi_B\rangle = 0$, $\langle\psi_A\rangle \neq 0$.

3. **2SF** — Two-component SF (SF of component A and SF of component B: $\langle\psi_A\rangle \neq 0$, $\langle\psi_B\rangle \neq 0$.

4. **PSF** — paired SF vacuum: a SF state of diatomic $A-B$ molecules. It requires $U_{AB} < 0$. $\langle\psi_A\rangle = \langle\psi_B\rangle = 0$, $\langle\psi_A\psi_B\rangle \neq 0$.

5. **SCF** — Super-counter-fluid: a state with the zero net SF current and equal and opposite SF currents of A and B components. Particles of sort A are paired up with holes of B-particles. It requires $U_{AB} > 0$. $\langle\psi_A\rangle = \langle\psi_B\rangle = 0$, $\left\langle\psi_A\psi^\dagger_B\right\rangle \neq 0$.

The SCF phase can be also derived from simplified two-site model [67] of the Hamiltonian (1.105). The main argument is that at commensurate total fillings on

each site and in the limit when interaction term is dominant the single-particle jumps change total onsite population. The required energy of this process is much greater than the energy necessary for *exchange* of two different particles, because in this case total onsite population unchanged.

These five listed above phases can be derived by considering proper limiting cases of parameters t_σ and $U_{\sigma\sigma'}$ in the Hamiltonian (1.105). Additionally authors of reference [70] perform Monte-Carlo (MC) simulations to find detailed phase diagram. According to MC simulations 2SF-MI transition may be of first order, which also can be shown with microscopic arguments given in [70].

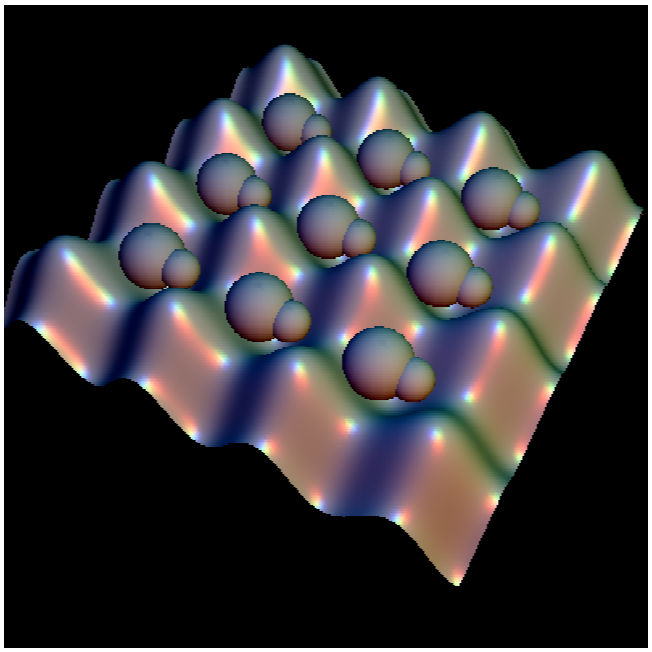

Figure 1.15: MI phase in a two-component mixture. Atoms of different kinds are schematically represented by the size of the spheres.

Authors of the reference [27] suggested how to form heteronuclear molecular SF using SF-MI transition. First they propose to load an OL with unpaired SFs of two different atomic species (for example ^{41}K and ^{87}Rb), thus having 2SF state. Then

after transition from 2SF to MI sate it is possible to have exactly one atom of each kind per lattice site as schematically shown on the figure FIG.1.15. Then with the help of photoassociation process (or other methods, see reference [27]) two atoms on each site are united in heteronuclear dimmers. After the dimmers K-Rb are created the system is essentially single-component. By modifying the OL parameters it is possible to "melt" MI phase into the SF phase of heteronuclear dimmers. Interestingly the MI molecular state (see FIG.1.15) can be used for quantum computation as suggested in the references [17, 18, 30].

Multi-component quantum mixtures (which also include boson-fermion and fermion-fermion mixtures) on OL are currently a very active filed of ultracold physics opening great possibilities for fundamental research and practical applications. The second problem of this thesis considers a so called *drag effect* between different components. It is frictionless entrainment of one component by the other and is a consequence of macroscopic quantum coherence and interaction in the system.

Chapter 2

Atomic Josephson vortex

The system we consider consists of two parallel atomic waveguides containing BEC. Proximity of the waveguides to each other allows tunneling of atoms between them, which is schematically depicted on FIG.2.1. Due to the tunneling and extended spatial dimension along the waveguides this system forms long Bose-Josephson junction (BJJ). The aim of this chapter is to show that long BJJ can sustain stable persistent circulating supercurrent, which by analogy with the superconducting case we call Bose (or atomic) JV. Experimentally such system can be realized in several ways discussed in section 1.5.3, but a particular realization of the experimental setup will not be discussed here. In the consequent sections we develop a general mean field approach to derive and solve equations of motions describing dynamics of the JV.

2.1 Model

We consider a simplified model of infinitely long straight waveguides. At infinity the waveguides are connected to separate large reservoirs, which allows to set chemical potentials $\mu_{1,2}$ independently for each waveguide. Uniform ground state atom density

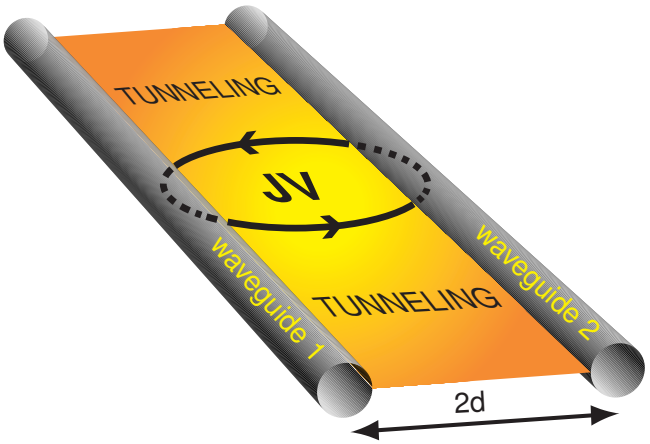

Figure 2.1: Schematic representation of the long BJJ.

then may be expressed through the chemical potentials. More realistic setups and influence of the boundary conditions are discussed in the later section 2.7. The system geometry is defined by the shape of the trapping potential schematically shown on Fig.2.2. It is essentially a 1D double well potential with tunable tunneling between the wells. The "tuning" of the tunneling rate may be accomplished by adjusting width (separation between the waveguides) or height of the inter-well potential barrier. The tunneling strength is spatially uniform along the whole span of the waveguides and characterized by the coupling constant γ. We assume that BEC in each waveguide is effectively 1D, which implies that BEC atoms do not have enough energy to leave the ground state of the tight transverse harmonic potential. In this case mean-field approach describes the long BJJ in terms of linearly coupled (via cross term $\sim \gamma$) quasi-1D GP equations. The whole dynamics occurs in a single spatial dimension, which we choose to be along x axis. Due to the absence of trapping confinement along the waveguides, the system of coupled GP equations is mathematically identical to the system of coupled defocusing NLS equations well known in the context of fiber optics with abundant research on solitonic sates in such systems. Nevertheless, despite

obvious formal similarities, the physics of solitons is very different in atomic and optical systems, especially if more realistic effects are considered (e.g. dissipation in BEC and effects of external forces).

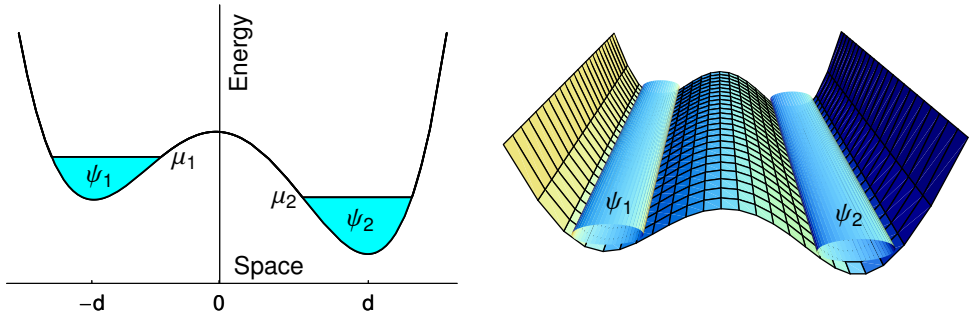

Figure 2.2: Schematic representation of a double-well potential forming long BJJ.

If the chemical potentials are equal $\mu_{1,2} = \mu$, then the Hamiltonian, as we will see, is symmetric with respect to interchange of the BECs in the different waveguides. Some solutions to the coupled GP equations, including, for instance, uniform ground state and GS solutions satisfy this symmetry. On the other hand, if the JV is formed in the BJJ this symmetry is spontaneously broken.

We will first consider BJJ formally by finding exact analytical and variational solutions to the coupled GP equations. In the later sections we develop a general phenomenological approach, which describes BJJ in terms of effective variables and allows analyzing rich phenomena of BJJ without knowledge of analytical solutions to the mean-field equations. It is important to emphasize that the quasi-1D regime under consideration is well described within the mean-field approach. Any typical disturbance of BEC wave function occurs on distances of the order of healing length l_c. If on this length there are many atoms $l_c n_0 > 1$ (where n_0 is 1D atomic density), then quantum effects can be ignored and the mean-field approach is valid.

2.1.1 Lagrangian of coupled waveguides

BEC in each waveguide is described by corresponding condensate wavefunction ψ_k, $k = 1, 2$. Dynamical equations can be derived from the action

$$S = \int \mathcal{L} dt dx \ , \tag{2.1}$$

where t is time and x is the axial coordinate along the waveguides. The Lagrangian density

$$\mathcal{L} = \mathcal{L}_1 + \mathcal{L}_2 + \mathcal{L}_{12} \tag{2.2}$$

consists of the parts describing the dynamics along x

$$\mathcal{L}_k = Re[i\hbar\psi_k^* \dot{\psi}_k] - \frac{\hbar^2}{2m}|\nabla\psi_k|^2 + \mu_k|\psi_k|^2 - \frac{g}{2}|\psi_k|^4, \tag{2.3}$$

and the Josephson tunneling

$$\mathcal{L}_{12} = \gamma\psi_1^*\psi_2 + c.c. \ , \tag{2.4}$$

where μ_k are waveguide's chemical potentials, m is atomic mass, $g = 4\pi\hbar^2 a/(m r_\perp^2)$— the effective 1D interaction constant [162] with $a > 0$ being 3D scattering length and $r_\perp$ standing for the effective width of the waveguides. We also will find useful expressions for Hamiltonian density

$$\mathcal{H} = \mathcal{H}_1 + \mathcal{H}_2 + \mathcal{H}_{12} \ , \tag{2.5}$$

$$\mathcal{H}_k = \frac{\hbar^2}{2m}|\nabla\psi_k|^2 - \mu_k|\psi_k|^2 + \frac{g}{2}|\psi_k|^4 \ , \tag{2.6}$$

$$\mathcal{H}_{12} = -\gamma\psi_1^*\psi_2 - c.c. \ . \tag{2.7}$$

2.1.2 Dissipative function

Significant damping of Josephson dynamics can occur due to tunneling of the normal component [115] between two BEC. Phenomenologically, the dissipation can be introduced through the dissipative function F_D, so that

$$\frac{d}{dt}\frac{\delta\mathcal{L}}{\delta\dot{\psi}_k^*} - \frac{\delta\mathcal{L}}{\delta\psi_k^*} = -\frac{\delta F_D}{\delta\dot{\psi}_k^*} \tag{2.8}$$

in accordance with the standard procedure [163]. In general, F_D must be positively defined function of the time derivative of physically observable quantities [163]. We choose it in the minimal form

$$F_D = \int dx \frac{\dot{\rho}^2}{2\sigma}, \tag{2.9}$$

where $\rho = |\psi_1|^2 - |\psi_2|^2$. All the information about normal component is included into the kinetic coefficient σ, which can be related to the dissipation rate of small Josephson oscillations ref.[115]. Employing eqs.(2.1-2.9) for small uniform relative phase $\phi(t)$ and density $\rho(t)$

$$\psi_{1,2}(t) = \sqrt{n \pm \frac{\rho(t)}{2}}\exp(\pm i\frac{\phi(t)}{2}) \tag{2.10}$$

we obtain damped Josephson oscillations

$$\ddot{\rho} + \omega_J^2\rho + \kappa\dot{\rho} = 0 \ , \tag{2.11}$$

where

$$\omega_J = 2\sqrt{\gamma(\mu+2\gamma)}/\hbar \ , \quad \kappa = 8\gamma(\mu+\gamma)/(\hbar^2 g\sigma), \tag{2.12}$$

are the Josephson frequency and the damping coefficient respectively. The value of κ, which determines a typical relaxation time $\tau \sim \sigma$, can be taken from the microscopic analysis [115].

2.1.3 Coupled Gross-Pitaevskii equations

We introduce the units of correlation length and time:

$$l_c = \hbar/\sqrt{m\mu} \ , \quad t_0 = \hbar/\mu \tag{2.13}$$

with $n_0 = \mu/g$ being the average 1D density in a single uncoupled ($\gamma = 0$) waveguide. Then, setting $\psi_k \to \sqrt{n_0}\psi_k$, the action S (2.1) becomes

$$S = \hbar S_0 \int dtdxL \ , \tag{2.14}$$

where $S_0 = l_c n_0$ justifies validity of the GP regime for $S_0 \gg 1$ [153]. Lagrangian (2.2) transforms as

$$L = L_1 + L_2 + L_{12} \ , \tag{2.15}$$

$$L_k = i(\psi_k^* \dot{\psi}_k + c.c.)/2 - |\nabla\psi_k|^2/2 + |\psi_k|^2 - |\psi_k|^4/2 \ , \tag{2.16}$$

$$L_{12} = \nu\psi_1^*\psi_2 + c.c. \tag{2.17}$$

where $\nu = \gamma/\mu$ is the only parameter determining dissipationless system dynamics. The dissipative function density takes the form

$$\tilde{F} = \frac{\hbar S_0 \dot{\rho}^2}{2\tilde{\sigma}} \quad , \quad \tilde{\sigma} = \frac{\hbar\sigma t_0^2}{n_0} \tag{2.18}$$

Employing eqs.(2.1-2.9) in these units,we obtain

$$i\dot{\psi}_1 - \frac{1}{\tilde{\sigma}}\dot{\rho}\psi_1 = -\frac{\nabla^2}{2}\psi_1 - \psi_1 + |\psi_1|^2\psi_1 - \nu\psi_2; \tag{2.19}$$

$$i\dot{\psi}_2 + \frac{1}{\tilde{\sigma}}\dot{\rho}\psi_2 = -\frac{\nabla^2}{2}\psi_2 - \psi_2 + |\psi_2|^2\psi_2 - \nu\psi_1. \tag{2.20}$$

The dissipative terms $\sim \dot{\rho}$ resemble the phenomenological dissipation introduced in ref.[164]. These conserve the total number of atoms. We note, however, that they *violate* the Galilean invariance [given by the transformation $\partial_t \to \partial_t - V\nabla_x$, $\psi_k \to \exp[i(Vx + V^2t/2)]\psi_k$, with V being the velocity of a new frame moving along x]. In this regard, it is important to realize a limited nature of the above phenomenological approach — it can only be applied in the case when the tunneling of the normal component *does not* conserve linear momentum (along the waveguides), that is, when scattering on imperfections of the trapping potential is significant.

2.2 Stationary solutions

Exact soliton solutions of the nonlinear partial differential equations expressed in terms of elementary or special functions are known just for a rather small set of special cases, including such well known equations as Sine-Gordon, Korteveg-de Vries, Ginsburg-Landau and nonlinear Schrödinger. There is no universal approach to finding such solutions. Luckily it is possible to obtain exact stationary solutions of system (2.19, 2.20) in terms of periodic elliptic functions (note that in the stationary case dissipative terms do not contribute because they are proportional to the time derivative of the relative density). These solutions describe either DS or JV or, more precisely, due to their periodicity, - "chains" of equally spaced DSs or JVs in the junction. The case of a single soliton in BJJ then is represented by the hyperbolic limit of elliptic solution. Because essential dynamics of BJJ can be derived from single soliton case, all analytical calculations are done with hyperbolic solutions. Numerical simulations, on the other hand, were performed using periodic elliptic solutions.

The method we use to obtain mentioned above solutions is based on reduction of the system (2.19, 2.20) to a single NLS or GL equation, solutions of which are already known. The reductions is done by assumptions of physically meaningful symmetries between the fields $\psi_{1,2}$. To find stationary solutions we set all time derivatives in equations (2.19, 2.20) to zero:

$$0 = -\tfrac{\nabla^2}{2}\psi_1 - \psi_1 + |\psi_1|^2\psi_1 - \nu\psi_2; \tag{2.21}$$

$$0 = -\tfrac{\nabla^2}{2}\psi_2 - \psi_2 + |\psi_2|^2\psi_2 - \nu\psi_1. \tag{2.22}$$

The most trivial non zero solution is constant

$$\psi_1 = \psi_2 = \sqrt{n} = \sqrt{1+\nu} \tag{2.23}$$

describing uniform density of BEC in each waveguide. Requirement of finite energy imposes boundary condition on any localized nontrivial solution (e.g. hyperbolic soliton solution): at $x = \pm\infty$ the solution must attain constant background value $\sqrt{n}$.

2.2.1 Hyperbolic Dark soliton ($\psi_1 = \psi_2$)

An obvious symmetry that reduces system (2.21, 2.22) to a single GP equation is $\psi_1 = \psi_2 = \psi$:

$$\left(-\frac{1}{2}\nabla^2 + |\psi|^2 - 1 - \nu\right)\psi = 0 \tag{2.24}$$

DS is well known solution of this equations

$$\psi_{DS} = \pm\sqrt{1+\nu}\tanh(\sqrt{1+\nu}x)\ . \tag{2.25}$$

In this case each waveguide contains a DS located at $x = 0$. The DS solution forms depletion of density in the uniform background value $\sqrt{1+\nu}$, which reaches zero at $x = 0$. At this point the DS phase shows an abrupt jump between constant values 0 and π. Behavior of the DS density and phase shown with the red line on FIG.2.3.

2.2.2 Hyperbolic Josephson vortex ($\psi_1 = \psi_2^*$)

The JV solution must describe persistent supercurrents circulating between the waveguides and, hence, we expect nontrivial relative phase formation. The most straightfor-

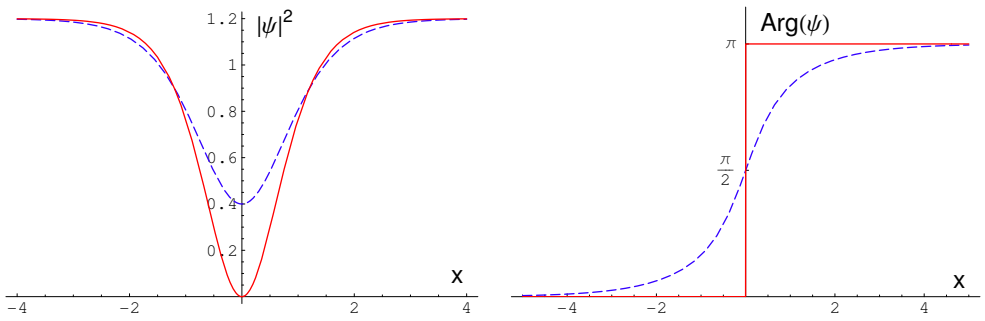

Figure 2.3: DS (red ——) and JV (blue − − −) density and phase in a single waveguide.

ward symmetry with nonzero relative phase is $\psi = \psi_1 = \psi_2^*$, which is combined time reversal and reflection symmetry. It reduces system (2.21, 2.22) to a single complex GL equation:

$$(-\frac{1}{2}\nabla^2 + |\psi|^2 - 1)\psi - \nu\psi^* = 0. \tag{2.26}$$

Here we describe two relevant solutions of the equation (2.26). First one is identical to (2.25), because, obviously, if fields $\psi_{1,2}$ are real we are back to equation (2.24). Otherwise, if $\psi_{1,2}$ are complex, the solution is

$$\psi_{JV} = \pm\left[\sqrt{1+\nu}\tanh\left(2\sqrt{\nu}x\right) \pm i\frac{\sqrt{1-3\nu}}{\cosh\left(2\sqrt{\nu}x\right)}\right] \tag{2.27}$$

Density and phase of this solution shown on FIG.2.3 as blue line. The JV phase changes smoothly from 0 at $x = -\infty$ to π at $x = +\infty$. Due to the symmetry $\psi_1 = \psi_2^*$, in the other waveguide phase changes from 0 at $x = -\infty$ to $-\pi$ at $x = +\infty$. The relative phase then changes from 0 to 2π. This induces closed localized circulation of the supercurrents between the waveguides in the vicinity of the phase change on a typical length $L_{JV} = 1/(2\sqrt{\nu})$. This is schematically shown on FIG.2.4. The circulating supercurrent roughly consists of parts propagating along the waveguides in

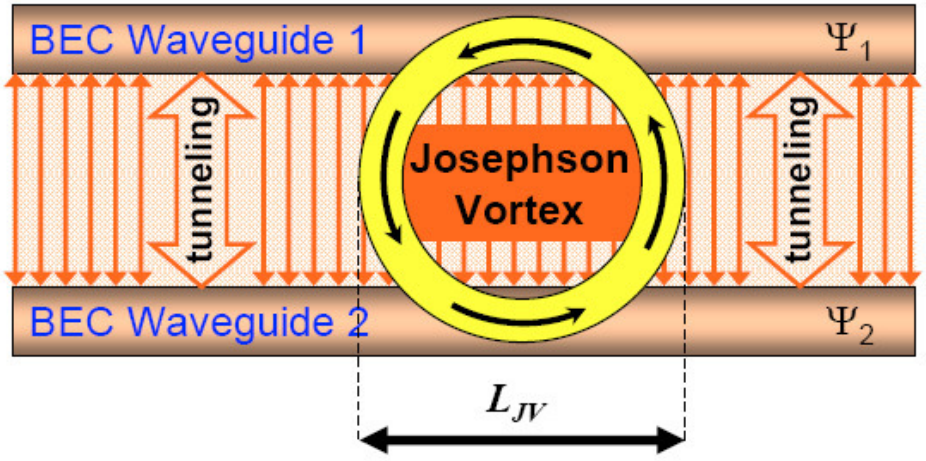

Figure 2.4: Schematic representation of localized supercurrent circulation.

opposite direction and opposite tunneling currents. By analogy with superconducting case we call it Bose JV. There is remarkable difference with superconducting case, though, which is traditionally described by the SG equation. In SG approach all density variations are neglected. In BJJ such description is insufficient. From FIG.2.3 we see that the JV has density depletion in the center, which increases as coupling ν grows. The JV solution, obviously, does not exist for $\nu > \nu_c = 1/3$. The minimum of JV density depletion reaches 0 at $\nu = \nu_c$, relative phase between the waveguides vanishes and JV transforms into the DS (2.25). As we will show this interconversion is *reversible*, i.e. we can get the JV back from the DS by simply decreasing ν below ν_c. Thus the time-reversal symmetry of the solution can be broken spontaneously. The DS↔JV interconversion effect is a *reversible* 1D analog of the 3D DS snake instability [132]. In contrast to the 3D, where the DS irrecoverably decays into vortex rings, the DS in the quasi-1D BJJ can be controllably restored from the JV by tuning ν above the critical value, with condition that the direction of circulation is chosen spontaneously.

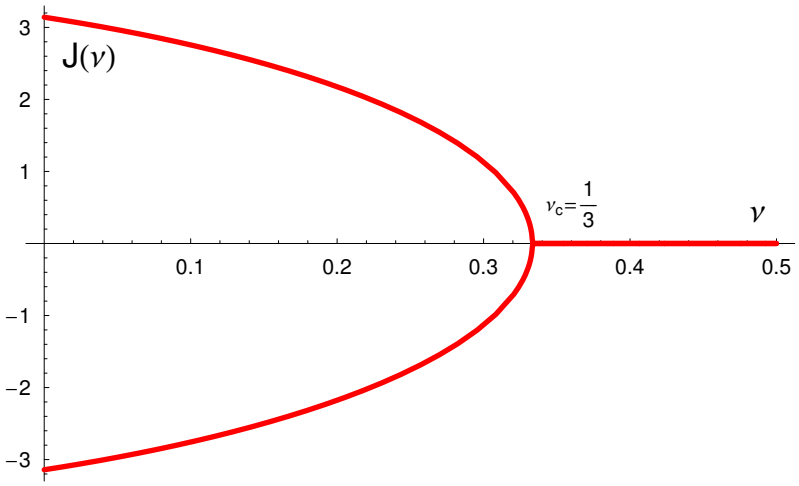

Figure 2.5: Pitchfork bifurcation of global supercurrent circulation $J(\nu)$.

A good measure of global circulation is total current along the waveguides:

$$J = \frac{1}{2}\,\mathrm{Im}\int dx\,(\psi_1^*\nabla\psi_1 - \psi_2^*\nabla\psi_2) \tag{2.28}$$

Substituting JV solution (2.27) in (2.28) we find

$$J = \pm\pi\sqrt{(1+\nu)\,(1-3\nu)} \tag{2.29}$$

Where sign depends on the direction of circulation: clockwise or counterclockwise. Substitution of the *real* DS solution (2.25) yields no circulation $J = 0$. Dependence of circulation J on coupling ν is plotted on FIG.2.5, which is a typical pitchfork bifurcation. Above the critical coupling value ν_c only DS exists with corresponding zero circulation. As soon as coupling is brought below ν_c, DS becomes unstable (see section 2.3) and spontaneously transforms into the JV with one of two possible circulations. Both circulations are equally probable and the choices of a particular circulation depends on initial conditions of interconversion process and, in realistic

systems, on interaction with environment (e.g. dissipation, trapping imperfections, etc.).

The history of equation (2.26) and its solutions (2.27) is quite interesting due to diversity of problems they describe. Bulaevskii and Ginzburg [20] were first who arrived at such equation in the context of temperature induced transformation between domain walls in ferromagnetics and ferroelectrics. Equations in ref.[20] were written in terms of real and imaginary parts of the complex field ψ representing components of magnetization along two orthogonal spatial directions. In ref.[120] a Lagrangian of a scalar complex field (associated with charge-density-wave condensates) generated equations of motion, which, in static case, were satisfied with solutions (2.27). It was noted by the authors of [120] that in the range of critical parameter (ν in our case) where both DS and JV solutions exist, the DS solution have higher energy, which suggests that it becomes instable as soon as ν is lowered below ν_c. Also authors of ref.[120] make an interesting observation, that the JV solution describes a crossover between two different mean-field models: SG and NLS models. Indeed, as we will show later at $\nu \to 0$ the JV solution (2.27) can be well approximated by the SG kink solution. In the opposite limit $\nu \to \nu_c$ the JV solution (2.27) transforms into the NLS kink, - the DS. Later Currie *et al.* [121] and Trullinger and DeLeonardis [123] developed statistical mechanics of the Lagrangian from ref.[120]. In 1979 Lajzerowicz *et al.* [122] considered transition between Ising-Neel and Bloch domain walls in an XY model driven by change of the system temperature and anisotropy. The static Ising-Neel and Bloch walls are formally described by the DS and JV solutions respectively. The authors of ref.[122] note that transition between the walls is accompanied by spontaneous breaking of chiral symmetry at the bifurcation point, meaning that flat (zero-chirality) Ising-Neel wall spontaneously transforms into right or left twisted Bloch wall. The dynamics of transformation was considered later in ref.[124]. Among

other phenomena equation (2.26) describes waves on the surface of a liquid [127], chain of coupled pendulums [128], longitudinal defects in roll systems (e.g. thermal convection rolls) [129], spiral waves in liquid crystals [130]. An excellent review of (2.26) and related equations can be found in ref.[126].

We must emphasize that despite formal similarity in *stationary* case all mentioned above systems are very different form the system of coupled BEC waveguides we consider. First of all equation (2.26) governs *scalar* (single component) complex filed, while coupled GP equations (2.19, 2.19) describe dynamics of *vector* (two-component) complex field. Second, Berry phase term in Lagrangian for the above systems can be very different from that in (2.3). Hence, despite being mathematically identical to the above systems in the *stationary* case, the *dynamics* of coupled GP equations (2.19, 2.19) (in particular, transitions between the SD and JV solutions) is remarkably different.

2.2.3 Josephson vortex with pinning potential

In future applications it maybe useful to pin the JV to a particular position in the junction or to adiabatically transport it from one position to another. These manipulations can be performed with help of an external potential. We give an exact stationary solution of a JV trapped by an axial potential of a special form. In the later sections we show numerically that it is indeed possible to drag the JV with this potential without destruction of supercurrent circulation. In general the pinning potential can have varieties of forms, but for practical reasons it is helpful to have one which allows an exact solution. This facilitates analysis and numerical simulations.

We assume the same shape of the pining potential $V = V(x)$ for both channels so

the condition ($\psi_1 = \psi_2^*$) still holds and we can rewrite equation (2.26) as

$$(-\frac{1}{2}\nabla^2 + |\psi|^2 + V - 1)\psi - \nu\psi^* = 0. \tag{2.30}$$

In order to find an exact solution of (2.30) we choose V self consistently in the following form

$$V = c\left(|\psi_{pin}|^2 - 1 - \nu\right) \tag{2.31}$$

where $|\psi_{pin}|^2$ is the stationary solution of the equation (2.30) and c is a constant. We emphasize that V duplicates the shape of *only stationary* solution density $|\psi_{pin}|^2$. If V is to be displaced in order to carry the JV along the junction, the solution will be perturbed by the motion from exact stationary form ψ_{pin}, but the shape of V will still be (2.31). As $|\Psi_{pin}|^2 = 1 + \nu$ for $x = \pm\infty$ the potential V asymptotically vanishes. So it affects BEC only in the vicinity of the JV. With (2.31) equation (2.30) becomes

$$\left(-\frac{1}{2}\nabla^2 + (1+c)\,|\psi|^2 - 1 - c\,(1+\nu)\right)\psi - \nu\psi^* = 0 \tag{2.32}$$

The JV solution of this equation is

$$\psi_{pin} = \pm\left[\sqrt{1+\nu}\tanh\left(2\sqrt{\nu}x\right) \pm i\frac{\sqrt{1-3\nu+c(1+\nu)}}{\sqrt{1+c}\cosh\left(2\sqrt{\nu}x\right)}\right] \tag{2.33}$$

Now we can substitute solution (2.33) into the potential (2.31):

$$V = -\frac{4c\nu}{1+c}\mathrm{sech}(2\sqrt{\nu}x)^2 \tag{2.34}$$

It is convenient to introduce the following parameter

$$\alpha = \frac{4c\nu}{1+c} \tag{2.35}$$

and we can make the following statement. If the potential V is chosen in the form

$$V = -\alpha \mathrm{sech}(2\sqrt{\nu}x)^2 \tag{2.36}$$

then the exact solution of the equation (2.30) is given by

$$\psi_{pin} = \pm \left[\sqrt{1+\nu} \tanh\left(2\sqrt{\nu}x\right) \pm i \frac{\sqrt{1+\alpha-3\nu}}{\cosh\left(2\sqrt{\nu}x\right)} \right] \tag{2.37}$$

The parameter α is the potential strength. This is just a simple modification of the JV solution (2.27). Note that comparing with (2.27) α shifts the threshold of the JV existence:

$$\nu_c = \frac{1+\alpha}{3} \tag{2.38}$$

2.2.4 Elliptic Josephson vortex solutions

The JV solution (2.27) is hyperbolic limit of two families of periodic elliptic waves. These stationary solutions are given in terms of the Jacobi elliptic functions $\mathrm{sn}(u,k)$, $\mathrm{cn}(u,k)$ and $\mathrm{dn}(u,k)$ with periods $4K$, $4K$ and $2K$ correspondingly, where $K(k)$ is the complete elliptic integral of the first kind and k is the elliptic modulus [133]. First solution $\psi_1 = \psi_2^* = \psi_{\uparrow\uparrow}$ can be thought as a chain of JVs all having the same circulation

$$\psi_{\uparrow\uparrow} = Q_{\uparrow\uparrow}\mathrm{sn}\left(2x\sqrt{\nu/m}\right) \pm iR_{\uparrow\uparrow}\mathrm{cn}\left(2x\sqrt{\nu/m}\right) \tag{2.39}$$

where

$$Q_{\uparrow\uparrow} = \sqrt{1+\nu\left(3-\frac{2}{m}\right)}, \quad R_{\uparrow\uparrow} = \sqrt{1-\nu\left(1+\frac{2}{m}\right)}.$$

and $m = k^2$. The other solution $\psi_1 = \psi_2^* = \psi_{\uparrow\downarrow}$ has the circulation alternating from vortex to vortex

$$\psi_{\uparrow\downarrow} = Q_{\uparrow\downarrow}\mathrm{sn}\big(2x\sqrt{\nu}\big) \pm iR_{\uparrow\downarrow}\mathrm{dn}\big(2x\sqrt{\nu}\big) \tag{2.40}$$

where

$$Q_{\uparrow\downarrow} = \sqrt{m}\sqrt{1+\nu(3-2m)}, \quad R_{\uparrow\downarrow} = \sqrt{1-\nu(1+2m)}.$$

In the solution of co-circulating vortices relative phase in the junction grows by 2π

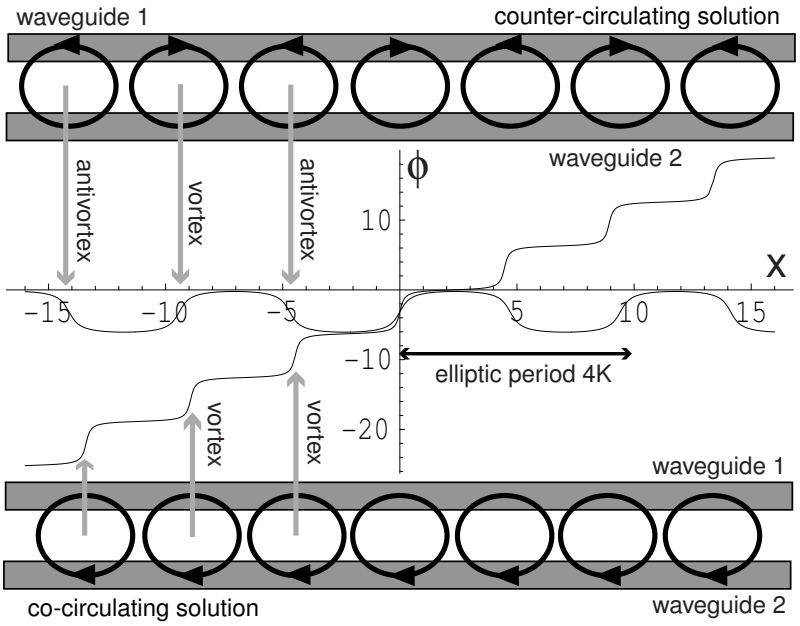

Figure 2.6: Correspondence between waveguides' relative phase and JV chains along the junction. $\nu = 0.3$, $m = 0.9$.

on each vortex and has ladder-like character, while the relative phase of the solution with counter-circulating vortices oscillates between $0 < \phi < 2\pi$ (see FIG.2.6). As $k \to 1$ distances between the neighboring JVs increase. The hyperbolic limit $k = 1$ corresponds to a single vortex in the junction and (2.39), (2.40) both are reduced to (2.27).

In all numerical simulations we used annular geometry with cyclic boundary conditions. Presence of JV or DS in the junction changes phase by $\pm\pi$ in each waveguide. To satisfy cyclic boundary conditions we placed two diametrically opposite solitons in the anular junction using solutions (2.39, 2.40) as initial conditions for JV and well known (see for example [134]) elliptic solution for DS. Choosing elliptic modulus $k \sim 1$ allows us to consider solitons practically independent and very close to the hyperbolic form (2.27).

2.3 Interconversion of Dark soliton and Bose Josephson vortex

2.3.1 Energy considerations

The DS formally exists for all values of the dimensionless coupling ν. The JV solution is valid only for $\nu < \nu_c = 1/3$. At the critical value ν_c, the JV transforms into the DS. Simple energy argument shows that the DS is an unstable state for $\nu < \nu_c$. Indeed, after subtracting energy of uniform background energies of the DS and JV can be found as

$$E = \int_{-\infty}^{\infty} (H(x) + 1 + \nu)dx \tag{2.41}$$

where $H(x)$ is Hamiltonian density (2.5). Substituting the DS and JV solutions (2.25, 2.27) into (2.41) we obtain the following expressions

$$E_{DS} = \frac{8}{3}(1+\nu)^{3/2}, \tag{2.42}$$

$$E_{JV} = \frac{8}{3}\sqrt{\nu}(3-\nu)\ , \tag{2.43}$$

which are plotted on the FIG.2.7. The energies E_{DS} and E_{JV}, as well as their ν-derivatives, become equal at $\nu = \nu_c$. For $\nu < \nu_c$, one finds $E_{DS} > E_{JV}$, which implies *instability* of the DS.

2.3.2 Modeling and simulating interconversion

Despite being identical to the problems of refs.[20, 120, 122, 123, 124, 129] in the static limit, dynamical equations (2.19, 2.20) cannot be mapped on these systems. Dynamics in our case is essentially two-component. Exact time dependent solutions

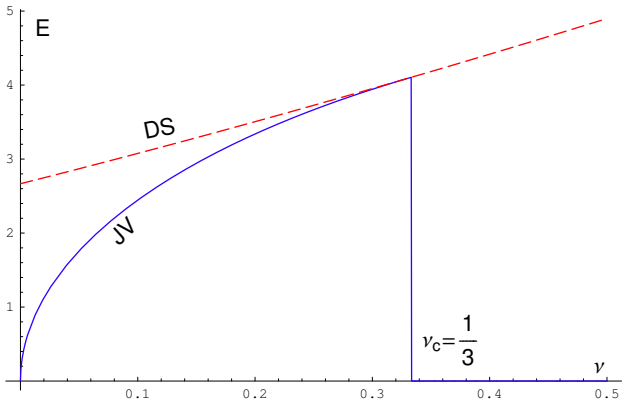

Figure 2.7: Energies of the DS (red $---$) and JV (blue ——).

of coupled GP equations (2.19, 2.20) are not known. Nevertheless dynamics of interconversion can be well described analytically in terms of effective variables. With a suitable ansatz field equations (2.19, 2.20) can be reduced to the effective point-mass equations. Variational analysis performed below is based on assumption that system is close to critical point ν_c of the interconversion. All expansions are made in terms of the small quantity $(\nu_c - \nu)$ and in all terms independent (in lowest order) of $(\nu_c - \nu)$ explicit value $\nu_c = 1/3$ is substituted.

The interconversion can be well described within the family

$$\psi_{1,2} = \sqrt{1+\nu}\tanh(sx) \pm i\frac{B\sqrt{s/2}}{\cosh(sx)}. \tag{2.44}$$

The DS (2.25) corresponds to $s = \sqrt{1+\nu}$ and $B = 0$ and the static JV (2.27) is given by $s = 2\sqrt{\nu}$ and $B\sqrt{s/2} = \sqrt{1-3\nu}$. To describe the dynamics of interconversion we choose $s = s(t)$ and $B = B(t) = a(t) + ib(t)$ to be some real and complex functions of time ($a(t), b(t)$ are real functions of t), respectively. Substituting (2.44) into (2.15)

Lagrangian becomes

$$L = \mathbf{i}\left(B^*\dot{B} - B\dot{B}^*\right) - \frac{4\left(1+\nu\right)^2}{3s} + \frac{4\left(1+\nu\right)s}{3} - \frac{1}{3}\left(B+B^*\right)^2 - \frac{\nu}{3}\left(B-B^*\right)^2 + \frac{8\nu+s^2}{3}\left|B\right|^2 + \frac{\nu}{3}\left|B\right|^4 \quad (2.45)$$

It is important that ansatz (2.44) does not yield the term containing $\dot{s}(t)$. However the dynamics of adjustment of the soliton size controlled by $s(t)$ is considered to be fast, if compared with slow interconversion ($\nu \to \nu_c$). Thus $s(t)$ can be considered as adjusting instantaneously to $B(t)$. Hence in adiabatic approximation the Lagrangian (2.45) can be minimized with respect to $s(t)$ to obtain an approximate solution for $s(t)$. Keeping only lowest order terms in $a(t), b(t)$ we find the following expression for the effective soliton size

$$s = \sqrt{1+\nu} - \frac{1}{4}\left(a^2+b^2\right) \quad (2.46)$$

Substituting (2.44) into the action and the dissipative function and performing the variational analysis based on the adiabatic approximation with respect to the mass flow along the waveguides, we find for $\nu \to \nu_c$

$$\dot{a} - \frac{8}{9}b - \frac{1}{2\sqrt{3}}(a^2+b^2)b - \frac{1}{\tilde{\tau}}\dot{b} = 0, \quad (2.47)$$

$$\dot{b} + \frac{3}{2}(\nu-\nu_c)a + \frac{1}{2\sqrt{3}}(a^2+b^2)a = 0, \quad (2.48)$$

where $\tilde{\tau} = (3\sqrt{3}/8)\tilde{\sigma}$. It is important to note that these equations describe no metastable solution. As $\nu \to \nu_c$ equations (2.47, 2.48) give $a = b = 0$ which correspond to the DS. For $\nu < \nu_c$ it is possible to transform the DS into JV by smoothly modifying the solution varying parameters a and b without passing any energy barrier. This consideration proves that the DS becomes absolutely unstable for $\nu < \nu_c$.

It is quite obvious that the interconversion of the DS ($a = b = 0$) and the JV ($b = 0,\ a = \pm 3^{3/4}\sqrt{\nu_c - \nu}$) proceeds on typical relaxation time τ of the BJJ [115]. Very close to the instability ($\nu \to \nu_c$) the "critical" slowing down $\sim \tilde{\tau}/|\nu - \nu_c|$ takes place. Thus, the DS may vanish in accordance with the mechanism of ref.[150] before it decays into the JV. It is important to realize that the above result is independent of a particular mechanism of dissipation. We have also performed direct numerical

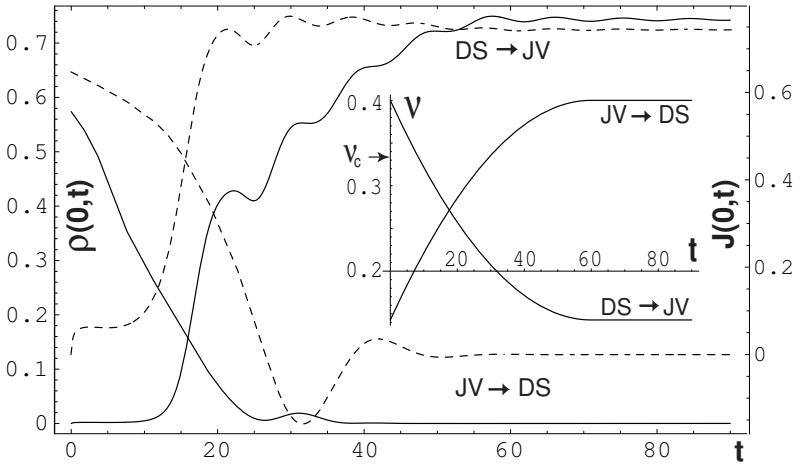

Figure 2.8: Interconversion of the DS and JV is displayed via the evolutions of single waveguide density $\rho(x,t)$ (solid lines) and current $J(x,t)$ (dashed lines) at $x = 0$. Slow change of ν passing through ν_c is shown on the inset. Transformation JV→DS (DS→JV) is manifested in the damped oscillatory transition of $\rho(0,t)$ and $J(0,t)$ from finite (zero) to zero (finite) values. Plots obtained from the numerical simulations of the full system (2.19, 2.20).

simulations of the full GP equations (2.19, 2.20) with the initial conditions taken as either DS or JV (located at $x = 0$) for periodic boundary conditions, with the space period being about 10 times larger than soliton size. To accommodate the phases variation by π, two-soliton solutions were considered. On Fig.2.8, the results of slow evolution of the coupling ν from below critical $\nu = 1/7$ (where JV is stable) toward above critical $\nu = 2/5$ (where the DS is stable) as well as its reverse is presented for the dissipation $\tilde{\sigma} = 0.5$. As perturbation, small uniform imbalance

of the waveguides population has been imposed on the initial conditions. Starting

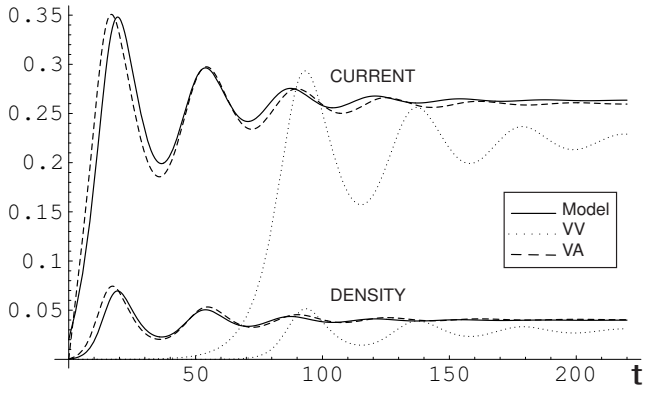

Figure 2.9: DS→JV decay close to the critical point: comparison of full system (2.19, 2.20) and model (2.47, 2.48) numerical simulations. $\nu = 32/100$, $\tilde{\sigma} = 1$.

from JV and increasing ν causes damped phase-slip oscillations during which the JV changes its vorticity (see curves marked $JV \rightarrow DS$), and, finally, current vanishes. Correspondingly, the density, first, acquires zero at finite time moments before the zero becomes permanent. This final stage indicates formation of the DS. If starting from the DS and decreasing ν, the sign of the JV vorticity is determined by sign of the initial density imbalance.

Variational ansatz of (2.47, 2.48) reproduces the full numerical solution with good accuracy. To verify this we set coupling value less, but very close to the critical: $\nu = 32/100 < \nu_c$. We used two slightly perturbed ($\sim 1\%$) DSs as initial condition and studied its decay into JVs. Depending on the form of perturbation, full system has two final static configurations, – vortex-vortex (VV) or vortex-antivortex (VA), – which it assumes after a few cycles of damped oscillations. We plot currents and densities vs. time at $x = 0$ (soliton center) and compare it to the behavior of the model system (2.47, 2.48). To find model current and density we obtained $a(t)$ and $b(t)$ from numerical simulation of (2.47, 2.48) and substituted them into ansatz (2.44).

The fact that VV configuration has time-lag and slightly different final density and current is due to interaction between two solitons in the junction. Elliptic modulus is very close to, but not exactly one: $k = .995 < 1$ and it makes VV and VA configurations somewhat different. As value of $k \to 1$ difference between VV and AV behavior diminishes.

2.3.3 Quasi-1D Fluctuations

The above analysis was performed at zero temperature and neglects quantum effects (deviations from the mean-field approach). In realty both quantum and thermal effects will result in restoration of the broken time reversal symmetry of the JV solution. Quantum tunneling between two JV circulations will produce the non-mean-filed ground state, which is characterized by full time reversal symmetry. Here no quantum mechanical effects are considered.

At a finite temperature T, which is more realistic situation, the time reversal symmetry restoration is possible due to thermally activated jumps between two JV circulations. This is thermal phase slip effect. Thus at finite temperatures T, phase-slip effects can destroy the JV circulation. The corresponding life-time, however, can be very long [173]. In our case, stability of the JV is determined by the finite energy barrier $\Delta E = E_{DS} - E_{JV}$ with respect to thermal (quantum) jumps between the opposite orientations of the current circulation. The probability of the thermal jump is $P \sim \exp(-\Delta E/T)$. If $\nu \to \nu_c$, we find

$$P \sim \exp(-4.5\sqrt{3}(\nu_c - \nu)^2 \frac{E^*}{T}), \tag{2.49}$$

where $E^* = \mu S_0 = \sqrt{\mu T_c}$, with $T_c = \hbar^2 n_0^2/m$ being the temperature of the quasi-

BEC [174] formation. To have long lived JV, temperature must satisfy the condition

$$T \ll 4.5\sqrt{3}(\nu_c - \nu)^2 E^*, \quad \nu \to \nu_c. \tag{2.50}$$

It is important that for $\nu \to \nu_c$ JV energy is finite $\mu S_0 \gg \mu$, which is usually much larger than T. Accordingly, in this limit, while thermal fluctuations can destroy the JV circulation by producing the phase slips, they are not capable of exiting vortex-antivortex pairs. However as $\nu \to 0$ the JV energy vanishes as $\sqrt{\nu} \to 0$ and thus finite T effects can induce pair production. At the same time the enrgy barrier between two ciculations turns out to be $\sim \mu$. Thus once created the JV retains its identity for a long time.

To suppress the thermal pair production effect, T must be less than the energy $2E_{JV}$ of the pair. Thus,

$$T \ll 16\sqrt{\nu}E^*, \quad \nu \to 0. \tag{2.51}$$

It is important to note that, if the conditions (2.50,2.51) are met, the JV size $L_{JV} \approx l_c/\sqrt{\nu}$ is smaller than a typical phase coherence size $L_\phi = \hbar^2 n_0/(mT) = l_c E^*/T$ of the quasi-BEC [174], so that 1D thermal fluctuations do not effect the JV shape.

2.4 Sine-Gordon approximation

The moving DS solution is known analytically (as gray soliton) [21, 22]. Despite being integrable in the case of one waveguide, the two coupled GP equations (2.19, 2.20) appear to be non-integrable. However, in the limit $\nu \to 0$, the JV can be well approximated by the SG equation. Indeed, in this case, the variation of the total

density can be ignored. Thus, the representation

$$\psi_{1,2}(x,t) = \sqrt{1 \pm \frac{\rho(x,t)}{2}} \exp(\pm i \frac{\phi(x,t)}{2}) \tag{2.52}$$

can be employed, with $|\rho| << 1$. Substituting this ansatz into Lagrangian and ignoring the gradient $\nabla\rho$, we obtain after the variation of action (in dimensionless units):

$$\begin{aligned} \dot{\varphi} - \rho - \tilde{\sigma}^{-1}\dot{\rho} &= 0, \\ -\dot{\rho} + \nabla_x^2\varphi - 4\nu \sin\varphi &= 0. \end{aligned} \tag{2.53}$$

If no dissipation is present ($\tilde{\sigma} \to \infty$), we find $\rho = \dot{\varphi}$, and eqs.(2.53) yield the dynamical SG equation

$$-\ddot{\varphi} + \nabla_x^2\varphi - 4\nu \sin\varphi = 0. \tag{2.54}$$

Its analytical solutions are well studied in the context of, e.g., the underdamped superconducting Josephson junctions [12]. In the case $\tilde{\sigma} \to 0$, one finds $\dot{\rho} = \tilde{\sigma}\dot{\varphi}$, and eqs.(2.53) give the overdamped SG equation [12]

$$-\tilde{\sigma}\dot{\varphi} + \nabla_x^2\varphi - 4\nu \sin\varphi = 0. \tag{2.55}$$

We note that, as $\nu \to 0$, the solution (2.44) satisfies the static SG equation.

It is important to note that, in the SG approximation, the JV is *always* stable. There is, simply, no room for the DS due to the imposed constraints. Similar situation has been discussed in ref.[172] for two-component BEC. The SG approximation is the standard approach for JVs in superconductors [12]. In our case, however, such an approximation is not appropriate once the interconversion effect is considered,

which also determines soliton instability at some critical speed. Indeed, before V approaches the sound barrier $V = 1$, the energy of the (underdamped) solution experiences "relativistic" growth $\sim \sqrt{\nu}/\sqrt{1-V^2}$. The size of the solution shrinks as $\sim \sqrt{1-V^2}/\sqrt{\nu}$. Thus, at some point, the size becomes comparable to the healing length l_c, and the phase slip will take place [172]. This effect is obviously not present in the SG approximation.

2.5 Josephson vortex and Berry phase effect

2.5.1 Phenomenology of the Bose JV

Here we will employ generic phenomenological description of the Bose JV which addresses the Berry phase induced force and the critical speed effect regardless of a particular model of the BJJ. The JV is characterized by spatially localized distributions

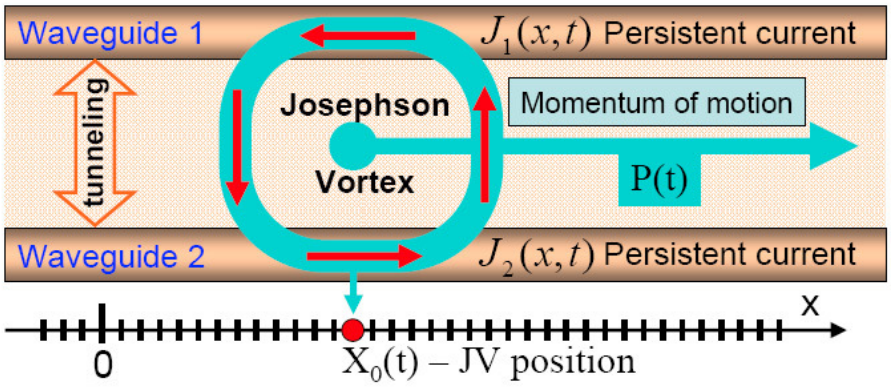

Figure 2.10: Schematic representation of JV dynamics along BJJ

of persistent currents $J_{1,2}(x)$ along the first and the second waveguides, respectively. The sum $J_+ = J_1 + J_2$ represents the total linear momentum density, which must be zero for the stationary JV. The difference $J_- = J_1 - J_2$ characterizes internal circulation of the supercurrent, which forms spontaneously when the Josephson coupling γ becomes less than some critical value γ_c [64]. The minimal effective Lagrangian can be formulated in terms of the total soliton momentum $P(t) = \int dx J_+(x)$, its center of mass velocity $V(t) = \dot{X}_0$, the circulation of the supercurrent $J(t) = \int dx J_-(x)$ (we consider contributions from the tunneling currents negligible) and the corresponding canonically conjugate variable $Q(t)$. It has a form

$$L_{eff} = \dot{X}_0 P + \dot{Q} J - H_{eff}, \tag{2.56}$$

with the effective Hamiltonian being

$$H_{eff} = \frac{P^2}{2M_+} + \frac{Q^2}{2M_-} + \alpha(\gamma - \gamma_c)J^2 + c_1 J^4 - c_2 \eta P J + c_3 J^2 P^2. \tag{2.57}$$

where M_+, M_-, $\alpha > 0$, $c_1 > 0$, c_2, $c_3 > 0$ are phenomenological coefficients dependent on a particular form of a microscopic description. These coefficients will be determined later within the variational approach applied to the model [64]. The Lagrangian (2.56,2.57) describes the spontaneous formation of the circulation $J \neq 0$ for $\gamma < \gamma_c$ [64] ($c_1 > 0$ insures stability beyond linear approximation) as well as coupling between the center of mass motion and the internal circulation. The term $\sim c_3$ describes the effect of the critical velocity: as $P \sim V$ exceeds some critical value, the effective coefficient $\alpha(\gamma - \gamma_c) + c_3 P^2$ becomes positive, which restores the time-reversal symmetry so that the circulation $J = 0$. This term is symmetric with respect to the exchanging of the waveguides. The term $\sim c_2$ describes the effect of the force induced by the chemical potential difference. Its nature can be understood as follows. When $\eta \neq 0$, a number of atoms $\sim \eta$ starts tunneling between the waveguides in the direction of smaller chemical potential. Accordingly, while one waveguide looses its total linear momentum $\sim \eta J$, the second gains it. Hence, the total momentum P attains a nonzero value $\sim \eta J$.

In the presence of dissipation one should introduce the dissipative function in terms of the velocities $\dot{X}_0$ and $\dot{Q}$ as

$$\mathcal{F} = \frac{\dot{X}_0^2}{2\sigma_+} + \frac{\dot{Q}^2}{2\sigma_-}, \tag{2.58}$$

with some kinetic coefficients $\sigma_\pm > 0$. Then the standard variational procedure with

respect to the conjugate variables yields the equations of motion

$$V - \left(\frac{1}{M_+} + 2c_3 J^2\right) P - c_2 \eta J = 0, \tag{2.59}$$

$$\dot{P} + \frac{V}{\sigma_+} = 0, \tag{2.60}$$

$$\dot{Q} - 2\left(\alpha(\gamma - \gamma_c) + c_3 P^2\right) J^2 - 4c_1 J^3 - c_2 \eta P = 0, \tag{2.61}$$

$$\dot{J} + \frac{Q}{M_-} + \frac{\dot{Q}}{\sigma_-} = 0. \tag{2.62}$$

Let's, first, consider the case $\eta = 0$ and small J close to the equilibrium. Then, eq.(2.59) gives $P = M_+ V$. For simplicity, we also consider the case of negligible dissipation with respect to the center of mass motion ($\sigma_+ \to \infty$), so that P is a conserved quantity as seen from eq.(2.60). Close to the equilibrium one can set $Q = 0$ in eqs.(2.61,2.62) and obtain

$$-2\left(\alpha(\gamma - \gamma_c) + c_3 M_+^2 V^2\right) J^2 - 4c_1 J^3 = 0. \tag{2.63}$$

This yields the critical velocity

$$V_c = V_1 \sqrt{\gamma_c - \gamma}\ , \tag{2.64}$$

above which only trivial solution $J = 0$ can exist, where $V_1 = \sqrt{\alpha/(c_3 M_+^2)}$.

When $V \ll V_c$, one can ignore the term $\sim c_2$ in eq.(2.61) and consider $J \neq 0$ as a fixed quantity in eqs.(2.59,2.60) for $\eta(t) \neq 0$. Then, excluding P, one finds that the center of mass velocity obeys the equation

$$\dot{V} + \frac{V}{M_+ \sigma_+} = \frac{f(t)}{M_+}, \quad f(t) = c_2 M_+ J \dot{\eta}, \tag{2.65}$$

where we have ignored the term $\sim c_3$ in eq.(2.59). As discussed above, the term $f(t)$ describes the force induced by time dependence of the difference of the chemical potentials η. The relation of this force to the Berry phase term in the full "microscopic" action will be considered below.

2.5.2 Variational approach

It is worth noting that all the phenomenological coefficients can be derived from a "microscopic" Lagrangian and a dissipative function. Here we will use a simplified approach which ignores dissipation and will consider model [64] as the "microscopic" Lagrangian. In terms of the fields $\psi_{1,2}$ describing each waveguide the Lagrangian,

$$L = L_B - H, \tag{2.66}$$

is given by the Berry term

$$L_B = \mathrm{Re} \int dx \left[i\hbar(\psi_1^* \dot{\psi}_1 + \psi_2^* \dot{\psi}_2) \right], \tag{2.67}$$

and by the Hamiltonian

$$H = \int \mathcal{H} dx \tag{2.68}$$

where Hamiltonian density $\mathcal{H}$ is given by (2.5). For small velocity of the JV, it is natural to use the variational ansatz which coincides with the stationary solution (2.27) at $V = 0$. Thus, we choose

$$\Psi_{1,2} = \sqrt{n_{1,2}}\ \mathrm{th}\left(s\left(x - X_0(t)\right)\right) + \frac{i\sqrt{s}Q_{1,2}}{\mathrm{ch}\left(s\left(x - X_0(t)\right)\right)} \tag{2.69}$$

with the parameter s giving the JV size. This ansatz is a generalization of the one used earlier (2.44) in the section 2.3.2. It includes the effect of the JV center of mass motion coupled to the internal degrees of freedom. The bulk densities $n_{1,2}$ can be obtained in the thermodynamical limit (when no JV is present) from eqs.(2.19, 2.20). Since we are interested in small deviations only, the corresponding explicit expressions are

$$n_{1,2} = (1+\nu)\left(1 \pm \frac{\eta}{1+2\nu} + o(\eta^2)\right), \tag{2.70}$$

where the indexes $1, 2$ correspond to $\pm$, respectively. The stationary solution centered at the origin (2.27) can be obtained from the ansatz (2.69) by setting $X_0 = 0$, $\sqrt{s}Q_1 = -\sqrt{s}Q_2 = \pm\sqrt{1-3\nu}$ and $s = 2\sqrt{\nu}$. Considering complex $Q_{1,2}$ and real X_0 as slow dynamical variables, one can substitute the ansatz (2.69) into the Lagrangian (2.66-2.68) and perform explicit integration over x . This procedure generates the effective Lagrangian L_e in terms of the variables $Q_{1,2}$, X_0, s and their time-derivatives. Obviously, such procedure is in line with separation of fast and slow variables, so that only slow dynamics should be considered to full extent. Close to the interconversion instability ($\nu \approx \nu_c = \gamma_c/\mu$), the slow variables are X_0 and J . Similarly to the section 2.3.2 the variable s is excluded adiabatically. Calculating the depletion δN of the number of particles caused by the presence of the JV, we find

$$\delta N = -\frac{2(n_1+n_2)}{s} + 2(|Q_1|^2 + |Q_2|^2) = C_N, \tag{2.71}$$

where the constant C_N is determined for the stationary JV by setting all the time derivatives to zero and minimizing the effective energy with respect to $Q_{1,2}$ and s. Considering small values η, it is enough to set $n_1 + n_2 = 2(1+\nu)$, which is the equilibrium value. Here we will consider values $Q_{1,2} \to 0$, so that the explicit solution

of eq.(2.71) for s becomes

$$s = \sqrt{1+\nu} + \frac{1-3\nu}{2\sqrt{1+\nu}} - \frac{|Q_1|^2 + |Q_2|^2}{2}. \tag{2.72}$$

As discussed in ref.[64], the value $\nu = \nu_c = 1/3$ is the critical point below which the JV forms spontaneously from the DS. Thus, the smallness of $Q_{1,2}$ automatically implies a proximity to the critical point. Then, for consistency of the effective action expressed in powers of $Q_{1,2}$, the value ν should be set to ν_c except in the quadratic term vanishing at the critical point.

It is worth discussing, first, the structure of the Berry-term part (2.67) of the full action. As mentioned above, the cross term $\sim \eta PJ$ leading to the force on the JV $\sim \dot{\eta}$ in the Lagrangian (2.56) can be viewed as generated by the Berry phase effect. Indeed, the Berry part is

$$L_B = -\int dx(\rho_1\dot{\varphi}_1 + \rho_2\dot{\varphi}_2) \ , \tag{2.73}$$

where ρ_k and φ_k are density and the phase, respectively, in the k-th waveguide. In the static solution (2.27) as well as in the ansatz (2.69) each phase changes by $\pm\pi$, so that,e.g., if at $x = -\infty$ one finds $\varphi_1 = \varphi_2 = 0$, then, at $x = +\infty$ there is $\varphi_1 - \varphi_2 = 2\pi$. If the JV is moving slowly, then $\dot{\varphi}_k \approx \dot{X}_0\nabla\varphi_k$. Thus, a substitution into the Berry part gives

$$L_B \approx \dot{X}_0 \int dx(\rho_1\nabla\varphi_1 + \rho_2\nabla\varphi_2) \approx \pi\dot{X}_0(\rho_1 - \rho_2) \ , \tag{2.74}$$

where spatial variations of the densities are ignored. Flipping the time derivative and realizing that $\rho_1 - \rho_2 \sim \eta$, one finds $L_B \sim -X_0\dot{\eta}$, which is the work done while making a displacement X_0 by the force $\sim \dot{\eta}$.

The relation between the observables P, J can be obtained as a result of substi-

tuting the ansatz (2.69) into (2.67). This yields

$$L_B = \dot{X}_0 P - 2(\dot{B}_+ Q_+ + \dot{B}_- Q_-), \tag{2.75}$$

where

$$Q_+ = \mathrm{Re}(Q_1 + Q_2) \ , \tag{2.76}$$

$$Q_- = \mathrm{Re}(Q_1 - Q_2) \ , \tag{2.77}$$

$$B_+ = \mathrm{Im}(Q_1 + Q_2) \ , \tag{2.78}$$

$$B_- = \mathrm{Im}(Q_1 - Q_2) \ . \tag{2.79}$$

The total momentum

$$P = -i \int dx (\psi_1^* \nabla \psi_1 + \psi_2^* \nabla \psi_2) \tag{2.80}$$

and the supercurrent circulation

$$J = -i \int dx (\psi_1^* \nabla \psi_1 - \psi_2^* \nabla \psi_2) \tag{2.81}$$

are given as

$$P = -\pi (1+\nu)^{3/4} \left[Q_+ + \frac{\eta Q_-}{2(1+2\nu)} \right], \tag{2.82}$$

$$J = -\pi (1+\nu)^{3/4} \left[Q_- + \frac{\eta Q_+}{2(1+2\nu)} \right]. \tag{2.83}$$

Thus, the parameters $Q_\pm$ can uniquely be expressed in terms of P, J. In particular, $Q_+ \sim P$ for $\eta = 0$. The Berry phase effect discussed above is reflected in the part $\sim \eta$ of eq.(2.82). It is also clear that the variable conjugated to J in eq.(2.56) is $Q \sim B_-$. Further analysis shows that the quantity $B_+ = \mathrm{Im}(Q_1 + Q_2)$ enters L_B in

a combination $\sim \dot{B}_+ P - r_b B_+^2 + o(B_+^4)$ with some $r_b > 0$. Thus, B_+ would generate higher time derivatives with respect to X_0, which should be neglected as long as the JV motion is slow. Accordingly, it is reasonable to set $B_+ = 0$ in eq.(2.69), so that $Q_{1,2}$ are chosen in the form

$$Q_{1,2} = \frac{Q_+ \pm Q_-}{2} \pm i\frac{B_-}{2}, \tag{2.84}$$

with the indexes $1, 2$ corresponding to $\pm$, respectively. Finally, employing the ansatz (2.69,2.84) in the "microscopic" Lagrangian (2.66) and expressing the variables (2.84) in terms of the observables P, X_0, Q, J as described above one arrives at the effective Lagrangian in the form (2.56), where the coefficients (in the chosen units) are

$$\frac{1}{M_+} = -\frac{\sqrt{3}}{2\pi^2}, \tag{2.85}$$

$$\frac{1}{M_-} = \frac{32\pi^2}{27\sqrt{3}}, \tag{2.86}$$

$$\alpha\,(\gamma - \gamma_c) = \frac{3\sqrt{3}}{4\pi^2}\left(\nu - \frac{1}{3}\right), \tag{2.87}$$

$$c_1 = \frac{3\sqrt{3}}{128\pi^4}, \tag{2.88}$$

$$c_2 = \frac{2\sqrt{3}}{5\pi^2}, \tag{2.89}$$

$$c_3 = \frac{9\sqrt{3}}{64\pi^4}. \tag{2.90}$$

As discussed above, in these expressions the difference $\sim \nu - \nu_c$ has been ignored except in the quadratic coefficient (2.87), which determines the instability. It is worth noting that far from the instability $\nu \ll \nu_c$ no simple expansion for the effective Lagrangian in terms of powers of $Q_{1,2}$ can be obtained. Accordingly, the expressions would become much more complicated.

2.5.3 Numerical simulation of the Berry phase effect

Sensitivity to the difference of the chemical potentials η can be a useful tool for manipulation of the JV position in the junction. To demonstrate this numerically we used η as an externally controlled variable to displace the JV on a distance much greater than its size and than to return it to its original position. The result of the simulations of the full system (2.19, 2.20) is displayed on FIG.2.11. The plot on the left represents density of a single waveguide by the intensity of white color. The dark curve is a trajectory of the JV center, where its density is minimal. Shown on the right, the time-dependence η is chosen as $\eta(t) = 0.1\sin(\frac{\pi t}{125})$. The simulations have been performed with the dissipative term comparable to other terms in the system with dissipative constant $\tilde{\sigma} = 2$.

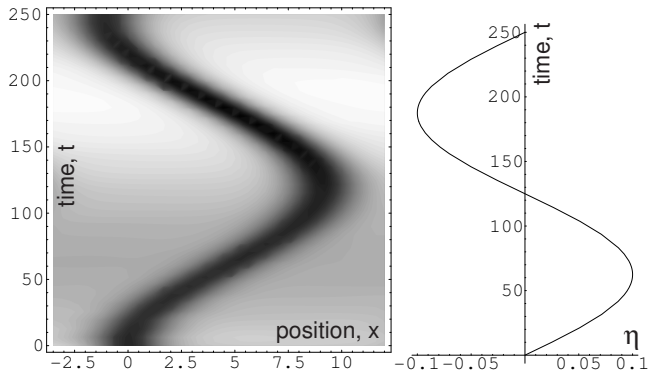

Figure 2.11: Motion of the JV along the junction (left) generated by change of relative chemical potential η (right) from numerical simulations of the system (2.19, 2.20). $\nu = 0.1$, $\tilde{\sigma} = 2$.

2.6 Creation and detection of Bose-Josephson vortex

2.6.1 Creation and detection by interconversion

Besides limitations on temperature (2.50,2.51), there is the requirement that the Josephson relaxation proceeds faster than (about 1 s) the traditional decay mechanism [150]. The optimal condition for fast formation of the JV is that the Josephson relaxation rate $\Gamma \approx \omega_p \gg 1Hz$, where $\omega_p = 2\sqrt{\nu}\mu$ stands for Josephson frequency. We evaluate $\Gamma = \omega_p(T/T_m)^{3/2}$ in the approximation of small barrier ref.[115] applied to the quasi-1d geometry when $T \gg \omega_\perp \gg \mu$. Here $\omega_\perp$ is the radial frequency of the waveguide and $T_m \approx \omega_\perp[\omega_p r_\perp/(\omega_\perp a)]^{2/3}$, with $r_\perp = 1/\sqrt{m\omega_\perp}$. To reconcile the above conditions for $\nu \ll \nu_c$ with eq.(2.51) (that is, $T_m < 16\sqrt{\nu}E^*$), we find the requirement for the 1d density

$$0.04\frac{\mu^{2/5}r_\perp^{3/5}}{\omega_p^{2/5}a^{3/5}} \ll n_0 \cdot r_\perp \ll \frac{r_\perp}{a}, \tag{2.91}$$

where the numerical coefficient comes from the factor 16 (as a factor $16^{-6/5}$) in eq.(2.51), and the last inequality stems from the condition $\mu \ll \omega_\perp$. We choose the following realistic parameters $r_\perp \approx 1\mu$m (implying $\omega_\perp = 3 \cdot 10^3 Hz$ for Na); $a \approx 3 \cdot 10^{-7}$cm; $\mu/\omega_p \approx 100$ [80]. Eq.(2.91) yields the 1D density range $10/r_\perp < n_0 < 300/r_\perp$. This translates into the 3D densities $n_{3D} = n_0/r_\perp^2$ as $10^{13}\text{cm}^{-3} < n_{3D} < 3 \cdot 10^{14}\text{cm}^{-3}$. The temperature for the fastest interconversion, occuring at the rate $\approx \omega_p$ (for,e.g., $\omega_p = 10Hz$), is $T_m \approx 100nK$. These values are the typical BEC parameters.

Observation by the interconversion can be based on, first, creating the DS simultaneously in the both waveguides. Then, moving them slowly apart (to have $\nu < \nu_c$) will result in vanishing of the DS into the JV, so that the zero in the densities will

heal (see Fig.2.8). Bringing the waveguides back together (to have $\nu > \nu_c$) will cause reappearing of the DS (see Fig.2.8). The very fact of this reversible transformation, besides being potentially utilized for creating the JV, can serve as an unambiguous evidence of the static Josephson currents. It is important that this effect, in contrast to the suggestion of ref.[108, 48], can be observed in the *overdamped* regime. Direct imaging of the JV currents could be done by the Bragg spectroscopy technique [175]. Analysis of the absorption imaging of the JV upon expansion (for 3D vortices, see [176]) will be presented in the later sections.

2.6.2 Creation by phase imprinting

The JV can be formed as a result of the decay of the DS, once the Josephson coupling γ is reduced below a critical value γ_c (or, in the chosen units, ν, with the critical value being $\nu_c = 1/3$). An alternative method is the phase imprinting. It is already a well established experimental tool for creation of the DS [21, 5, 31]. It consists of exposing a BEC to a pulse of a far detuned laser beam which acts as a temporary external potential $U(x,t)$. According to the impulse approximation, the duration of the pulse δt must be short compared to the correlation time of the condensate $t_0 = 1/\mu$, so that no change of the BEC density occurs during the pulse — atoms just acquire finite speeds without performing any significant displacements. The phase, on the other hand, accumulates according to $\delta\varphi(x) = \int dt U(x,t)$ and the wave function ψ before the pulse is transformed as $\psi \to e^{-i\delta\varphi}\psi$ after the pulse. To create a DS, one needs to expose a half-plane of an elongated BEC to a laser pulse with a spatial variation reminiscent of the typical DS phase profile (the π-step). In order to produce the JV, one needs to apply a pulse with spatial profiles $U_{1,2}(x,t)$ specific for each waveguide. These should reflect the structure of the JV phases in each waveguide: $\varphi_{1,2} = 0$ at

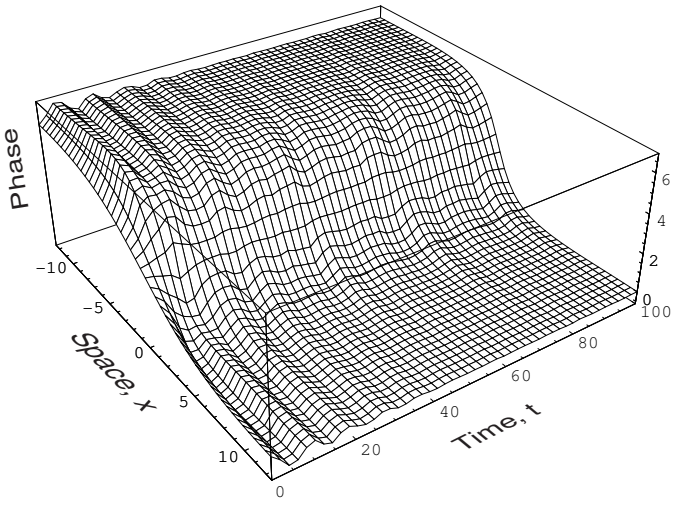

Figure 2.12: Evolution of the relative phase after the imprinting as follows from eqs.(2.19, 2.20). $\tilde{\sigma} = 6$, $\nu = 0.1$.

,e.g., $x = -\infty$ and $\varphi_1 = -\varphi_2 = \pm\pi$ at $x = +\infty$, with smooth transition in between at a typical length comparable to the JV size $= 1/(2\sqrt{\nu})$. Accordingly, $U_{1,2}(x,t) = 0$ at $x = -\infty$ and $U_1(x,t) = -U_2(x,t)$ at $x = +\infty$, with the "crossover" region being approximately equal to the JV size and the time integral $\int dt U_1(x,t) = \pi$ at $x \to +\infty$.

It is important to note that, once the above "topological" requirements are satisfied, the JV forms with minimal disturbances regardless of other details of the laser beams profiles. The most robust characteristic of the evolving solution turns out to be the phase difference between the waveguides. In the case of the DS, the complete density depletion must form at the DS center. Thus, the adjustment is accompanied by a strong perturbation in the form of the density waves [21, 5, 31]. The depletion at the JV center is also strong, if ν is close to the critical value 1/3. Accordingly, the densities in each waveguide will experience significant perturbations. Yet, the phase difference relaxes quite smoothly to the equilibrium profile. To demonstrate this feature, we ran the numerical simulations with the initially imprinted profile

of the phases given by the tanh-type variations of the light intensities as described above. The result of the following evolution of the phase difference is represented on FIG.2.12. As can be seen, the equilibrium phase profile establishes after few relatively small oscillations even though the initial extension of the (imprinted) phase was about two times longer than the equilibrium JV size.

2.6.3 Detection by interference

Experimental visualization is typically done by absorption imaging [157, 7, 176], with its intensity proportional to the density n of the expanding cloud. In contrast to bulk vortices, which can be detected by observing their cores, the JV does not have a core. Yet, the phases exhibit the π-jumps. Thus, the interference of the expanding clouds released from the waveguides should demonstrate a corresponding feature.

In quasi-1D regime a good approximation for the waveguides wave functions in transverse directions is a product of Gaussians $G(y,z) = \exp\left(-(y^2+z^2)/2d^2\right)$. Thus, in 3D, the two waveguides separated by a distance $2z_0$ can be described by the following ansatz:

$$\Psi_0(\vec{R}) = \Psi_0^+ + \Psi_0^- \tag{2.92}$$

$$\Psi_0^\pm = f(x)\psi_{1,2}(x)G(y, z \pm z_0) \tag{2.93}$$

where $\psi_{1,2}(x)$ are the solutions (2.25, 2.27) corresponding to either the DS ($Q_{1,2} = 0$) or the JV and the sign $\pm$ is different for different waveguides. The envelope $f(x) = (1 - (4x^2/L))$, with L, the axial system size, being much larger than the JV, reflects finiteness of the BEC clouds.

As long as the transverse dimension d is much smaller than any axial feature, the expansion occurs primarily in the transverse direction. Thus, the density decreases,

practically instantaneously, so that the expansion is essentially free of interaction. This can be formulated as the requirement $(d/l_c)^2 \ll 1$. Indeed, the mean-field interaction is given by the chemical potential $\mu \sim n(t)$, where $n(t) \sim 1/R^2(t)$ stands for a typical density of the expanding cloud scaled by its radius $R(t) \approx \sqrt{d^2 + (t/d)^2}$ (in chosen units). The interaction-induced additional phase shift can be estimated as $\Delta\phi \approx \int_0^\infty \mu dt \sim \int_0^\infty n dt \approx (d/l_c)^2 \ll 1$, where the initial density is taken as $n = 1$ in the chosen units. Hence, under this condition, the density after time t of free expansion becomes

$$n(\vec{R}, t) = \frac{1}{t^3} \left| \int d^3R' \exp\left(\frac{i(\vec{R} - \vec{R}')^2}{2t} \right) \Psi_0(\vec{R}') \right|^2 . \tag{2.94}$$

A numerical factor in (2.94) is set to 1, because it defines only overall intensity (not the structure) of the absorption image.

When two expanding uniform BECs overlap they form an interference pattern (IP) of parallel fringes [157, 7]. The specific signature of a rotational vortex in the IP is a so-called edge dislocation. It was predicted in ref.[149] and then seen experimentally in ref.[176]. Here we will discuss how the JV can be recognized in the IP.

For any feature with a size $\sim L_s$ comparable with the healing length to become optically resolvable it must be enlarged (typically about 10 times) during the expansion. We consider the situation when axial expansion of the cloud of length L can be ignored. This imposes the limitation $\sqrt{t} \ll L$ in the chosen units. We also ignore quasi-1D thermal fluctuations. In other words, the phase-correlation length L_φ [153] is taken larger than the system size L. In reality this is too strong of a requirement — the discussed feature can be seen when $L_\varphi \geq L_s$.

Employing the ansatz (2.92,2.93), the density after time t (such that $R(t) \gg d$,

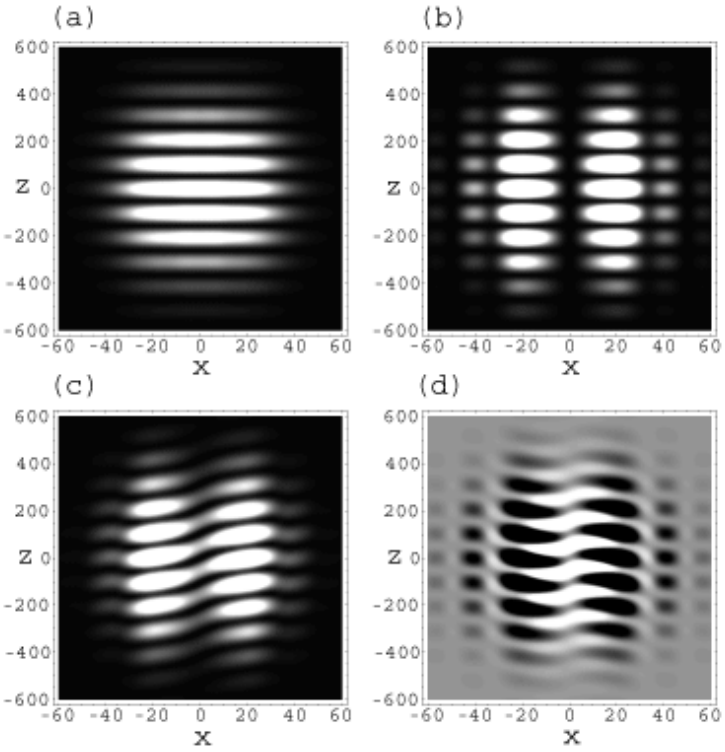

Figure 2.13: Interference patterns of two expanded overlapping BEC clouds released from the waveguides as given by direct numerical integration of (2.94). Waveguides initially contained: (a) uniform BECs, (b) two DS aligned at $x = 0$, (c) JV solution located at $x = 0$. The image (d) is the relative intensity between (b) and (c); $\nu = 0.01$, $t = 100$, $d = 2^{-3/2}$, $z_0 = 3$.

that is, $t \gg d^2$) becomes

$$\begin{aligned} n(x,y,z) &= \frac{\mathrm{e}^{-\frac{(y^2+z^2)d^2}{t^2}}}{t^3} \Big| \int dx_1 \mathrm{e}^{-ix_1^2/2t} f(x_1) \\ &\Big(\sin(\frac{zz_0}{t}) \cos(\frac{xx_1}{t}) \psi''(x_1) + \\ &i \cos(\frac{zz_0}{t}) \sin(\frac{xx_1}{t}) \psi'(x_1) \Big)\Big|^2 \end{aligned} \tag{2.95}$$

where the overall factor is dropped, and $\psi'(x) = \sqrt{1+\nu}\tanh(sx)$ and $\psi''(x) = Q_0/\cosh(sx)$ are, respectively, the real and imaginary parts of the JV solution given by $s = 2\sqrt{\nu}$, $Q_0 = \sqrt{1-3\nu}$. It is instructive to consider three distinctive cases: i)

two uniform condensates, which can be reproduced from eq.(2.95) by setting $\psi' = 0$ and $\psi'' = 1$; ii) two identical DSs at $x = 0$, which can be obtained by setting $\psi'' = 0$; and iii) the JV. In the case i), taking the limit $L \to \infty$ and performing explicit integration, one finds the well known parallel fringes $n(x, y, z) \sim \cos^2(zz_0/t)$. In the case ii), there is a zero at $x = 0$. Its width can be estimated from eq.(2.95) as $\delta x \approx \sqrt{t}$ in the limit $\sqrt{t} \gg 1/s$, that is, when the DS length $L_s = 1/s$ has expanded significantly: $L_s \ll t/L_s$. The actual density profile can be obtained analytically for $1/s \ll |x| \leq \sqrt{t}$ as

$$n_{DS}(x, y, z) = \frac{4(1+\nu)\mathrm{e}^{-\frac{(y^2+z^2)d^2}{t^2}}}{t^3} x^2 \cos^2(\frac{zz_0}{t}). \tag{2.96}$$

It features the parallel fringes with the central zero as shown in Fig.3b.

The JV IP can easily be understood by analyzing the vicinity $x = 0$. Indeed, for $1/s \ll |x| \leq \sqrt{t}$, the $\tanh(sx)$ function can be replaced by a step function and $Q_0/\cosh(sx)$ effectively becomes $\delta(x) \int dx Q_0/\cosh(sx) = \pi Q_0 \delta(x)/s$. Thus, the density profile due to the JV becomes

$$\begin{aligned} n_{JV}(x, y, z) &= \frac{\mathrm{e}^{-\frac{(y^2+z^2)d^2}{t^2}}}{t^3} (2\sqrt{1+\nu}\cos(\frac{zz_0}{t})\, x \\ &+ \frac{\pi\sqrt{1-3\nu}}{2\sqrt{\nu}} \sin(\frac{zz_0}{t}))^2. \end{aligned} \tag{2.97}$$

The profile of the zeros of the density $n = n(x, z, t)$ defines the feature specific for the JV. In the DS case, zeros belong to the set of mutually orthogonal lines $x = 0$ and $z = \pi(n + 1/2)t/z_0$, with n integer. In the JV case, represented by eq.(2.97), the

lines of zeros do not cross any more and obey the condition

$$x = \frac{\pi}{4}\sqrt{\frac{1-3\nu}{\nu(1+\nu)}}\tan\left(\frac{sz}{t}\right) \tag{2.98}$$

The inclined tangential feature seen on Fig.3c is a consequence of the smooth relative phase change from 0 to 2π in the JV. Direct numerical integration of (2.94) with initial condition (2.92,2.93) confirms this result. On Fig.(2.13) we have plotted the column density (integrated over y) at $t = 100$ ($t = 50ms$ in usual units, which is a typical experimental expansion time after which the absorption image is taken).

It should be noted that the above presented IP corresponds to the case when the separation between the waveguides z_0 is significantly larger than the transverse extension d. Obviously, in this situation the tunneling ν is essentially zero. If one tries to decrease z_0/d, the visibility of the fringes worsens due to the exponential factor in (2.95) so that for $z_0/d \sim 1$ just one central fringe is seen. Thus, in order to achieve a good resolution, the clouds should be quickly separated from each other and, then, immediately released. Under these conditions, the JV solution formed at a closed proximity between the waveguides will have no time to be distorted by the inter-particle interactions after the tunneling is cut off. Obviously, the duration of the waveguides' separation from some distance $z_0 \approx d$ (when the tunneling is finite) to $z_0 \approx 10d$ (when the tunneling is, practically, zero) is limited from below by the inverse frequency $\approx d^2$ of the radial confinement. From above, it is limited by the axial response time $1/\mu \approx l_c^2$. This requirement can safely be satisfied if $(d/l_c)^2 \ll 1$,that is, in the quasi-1D regime.

2.7 Applications

2.7.1 Josephson vortex pump

The vortex can be used to transfer a portion of the BEC atoms between BEC reservoirs (see Fig.2.14). The rate of the atom deposition/depletion in the first reservoir is

$$\dot{N}_1 = J_1 \ , \tag{2.99}$$

where

$$J_1 = \rho_1 \nabla_x \varphi_1 \tag{2.100}$$

is the current along the first waveguide taken at the point where the coupling is zero (the right end of the waveguides). It is given by the density ρ_1 and the phase φ_1 at the boundary. Thus,

$$\Delta N = \int_{-\infty}^{+\infty} dt J_1 \ . \tag{2.101}$$

If the reservoirs are large enough, the JV solution can be considered as undeformed at the boundary. Hence, one can set $J_1 = J_1(x - x_0(t))$, where $x_0(t)$ is the position of the JV, and replace the integration

$$\int dt J_1 = \int (dx/V(x)) J_1 \tag{2.102}$$

with $V(x) = dx_0(t)/dt$. If the JV moves uniformly, this gives

$$\Delta N = \frac{1}{V} \int \rho_1 \nabla \varphi_1 dx. \tag{2.103}$$

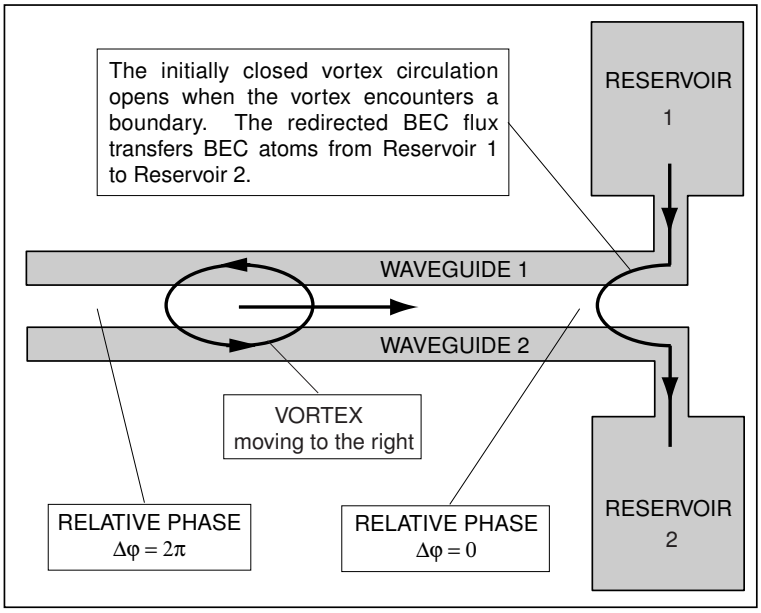

Figure 2.14: Schematic representation of the vortex pump.

For small V, we substitute the static JV solution. Thus, the explicit integration gives (in the physical units)

$$\Delta N = \frac{\pi S_0 V_s}{V}\sqrt{(1+\nu)(1-3\nu)}\ , \tag{2.104}$$

where $V_s = \hbar/(ml_c)$ is the speed of sound. The GP regime $S_0 \gg 1$ [153] implies $\Delta N \gg 1$. In reality, boundary with the reservoirs may modify eq.(2.104).

2.7.2 Mobile qubit

The field of quantum information is rapidly developing, because of the great prospects on calculating power of quantum computers. The elementary unit of a quantum commuter is a so called *qubit*, a quantum alternative to classical bit. The big difference between quantum and classical bits is the number of states they can be prepared in. A classical bit has only two possible states: 0 and 1, while a qubit, besides the 0 and

1 states, can be prepared in an infinite amount of their linear quantum superpositions. To create a qubit one needs a quantum system with an observable quantity, measurement of which yields two outcomes. For instance it can be spin of an electron with possible outcomes spin-up and spin-down or two possible polarizations of a photon. Theoretical research on quantum information and computation already accounts for very large body of works with numerous algorithms worked out and quantum circuits designed which, if practically implemented, could process quantum information and perform very powerful calculations. The only missing part is a reliable physical "hardware" allowing routine manufacturing of quantum computers. Currently there are drawbacks of almost fundamental scale on the way of creating a realistic quantum computer. Though single qubits and even their small circuits were already implemented, current technology is far from realization of a practically "useful" quantum computer able to compete with existing classical ones. One of the big problems is phenomenon of quantum decoherence. The coherence times of modern qubits resulting from interactions with environment are relatively short and quantum information thus can not be reliably stored and processed. This is why recently the search shifts towards mesoscopic quantum systems as possible candidates for quantum computing hardware. For example Josephson charge or flux qubits or quantum dots. Currently there are not that many mesoscopic system suggested for quantum computers. Therefore the challenge is to find a system that can offer, besides the longer coherence times, flexibility and accessibility of preparation and readout protocols, reliability of functioning and simplicity of designs for storage and processing of quantum information. BEC offers a few different experimental setups to achieve this purpose among which vortex states in BEC [76], implementation of the drag effect (see section 3) in a toroidal system [44], two Josephson-coupled BECs [25], and optical lattices [61].

Here we briefly outline how to design a qubit based on a JV. At low temperatures, quantum tunneling between two circulations of the JV will restore the symmetry for $\nu < \nu_c$ due to the quantum phase-slip. This results in a soliton, which, on one hand, is an essentially quantum object with respect to its internal structure — a superposition of opposite vorticities, and, on the other hand, can propagate like a heavy classical particle ($S_0 \gg 1$) along the BJJ-waveguides. The details of the JV qubit design such as preparation, readout, and practical range of relevant parameters are left for the future analysis.

Interestingly enough very recently phase slip qubit was suggested for superconductors. Authors of reference [89] note that quantum tunneling at low temperatures can have a significant rate in superconducting wires. They propose to design a qubit from a loop of a superconducting nanoscale wire biased with magnetic flux of half a flux quantum. It will produce two possible circulations of superconducting current inside the wire, which are degenerate macroscopic quantum states. Quantum phase slip then provides coupling between these two states necessary for a qubit.

An important feature of the JB qubit is its mobility. Most of currently suggested qubits are static, which means that the hardware they are located at must be "mobile", that is must contain changing external fields for preparation and readout of different quantum states. This fact was noted by the authors of reference [100] who propose a computational scheme with mobile electron spin qubits. Their qubit is an electron moving inside a quantum wire with sates defined as spin orientations. The authors argue that a *mobile* qubit can have a great advantage with respect to static ones. In particular the hardware consisting of various quantum gates through which the qubit is moving is stationary, which can reduce decoherence and enhance robustness against errors.

Chapter 3

Drag effect in two-component lattice superfluids

Coherence is one of the most fundamental properties of BEC. Most plainly it was demonstrated in the matter-wave interference experiments when expanding and overlapping BEC clouds produced interference patterns in absorption images. Another basic example probably would be superfluidity demonstrated with creation of rotational vortices and frictionless motion of an obstacle through BEC. An essential feature specific to BEC in ultra-cold dilute gases is interaction between the atoms. In many cases interaction not just modifies the ideal system behavior, but gives rise to entirely new features , such as superfluidity, solitonic states, macroscopic self-trapping of Josephson oscillations, etc.

In previous chapters we considered one component weakly interacting bosons. Various phenomena inherent only to multi-component quantum mixtures can demonstrate surprising counterintuitive behavior. One of these phenomena is so called *drag* effect between different superfluid (SF) components, also known (mostly in astrophysical community) as *entrainment* to emphasize the nondissipative nature of this

drag and to distinguish from "usual" drag between fluids associated with friction and energy dissipation.

The drag effect is described by a specific term in the free energy proportional to the scalar product $\mathbf{v}_1 \cdot \mathbf{v}_2$ of SF velocities of two different components. Another way to look at this term is to realize that it can be obtained from the square of relative supercurrent velocity $(\mathbf{v}_1 - \mathbf{v}_2)^2$. The term also has a prefactor which depends on the interaction and it was shown in ref.[44] that in the case of two-component superfluid (2SF) the prefactor depends on the intercomponent scattering length. The drag term can be obtained from *second order* terms of the free energy expansion in small density and phase fluctuations [44]. We note that the GP equation is obtained in the zero-order approximation, which means that the standard description of Josephson effect in terms of the linearly coupled GP equations does not include the drag. The modifications of the Josephson oscillations between weakly coupled BECs were discussed in ref.[44] with respect to the SQUID-type geometry. Summarizing previous work in this field we may say that the drag effect is an inherent attribute of macroscopically coherent quantum systems and represents redistribution of supercurrent between two superfluid or superconducting components [43] caused by the interaction. The effect was considered for the first time by Andreev and Bashkin in 1975 [6]. The authors introduced a three-velocity hydrodynamic model of mixtures of liquid Helium ^{3}He and ^{4}He. A very similar system, - mixture of two hyperfine spin states of liquid Helium ^{3}He, - was considered in ref.[83]. Another interesting system predicted to show the drag effect is a neutron star where superfluid components are BECs of neutrons and proton Cooper pairs [6, 8]. The drag effect was also considered in superconductors [32], quantum Hall systems [33], quantum wires [103], a bilayer system of charged [110, 111] and neutral [43] bosons, and in two-component Bose gas [44].

In this chapter we discuss the mutual drag in strongly interacting 2SF in optical

lattices. We will show that the drag effect in optical lattices is drastically different from the Galilean invariant Andreev-Bashkin effect. There are two competing drag mechanisms: the vacancy-assisted motion and proximity to a quasimolecular state. In a case of strong drag, the lowest energy topological excitation (vortex or persistent current) can consist of several circulation quanta. In the SQUID-type geometry, the circulation can become fractional. We present both the mean field and Monte Carlo results. It is important to note that in OL regime of strong interaction is readily achievable, and in this case the drag effect becomes crucial.

3.1 Drag and effective mass

Multi-component quantum mixtures in OL are a source of new and rich many-body physics. The one-component bosons in OL have been exhaustively studied theoretically [135] and experimentally [136], especially in the context of the quantum phase transition between SF and Mott insulator. The study of multi-component boson systems in OL has just began. Theoretical investigations predict variety of new quantum phases with unusual properties [137, 138, 139, 140, 141, 142]. Two interesting recent examples include topological excitations – vortices and persistent currents with non-standard winding properties in 2SF [139, 140].

Crucial, but largely unaddressed effect is the impact of strong interaction on properties of superfluid phases where each component ψ_a has its finite expectation value $\langle\psi_a\rangle$. In a one-component superfluid, the strong interaction causes large depletion of the condensate. The same is expected in 2SF. Besides depletion, another interesting manifestation of the strong interaction is the inter-component drag similar to the Andreev-Bashkin effect [6] in helium isotope mixtures. In general, the drag effect between non-convertible species at zero temperature is represented by the cross-terms in

the expansion of the ground state energy in terms of small gradients of the superfluid phases $\nabla\varphi_a$, $a = 1, 2$,

$$\delta E = \int d\mathbf{x} \left[\frac{1}{2} \sum_{a,b} \rho_{ab} \nabla\varphi_a \nabla\varphi_a \right] , \tag{3.1}$$

with ρ_{ab} standing for the superfluid stiffnesses. The cross-term ρ_{12} is responsible for the drag. It is due to interaction effects and is not confined to some particular term in the full microscopic many-body Hamiltonian. Depending on its sign, this term describes either a mutual unidirectional flow or a counterflow of the components. The Galilean invariance argument, often attributed to Landau, imposes two constraints on ρ_{ab}. These constraints are responsible for the Andreev-Bashkin effect in superfluid mixtures of liquid helium isotopes in which ρ_{12} is uniquely related to the ratio of bare m_1 and effective m_1^* masses of minority atoms in the host superfluid of the majority component. The Galilean transformation to a frame moving with velocity $\mathbf{V}$ requires that the phase of each component changes as

$$\varphi_i \to \varphi_i - (m_i/\hbar)\, \mathbf{V} \cdot \mathbf{r} , \tag{3.2}$$

where m_i are the *bare* masses. The energy (3.1) transforms as

$$\delta E \to \delta E - \mathbf{PV} , \tag{3.3}$$

where

$$\frac{\mathbf{P}}{\hbar} = \int d\mathbf{x} \, (N_1 \nabla\varphi_1 + N_2 \nabla\varphi_2) \tag{3.4}$$

is the total momentum expressed in terms of particle densities $N_{1,2}$ of each component.

This yields

$$N_1 = \rho_{11} m_1 + \rho_{12} m_2 \ , \qquad N_2 = \rho_{12} m_1 + \rho_{22} m_2 \ . \tag{3.5}$$

Introducing effective masses m_1^*, m_2^* as

$$\rho_{11} = \frac{N_1}{m_1^*} \, , \quad \rho_{22} = \frac{N_2}{m_2^*} \, , \tag{3.6}$$

we reproduce the result [6],

$$\rho_{12} = \frac{N_1}{m_2} \left(1 - \frac{m_1}{m_1^*} \right) \tag{3.7}$$

as well as the relation

$$N_1 m_1 \left(\frac{m_1}{m_1^*} - 1 \right) = N_2 m_2 \left(\frac{m_2}{m_2^*} - 1 \right) \ . \tag{3.8}$$

In other words, conservation of the total momentum requires that the difference of the bare and effective masses is compensated by the flux of the other component. Note that $\rho_{12} > 0$ since $m_{1,2}^* > m_{1,2}$.

In the case of strong mass renormalization, $(m_1^*/m_1) - 1 \geq 1$, quite spectacular effects should be expected [143] from the topological excitations - vortices. Specifically, the *lowest energy* single-circulation vortex of the majority component ($\rho_{22} \gg \rho_{11}$) should carry several circulation quanta $q = 1, 2, ..$ of minority component. The equilibrium value of q is obtained by minimizing the factor $m_2 q^2 + 2 \left(m_1^* - m_1 \right) q$ in the energy of the vortex complex (or persistent current). These $q + 1$ vortex complexes exhibit transformations with respect to the value of q depending on external conditions that determine the value of m_1^*. If the interaction is weak, ρ_{12} can be calculated as an expansion in the gas parameter [43].

In this chapter we address the drag effect in a *lattice* 2SF in strongly interacting limit, and show that it is radically different from the Galilean-invariant case. The lattice plays a central role in violating the relation [6] between ρ_{12} and m_1/m_1^* (and the constraints (3.5)). We also argue that the value of q is affected by proximity of the 2SF to the quasi-molecular phase.

In OL, in contrast to the Galilean-invariant system, the lattice provides a preferred reference frame, so that the (hydrodynamic) properties of the two-component mixture are determined not by the relative velocity of components but by their individual velocities with respect to the lattice. Furthermore, the effective mass in OL is formed largely by the width and depth of laser-generated potential wells rather than by a trailing cloud of the second component. Another crucial difference is that in OL number of vacancies is a conserved quantity. Below we perform the mean field and Monte Carlo analysis of the mutual drag in 2SF in three different physical situations: a soft-core system close to molecular condensation, a hard core system with finite intercomponent exchanges, and a hard core system with vacancy-assisted motion without the intercomponent exchanges.

3.2 Drag due to proximity to the quasi-molecular state

Here we discuss a generic mechanism leading to the $q+1$-topological complexes in the 2SF. Strong drag effect occurs if a two-component boson system is close to a transition into the quasi-molecular state in which the only broken symmetry has the order parameter

$$\Phi_q \sim \exp(i\varphi^{(q)}) \sim \langle \psi_1 \psi_2^q \rangle \neq 0 \quad OR \quad \langle \psi_1 \psi_2^{\dagger q} \rangle \neq 0 \; . \tag{3.9}$$

In pure molecular state with undefined individual phases $\varphi_{1,2}$ we have $\langle\psi_{1,2}\rangle = 0$. The phase-gradient energy is given by the molecular superfluid phase $\varphi^{(q)}$ as

$$\delta E = \frac{1}{2}\int d\mathbf{x}\ \rho_q(\nabla\varphi^{(q)})^2\ , \tag{3.10}$$

with ρ_q being molecular superfluid stiffness. The molecular order parameter persists in the 2SF phase so that the additional broken $U(1)$ symmetry emerges continuously [140]. The two phases $\varphi_{1,2}$ become well defined in the 2SF state with the molecular phase being locked as

$$\varphi^{(q)} = \varphi_1 + q\varphi_2\ . \tag{3.11}$$

This locking can be understood as a consequence of virtual processes of transformation of a $(q+1)$-molecule into q B-atoms and one A-atom. The corresponding contribution to the energy functional is

$$\Delta E \sim \int d\mathbf{x}\,\Phi_q\psi_1^*\,(\psi_2^*)^q + H.C. \tag{3.12}$$

This term (*cf.* the diatomic molecules with $q = 1$ [144]) ensures the relation (3.11) in the longwave limit. Then the energy (3.1) becomes

$$\delta E = \int d\mathbf{x}\left[\frac{\rho_q}{2}(\nabla(\varphi_1 + q\varphi_2))^2 + \frac{\rho_1'}{2}(\nabla\varphi_1)^2 + \frac{\rho_2'}{2}(\nabla\varphi_2)^2 + \rho_{12}'\nabla\varphi_1\nabla\varphi_2\right] \tag{3.13}$$

with ρ_{ij}' continuously changing from zero in the molecular phase to some finite values in the 2SF phase. It is important that the molecular stiffness ρ_q is not a critical property of the system - it does not change while crossing the phase boundary. Thus, at least close to the phase boundary, minimization of the vortex energy gives $\varphi_1 = -q\varphi_2$, that is, the $q+1$ vortex. In reality, the relations $|\rho_{ab}'| \ll \rho_q$ can hold quite far

from the phase boundary. This implies that the $q+1$ topological excitation exist deep in the 2SF phase. We demonstrate this numerically for $q = 1$ (see FIG.3.1 below).

It is convenient to introduce the drag coefficient k as a ratio $k = \rho_{12}/\rho_{11}$ of the cross-stiffness to the smallest diagonal stiffness, $\rho_{11} \leq \rho_{22}$. Then, as the minimization of the energy (3.1) shows, when $|k| > 0.5$, a vortex of the dominant component can lower its energy if it carries the circulation of the other component $q = \pm 1$. In symmetric case ($\rho_{11} = \rho_{22}$), the integer q closest to k determines the $q + 1$ vortex (or persistent current) as the minimal topological excitation. It is important to note that even small $|k|$ causes attraction between either vortices of equal circulations ($k < 0$) or between vortex and anti-vortex ($k > 0$) in different components, so that if both exist they will form a complex. Crossing the boundary $|k| > 0.5$ has strong impact on mechanisms of vortex creation and stability. For example, stirring the component with the largest stiffness (ρ_{22}) above the threshold will cause creation of the complex instead of a single vortex of the stirred component. Also, a single vortex of the component 2 becomes unstable with respect to inducing creation of vortex of the other component.

The Hubbard lattice model with molecular phases,

$$H = \sum_{\alpha,<ij>} \Big[-t_\alpha a^\dagger_{\alpha,i} a_{\alpha,j} + H.c. \Big] + \sum_{\alpha,\alpha',i} U_{\alpha,\alpha'} n_{\alpha i} n_{\alpha',i} \ , \tag{3.14}$$

has been extensively studied analytically [138, 142] and numerically [140, 141]. Here $U_{\alpha,\alpha'}$ is the interactions matrix, t_α describes the nearest-neighbor jumps of component α; $a^\dagger_{\alpha,i}$, $a_{\alpha,j}$ are the construction bosonic operators, and $n_{\alpha i} = a^\dagger_{\alpha,i} a_{\alpha,i}$ are the on-site occupancies. As discussed in Refs.[140, 141], the quasi-molecular phase ($U_{12} < 0$), namely, the paired superfluid, is in many respects isomorphic to the super-counterfluid state ($U_{12} > 0$) [138] . Both states can undergo second order phase transition into the

2SF phase so that the order parameter $\Phi_{q=1} = \langle \psi_1 \, \psi_2 \rangle$ (or $\Phi_{q=1} = \langle \psi_1 \, \psi_2^\dagger \rangle$) remains finite and robust. Obviously, in the 2SF phase, the $q = 1$ composite vortices are the lowest topological excitations. As pointed out in ref.[145], the Hamiltonian (3.14) also allows molecular phases with arbitrary integer value of q. This issue, though, requires separate analysis.

3.3 Hard core limit $U_{ab} \to \infty$ of the Hamiltonian (3.14)

This limit can exhibit quite interesting physics of strong quantum fluctuations even far from any phase transition [139]. Obviously, when $N_A + N_B = 1$ (N_A, N_B are the average on-site occupancies of the species A, B), the system in the hard core limit (HC) is the Mott insulator. Its ground state is degenerate with respect to possible permutations of bosons A and B. This degeneracy, which is a consequence of the HC approximation, is lifted by any infinitely small inter-component exchanges. Accordingly, the two-component HC model should be considered as a limit of the model in which the inter-component interaction $V_{int} = U_{12}$ is finite and increasing. In contrast to free space, increasing V_{int} leads to decrease of *all* superfluid stiffnesses because all transport is suppressed as $\sim t_1 t_2 / V_{int}$. This is clearly at variance with the free space constraints (3.5) which prohibit uniform decrease of all stiffnesses at fixed densities.

The two-component Hamiltonian with residual soft-core inter-component repulsion is represented in terms of the HC construction operators $a_i^\dagger$, a_i and $b_i^\dagger$, b_i with

Pauli commutation relations for the A and B components

$$H = \sum_{<ij>} \Big[-t_1 a_i^\dagger a_j - t_2 b_j^\dagger b_i + H.c. \Big] + \sum_i V_{int} a_i^\dagger a_i b_i^\dagger b_i \tag{3.15}$$

with summation $< ij >$ over the nearest-neighbor sites. At total filling 1, this Hamiltonian has two phases - 2SF, where both SF order parameters are defined, and super-counterfluid (SCF), where the only SF order is observed in $\langle a_i b_j^\dagger \rangle$. Transition between

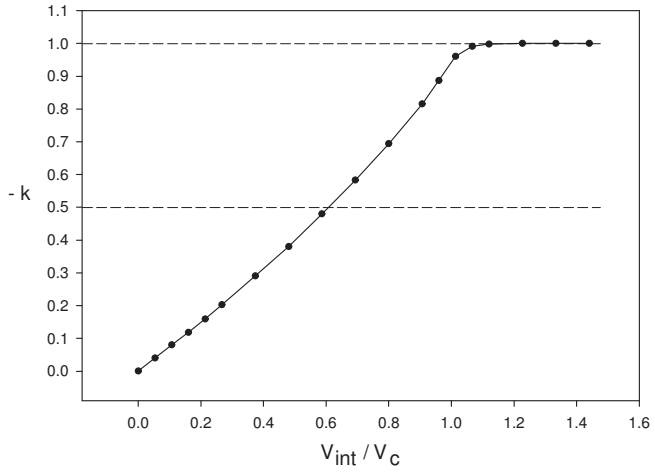

Figure 3.1: The drag coefficient k for the J-current analog of the Hamiltonian (3.15) as a function of the relative interaction, with the value $V_{int}/V_c = 1$ corresponding to the 2SF-SCF phase transition. The horizontal dashed lines indicate a domain where $1 + q$-vortex complex with $q = 1$ has lower energy than any single circulation vortex. Error bars are much smaller then symbol sizes. Solid line is the eye guide.

these two phases is continuous in the universality class U(1) [140] and occurs in the symmetric case $t_1 = t_2 = t$ at some value $V_{int} = V_c$, $V_c/t \sim 1$. As discussed above, the drag effect is strong in the 2SF phase even far from the transition. We proved this by performing the Worm algorithm [146] Monte Carlo simulations of the two-color J-current model [147, 140, 141] at zero temperature on a $2D$ square lattice. This model is a discrete-time grand-canonical analog of the Hamiltonian (3.15) with the hard-core constraints. In other terms it is a "topological" analog of the Hubbard model in a

sense that it qualitatively has the same low energy properties and the same topology of the world lines of particles. The stiffnesses were determined from the statistics of the winding numbers similarly to Refs. [148, 140, 141]. The SCF phase was identified by observing $\rho_{11} = \rho_{22} = -\rho_{12}$. The negative value of ρ_{12} is due to counterflow of the components - each winding of A-worldline is accompanied by opposite winding of B-worldline. In FIG.3.1, the drag coefficient k is plotted as a function of the relative interaction strength. As can be seen, the domain $1/2 < |k| < 1$ in the 2SF (between the dashed lines), where the composite $1+q$-vortex with $q = 1$ has lower energy than any single vortex, is not restricted to the vicinity of the critical point V_c but occupies about half of the phase diagram. Here $\rho_{12} < 0$, indicating that both components participate in the counterflow even in the 2SF state.

3.4 Vacancy assisted drag

If the total filling is different from 1, system is always in 2SF phase at $T = 0$. In this case, another mechanism contributes to the drag – the vacancy assisted transport. Atoms tunnel to the *unoccupied* sites (vacancies) much faster than the rate of the A-B exchange with large V_{int}. The vacancies stimulate mass flow in one direction and move in the opposite one. As a result, both components A and B move in one direction, which means that $\rho_{12} > 0$. This situation implies crossover when ρ_{12} changes sign at some special point with *no drag,* $\rho_{12} = 0$. Since no symmetry change takes place, this is not a phase transition. The crossover from $k < 0$ to $k > 0$ takes place as V_{int} increases at fixed number of vacancies.

Note that the drag coefficient k must increase when the number of vacancies $x_v = 1 - N_A - N_B$ *decreases*. This counterintuitive result stems from the nature of vacancies. In one component case, conservation of the number of vacancies N_V makes

them similar to particles. The HC limit links the flow of vacancies with the opposite flow of atoms. In the two-component case, the situation is similar with one crucial difference – a vacancy is not uniquely associated with a particular sort of atoms. Thus, motion of a *single* vacancy through a lattice in one direction leads to flows of *both* components in the opposite direction. This implies strong drag with positive k. When x_v increases, system becomes more like a low density and, thus, weakly interacting mixture of two sorts of atoms with correspondingly small k.

To analyze the mutual drag and the possibility of complex vortices in the vacancy dominated regime we modified the HC model by imposing the additional constraint $a_i b_i = 0$ on (3.15) and introducing the chemical potentials term $-\mu_1 N_A - \mu_2 N_B$ for each component to keep control of the filling factors. As discussed in Ref.[139], this limit can exhibit long range phase separation as well as short scale fluctuative phase separation corresponding to minority particles acquiring large cloud of vacancies.

If $1 - N_B > N_A$, it is convenient to introduce a description in which the vacuum corresponds to all sites filled by B particles. Then, the number $n = 1 - N_B$ of B holes is shared between N_A atoms and remaining $x_v = n - N_A > 0$ vacancies. In the limit $N_A \ll N_B \sim 1$ transport of vacancies can be considered as transport of B holes with the effective Hamiltonian

$$H = \sum_{<ij>} \left[-t_1 a_i^\dagger a_j v_j^\dagger v_i - t_2 v_j^\dagger v_i + H.c. \right] \ , \tag{3.16}$$

where $v_i^\dagger$, v_i are the Pauli operators for B holes. In order to describe the mutual drag within the mean field approximation, one should replace the field operators a, v by the functions $a = \sqrt{x_1}\exp(i\varphi_1)$, $v = \sqrt{x_v}\exp(-i\varphi_2)$ with the slowly varying phases and perform the gradient expansion. The minus in front of $i\varphi_2$ indicates that flow of holes and actual flow of mass are opposite. This automatically generates the term

$\sim t_1 x_1 x_v (\nabla(\varphi_1 + \varphi_2))^2$ in effective energy from the first term in Hamiltonian (3.16). Obviously, the ratio of the stiffnesses becomes $k = \rho_{12}/\rho_{11} = 1$ which corresponds to *positive* cross-term typical for the vacancy assisted transport meaning that the mean field captures well the physics of the vacancy assisted transport. However, the prediction $k = 1$ and, therefore, $q = 1$, is not supported numerically.

We have performed Worm algorithm [146] Monte Carlo simulations of the two-color J-current model [147, 140, 141] at zero temperature in $2D$ square lattice in the HC limit with partial filling. This model is similar to described above (3.15) with an

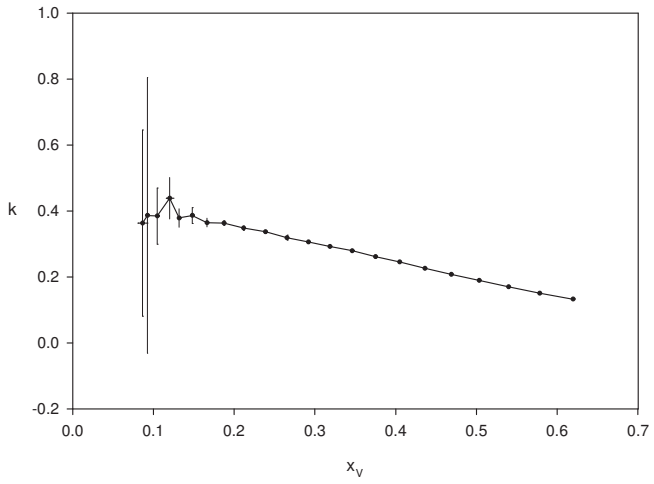

Figure 3.2: The drag coefficient k for the J-model analog of the Hamiltonian (3.15) in the limit $V_{int} \to \infty$ as a function of concentration of vacancies x_v for symmetric case: $N_A = N_B$, $t_a = t_b$. Error bars are shown for all points.Solid line is the eye guide.

additional requirement of no double occupancy. We have found (see FIG.3.2) that for $x_v \gtrsim 0.15$, $k < 0.42 \pm 0.02$, and, thus, no topological complexes can exist as the lowest energy topological excitations in this regime. At this point we do not have a simple explanation for this variance between numerical and mean field results. Most likely, the mean field result is not applicable for large x_v in the symmetric mixture when the vacancies cannot be uniquely identified with the holes in the majority component.

As the number of vacancies is tuned to become $x_v \leq 0.15$, all stiffnesses exhibit large error bars which can be attributed to the regime of strong quantum fluctuations [139] associated with the degeneracy of the ground state in the HC limit. The precise nature of this effect requires separate analysis. For finite V_{int}, depending on N_A, N_B, the ground state can exhibit various types of ordering including the checkerboard insulator [142]. Then, decreasing x_v at $N_A = N_B \to 0.5$ will result in the first order phase transition with strong fluctuations, similar to those in FIG.3.2, due to the domain formation.

3.5 Fractional q and detection

In the case of finite drag with $|k| < 0.5$ *fractional* phase circulation $q = k$ can be observed when persistent current is interrupted by a Josephson junction which lifts the requirement of the integer of 2π windings by creating the phase jump across the junction. Then, phase winding is determined solely by the minimization of energy.

In this chapter it was shown that the drag in lattice is not controlled by particle effective masses and that strong mutual drag can result in composite topological structures. The simplest mean field approximation does not adequately describe the strong drag. The $(q+1)$-vortex complexes can be observed by absorptive imaging technique similar to imaging of vortices in one-component Bose-Einstein condensates [149]. Typical pattern should include extra q fringes in one component.

3.6 Numerical Monte-Carlo simulations

Numerical simulations of the drag effect presented in the previous sections are based on the MC method, which is one of the most powerful computational techniques for

many-body systems. MC method is rather a broad term for a collection of computational algorithms. It is essentially a *stochastic* method, which distinguishes it from *deterministic* methods (such as for example molecular dynamics method). In this thesis MC simulations were based on a specific so called *worm algorithm* (WA) [146]. To be the most suitable for WA MC simulations the Hamiltonian (3.14) must be transformed to the form of the J-current model [147], with which we are going to proceed next.

To be able to control average onsite filling number, we introduce chemical potentials into the Hamiltonian (3.14)

$$H = -\sum_{\alpha,\langle i,j\rangle}\Big[t_\alpha \hat{a}^\dagger_{\alpha i}\hat{a}_{\alpha j} + \text{H.c.}\Big] + \sum_{\alpha,\alpha',i} U_{\alpha\alpha'}\hat{n}_{\alpha i}\hat{n}_{\alpha' i} - \sum_{\alpha,i}\mu_\alpha \hat{n}_{\alpha i} \tag{3.17}$$

Note that though the system is uniform and chemical potential μ_α is independent of the site index, the component index α allows to set average densities of different components independently. An intermediate step in deriving J-current model is reduction of the Hamiltonian (3.17) to the form describing quantum rotors. In order to do this one has to represent creation and annihilation operators in (3.17) as

$$a_{\alpha j} \approx \sqrt{n_{0\alpha} + \hat{\delta}_{\alpha j}}\, e^{\mathbf{i}\hat{\theta}_{\alpha j}} \tag{3.18}$$

where $\hat{\delta}_{\alpha j}$ is the operator of small density fluctuations around average density $n_{0\alpha}$ and $\hat{\theta}_{\alpha j}$ is the phase operator. Substituting this ansatz into (3.18) and expanding up to the second order in small quantities $\sim \hat{\delta}_{\alpha i}$ one can obtain the Hamiltonian describing a system of coupled Josephson junctions

$$H_{JJ} = -\sum_{\alpha,\langle i,j\rangle} t_\alpha \cos\left(\hat{\theta}_{\alpha i} - \hat{\theta}_{\alpha j}\right) + \sum_{\alpha,\alpha',i} U_{\alpha\alpha'}\hat{\delta}_{\alpha i}\hat{\delta}_{\alpha' i} - \sum_{\alpha,i}\mu_\alpha \hat{\delta}_{\alpha i} \tag{3.19}$$

The constants in the Hamiltonian (3.19) were redefined (for details see [147]) and, because eigenvalues of the operator $\hat{\delta}_{\alpha i}$ run from $-\infty$ to ∞, quantitative comparison of (3.19) with (3.17) can be achieved only for very large $n_{0\alpha}$. Nevertheless (3.19) and (3.17) are expected to be in the same universality class for any $n_{0\alpha}$ [147]. The next step is to realize that the H_{JJ} is equivalent to the quantum rotors Hamiltonian. Indeed, because variables $\hat{\delta}_{\alpha i}$ and $\hat{\theta}_{\alpha i}$ are canonically conjugate, defining angular momentum of a quantum rotor as

$$\hat{\delta}_{\alpha j} = -\frac{1}{\mathbf{i}} \frac{\partial}{\partial \hat{\theta}_{\alpha j}} \tag{3.20}$$

we can write

$$H_{QR} = -\sum_{\alpha,\langle i,j\rangle} t_\alpha \cos\left(\hat{\theta}_{\alpha i} - \hat{\theta}_{\alpha j}\right) + \sum_{\alpha,\alpha',i} U_{\alpha\alpha'} \left(\frac{1}{\mathbf{i}} \frac{\partial}{\partial \hat{\theta}_{\alpha i}}\right) \left(\frac{1}{\mathbf{i}} \frac{\partial}{\partial \hat{\theta}_{\alpha' i}}\right) + \sum_{\alpha,i} \mu_\alpha \left(\frac{1}{\mathbf{i}} \frac{\partial}{\partial \hat{\theta}_{\alpha i}}\right) \tag{3.21}$$

Properties of the quantum rotors system are derived from partition function

$$Z = \mathrm{Tr} \exp\left(-\beta H_{QR}\right) \tag{3.22}$$

where $Tk_B = 1/\beta$. According to [147] this partition function can be rewritten as a path integral over M time slices τ_j between $\tau = 0$ and $\tau = \beta$. Representation of temperature as discrete imaginary time axis is an approximation, which becomes exact in the proper thermodynamic limit as temperature goes to zero ($\beta \to \infty$). Discrete imaginary time axis is used as additional dimension and, thus, we obtain a $d + 1$ dimensional lattice, where d is spatial dimension of original BH Hamiltonian (3.17). Straightforward generalization of calculations in the reference [147] leads to

the following two-color J-current Hamiltonian.

$$H_{JC} = \sum_{i,\alpha} \left[\sum_{\alpha',\nu} K_{\alpha\alpha'} \left(J^{\nu}_{i\alpha} J^{\nu}_{i\alpha'} \right) - \mu J^{\tau}_{i\alpha} \right] \tag{3.23}$$

where quantity J^{ν} represents current along direction $\nu = \mathbf{r}, \tau$, which is the index of spatial $\mathbf{r}$ and temporal τ bonds in the lattice. Summation i runs over all sites of the spatiotemporal lattice. Then each lattice site is summed over spatial and temporal directions ν and component index α. Note, nevertheless, that chemical potential terms contain only temporal bonds, because the meaning of τ-component $J^{\tau}_{i\alpha}$ of "relativistic" current $J^{\nu}_{i\alpha}$ is particle density (more precisely deviation of boson number from its mean value). Coefficients $K_{\alpha\alpha'}$ depend on t_{α}, $U_{\alpha\alpha'}$ and effective

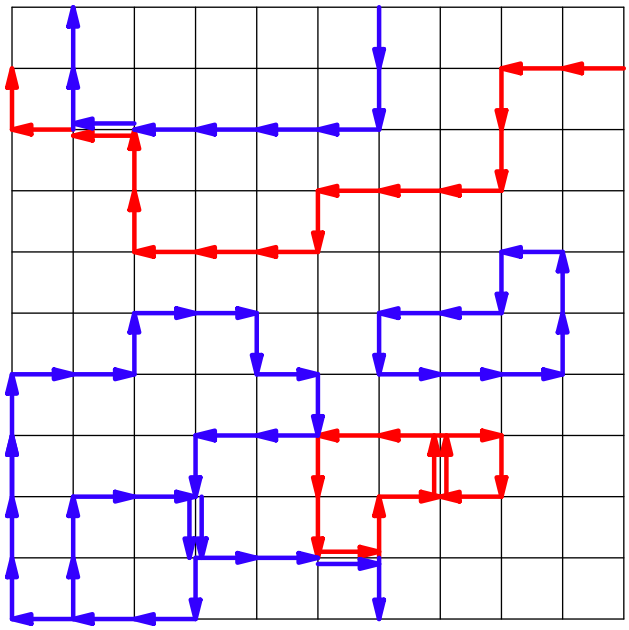

Figure 3.3: A typical configuration of closed-loop currents in the two-component (two-color) J-current model.

temperature $\Delta\tau = \beta/M$. The currents are divergenceless

$$\partial_\nu J^\nu = 0 \tag{3.24}$$

This simply means that on each lattice site for a specific component the sum of incoming currents equals to the sum of outgoing currents. The condition of zero divergence is satisfied, if currents configurations on the spatiotemporal lattice consist of closed loops as shown on the FIG.3.3. Different colors correspond to the atoms of different components. An arbitrary number of current loops can be present on the lattice and they can intersect and overlap. The total current J_α on a particular bond is given by the sum of same-color-arrows.

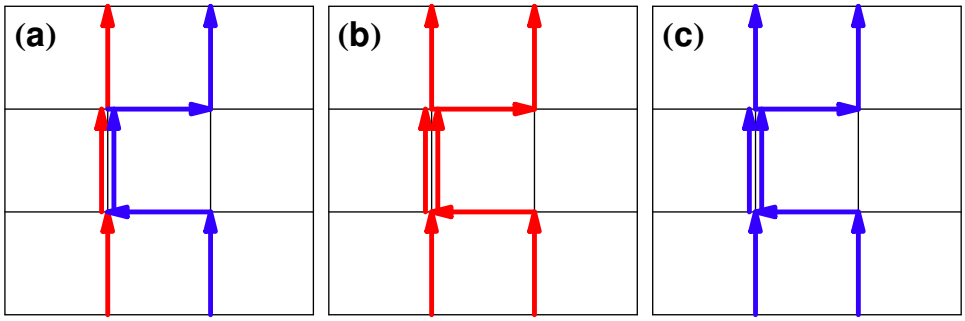

Figure 3.4: In the hard-core limit (a) only currents of different color can share the same bond, while the currents of same color cannot and configurations (b) and (c) are forbidden. In contrast most general J-current model allows the presence of a few currents of the same color on one bond and configurations (b) and (c) are allowed.

In the hard core limit (3.15) of BH model (when only intercomponent soft-core interaction present) the off-diagonal terms $U_{\alpha\alpha'} = 0$ in the 3.17 and, as a consequence of $K_{\alpha\alpha'} = 0$, while $K_{\alpha\alpha} \neq 0$. This leads to a topological restriction on possible current configurations demonstrated on FIG.3.4. In the hard core limit maximum occupancy of a bond is 2 corresponding to one current of each color (soft-core intercomponent

repulsion). Two currents of the same color cannot occupy the same bond (hard-core self-interaction for a particular component).

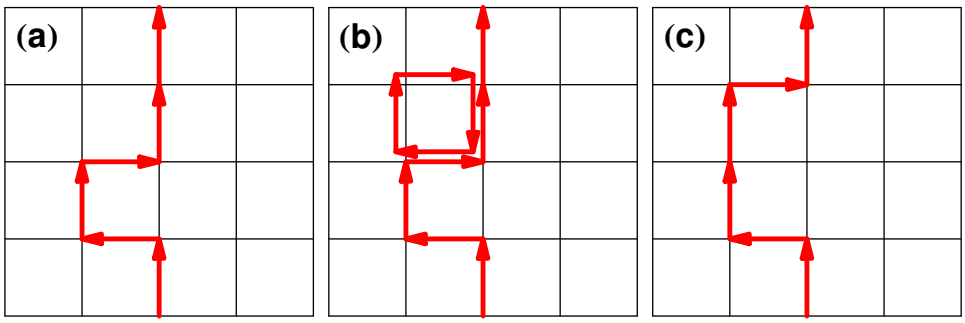

Figure 3.5: To the original loop (a) an elementary loop is added (b) which changes the shape of the original loop (a) to a new shape (c). The currents of the elementary loop are slightly displaced from bonds to improve visual distinction from original loop.

After the problem is reformulated in the J-current form, configuration space is considered consisting of all possible arrangements of closed loops existing in spatiotemporal lattice (possibly subject to certain topological constraints depending on a model). Numerical simulation of such a system with MC method is achieved by stochastic updates of loop configurations in accordance with their statistical weights. The simplest possible update is local: addition of an elementary loop to the system (smallest possible loop going around a plaquette formed by nearest neighboring sites). Loops of many possible shapes and sizes can be created in this way as shown on FIG.3.5, yet global topology of the loops cannot be changed (periodic boundary conditions are imposed on the lattice). For example, a loop that does not wind around the whole system cannot be transformed into a loop that does by addition of elementary loops. To resolve this problem global updates (addition of loops winding around the whole system) can be introduced in addition to local updates. Nevertheless, the acceptance ratio of such loops is exponentially small and this strategy is ineffective for large systems.

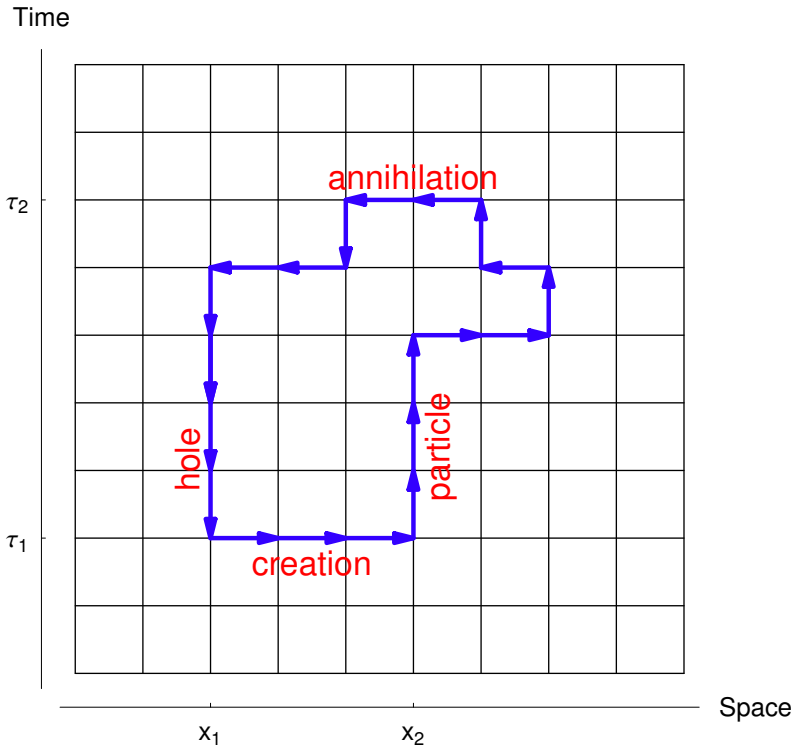

Figure 3.6: A current along a time-bond against the time axis direction is interpreted as motion of a hole in the positive time direction. At the time moment τ_1 a particle jumps from position x_2 leaving behind a hole at position x_1. The particle and hole then propagate through the lattice and annihilate at time τ_2.

Loops that wind around the whole system have great physical significance. For example addition of a loop that winds once around the system in time-direction is equivalent to addition of a particle ot hole (depending on the loop direction). Indeed if a loop does not wind around the system it can be interpreted as the process of creation, propagation and annihilation of a particle-hole pair as shown on the FIG.3.6. Obviously when a loop winds up around the whole system there is only propagation of particle or hole. To be able to introduce global loops into the system effectively we used WA [146] in the MC simulations. The basic idea is to enlarge the configuration space to include one disconnected loop (worm) for each component. Two worms were

used in the numerical simulations of the two-component drag effect. More results of the WA MC simulations of the two-color J-current model can be found reference [71]. Elementary and global closed loop updates are not used at all. Local updates are performed *only* for the end points of the worm. The end points can reconnect at some time creating a closed loop and, thus, updating the closed loops configuration. Obviously such algorithm can transform a loop not winded around the system to the winded one and vice versa. Despite being a local metropolis scheme the WA is very efficient and shows no slow down at critical points.

Chapter 4

Summary of the results and future work

4.1 Results of the Atomic Josephson Vortex study

1. Long quasi-one-dimensional bosonic Josephson junction can sustain stable circulating supercurrent — bosonic Josephson vortex, which is a topological soliton solution degenerate with respect to two possible directions of circulation;

2. Exact analytic solution for stationary Josephson vortex is found;

3. Josephson vortex exists only below certain critical coupling γ_c, where the dark soliton is absolutely unstable.

4. By tuning of the Josephson coupling above or below γ_c the Josephson vortex can be *reversibly* interconverted with dark soliton. Transitions between dark soliton and Josephson vortex are spontaneous and correspond to breaking (vortex) and restoration (dark soliton) of the time reversal symmetry.

5. The Josephson vortex can be controllably displaced along the junction by imposing tunneling current created by misbalance of chemical potentials between the waveguides.

6. In quasi-one-dimension, motion of an atomic Josephson vortex is strongly coupled to the current circulation through the phase-slip effect. This leads to a destruction of the circulation for the vortex speeds above a certain value determined by the Josephson coupling.

7. In contrast to the standard approach to Josephson vortices in superconductors within the Sine-Gordon formalism, a description of the coupling between the center-of-mass motion and the circulation necessarily involves both density and phase variations.

8. The Josephson vortex can be created with the phase imprinting technique directly or indirectly by, first, creating the dark soliton and then by adiabatic decrease of the Josephson coupling transforming the dark soliton to the Josephson vortex.

9. The Josephson vortex can be detected by absorption imaging due a specific feature it produces in the column density of released from the waveguides atomic clouds.

10. Josephson vortex can be used for controlled and coherent transfer of BEC atoms between two separated reservoirs.

11. Josephson vortex is suggested to be used as a mobile qubit.

4.2 Results of the drag effect study

1. There are two main mechanisms of the strong drag effect in optical lattices. They are induced, respectively, by proximity to quasi-molecular states (formed due to strong enough attractive as well as repulsive inter-atomic interaction) and by vacancy assisted transport. These mechanisms in optical lattices are drastically different from the Galilean-invariant Andreev-Bashkin drag effect in liquid helium, where the drag is controlled by particle effective masses. The simplest mean field approximation does not adequately describe the strong drag in optical lattices.

2. In the proximity induced drag, the phases of the separate superfluid components and the phase of the molecular superfluid are locked. This leads to formation of vortices with 1 circulation of one component (say, A) and $q = 1, 2, 3, ...$ circulations of the other (say, B), if the quasi-molecular state is given by the formula A_qB. In the case of the attractive interaction, the drag coefficient is positive.

3. In the case of the supercounterfluid — bound states of atoms of one sort and holes of the other (repuslive interaction)— the components flow predominantly in the opposite directions, resulting in negative drag coefficient.

4. In the vacancy assited drag, since a vacancy does not have an association with particular component, motion of a vacancy induces flow of both components in the same direction, which results in positive drag coefficient similarly to the case of the proximity to the quasi-molecular state A_qB . This effect increases as the vacancy density decreases. However, no bound vortex complexes can form in this regime because the drag coefficient is found to be always below the

threshold for formation of such complexes.

5. Different drag mechanisms compete in the case of repulsive interaction. Hence the result of this competition can be vanishing drag.

6. The microscopic arguments explaining drag effect in different cases were supported by Monte-Carlo numerical simulation based on the Worm Algorithm developed for two-color J-current model. The drag was identified through the nonvanishing off-diagonal (inter-component) terms of the superfluid stiffness obtained from the statistics of winding numbers.

7. Monte-Carlo simulations showed that $q + 1$ topological structures with $q = 1$ can exist in a wide range of the system parameters.

8. In some cases fractional phase circulation q can be observed when persistent current is interrupted by a Josephson junction which lifts the requirement of the integer of 2π windings by creating a phase jump across the junction.

9. The $q + 1$ vortex complexes can be observed by absorptive imaging technique similar to imaging of vortices in one-component Bose-Einstein condensates. A typical pattern should include extra q fringes in one component.

4.3 Directions of future work

Atomic vortex solution obtained in this work neglects quantum effects. Logically one of the problems (currently in progress) is quantization of the Josephson vortex. Quantum tunneling between two possible supercurrent circulations will lift degeneracy of the Josephson vortex with respect to circulation directions. This can find applications in the design of mobile Josephson vortex qubit able store and process

quantum information as well as transport it coherently along the junction. Important subproblems are: the interaction with environment, dissipation and decoherence times, rate of quantum tunneling between circulations of supercurrent, estimates of the qubit efficiency for a realistic experimental setup, design of preparation and read-out procedures.

Another problem (currently in progress) is influence of dimensionality of the system on quantum phase transitions in multi-component mixtures in optical lattices. In particular, quantum phase transition between two-component superfluid phase and single-component molecular superfluid phase (heteronuclear quasi-molecules) is studied in $2+1$ and $3+1$ dimensions in optical lattice. Monte-Carlo simulations show significant deviations from the mean-field predictions for the phase diagram in the coordinates interaction V versus density of atoms n in $2+1$. Specifically, the critical line above which only paired phase exists is described by the dependence $V \sim n^a$ with $a \approx 0.07 \pm 0.02$ in the limit $n \to 0$. No unambiguous explanation of the mechanism responsible for such anomaly exists so far.

4.4 Publications

The main results of this thesis have been published in the following articles

1. V. M. Kaurov and A. B. Kuklov, *Atomic Josephson vortices*, Phys. Rev. A **73**, 013627 (2006);

2. V. M. Kaurov, A. B. Kuklov, and A. E. Meyerovich, *Drag Effect and Topological Complexes in Strongly Interacting Two-Component Lattice Superfluids*, Phys. Rev. Lett. **95**, 090403 (2005);

3. V. M. Kaurov and A. B. Kuklov, *Josephson vortex between two atomic Bose-Einstein condensates*, Phys. Rev. A **71**, 011601 (2005).

and presented at the following meetings

1. Annual American Physical Society March Meeting 2006;

2. Annual American Physical Society March Meeting 2004;

3. Annual American Physical Society March Meeting 2003.

The results are also to be presented at the Cuenca (Spain) conference *Solitons and nonlinear phenomena in degenerate quantum gases* in September, 2006.

Appendix A

List of Abbreviations

1D One-dimensional

2D Two-dimensional

3D Three-dimensional

2SF Two-component superfluid

BEC Bose-Einstein Condensate

BH Bose-Hubbard

BJJ Bose Josephson junction

GP Gross-Pitaevskii

JILA The Joint Institute for Laboratory Astrophysics

MQST Macroscopic quantum self-trapping

MI Mott insulator

MIT Massachusetts Institute of Technology

OL Optical lattice

ODLRO Off-diagonal long-range order

PSF Paired superfluid vacuum

QMC Quantum Monte Carlo

SCF Super-counter-fluid

SF Superfluid

SG Sine-Gordon

SJJ Superconducting Josephson junction

TG Tonks-Girardeau

Bibliography

[1] Albiez M., Gati R., Flling J., Hunsmann S., Cristiani M, and Oberthaler M. K., Phys. Rev. Lett. **95**, 010402 (2005).

[2] J.F. Allen and A.D. Misener, Nature **141**, 75 (1938).

[3] M. A. Alpar, S. A. Langer, and J. A. Sauls, Astrophys. J. **282**, 533 (1984).

[4] Anderson, M. H., J. R. Ensher, M. R. Matthews, C. E. Wieman, and E. A. Cornell, Science **269**, 198 (1995).

[5] B. P. Anderson, P. C. Haljan, C. A. Regal, D. L. Feder, L. A. Collins, C. W. Clark, and E. A. Cornell, Phys. Rev. Lett. **86**, 2926 (2001).

[6] A. F. Andreev, E. P. Bashkin, Sov. Phys.-JETP, **42**, 164 (1976) [Zh. Eksp. Teor. Fiz. **69**, 319 (1975)].

[7] M. R. Andrews, C. G. Townsend, H.-J. Miesner, D. S. Durfee, D. M. Kurn, and W. Ketterle, Science **275**, 637 (1997).

[8] E. Babaev, Phys. Rev. D **70**, 043001 (2004).

[9] Balibar Sebastien, Seminaire Poincare **1**, 11 (2003).

[10] Balibar Sebastien, *Rotons, Superfluidity and Helium crystals*, Fritz London Prize Memorial Prize lecture (2005).

[11] R. Barnett, D. Petrov, M. Lukin, and E. Demler, Phys. Rev. Lett. **96**, 190401 (2006).

[12] Barone A., Paterno G., *Physics and Applications of the Josephson Effect*, John Wiley & Sons, New York - Singapore, 1982.

[13] F. Bloch, "Reminiscences of Heisenberg and the early days of quantum mechanics", Physics Today **Dec. 1976**, 23.

[14] Bloch I., J. Phys. B **38**, S629-S643 (2005).

[15] Bogoliubov N. N., J. Phys. U.S.S.R., **11**, 23 (1947).

[16] Bose, S. N., Z. Phys. **26**, 178, (1924).

[17] G. K. Brennen, C. M. Caves, P. S. Jessen, and I. H. Deutsch, Phys. Rev. Lett. **82**, 1060 (1999).

[18] G. K. Brennen, I. H. Deutsch, and C. J. Williams, Phys. Rev. A **65**, 022313 (2002).

[19] L. de Broglie, PhD thesis, reprinted in *Ann. Found. Louis de Broglie* **17** (1992) p. 22.

[20] L. N. Bulaevskii and V. L. Ginzburg, Sov. Phys. JEPT **18**, 530 (1964)]

[21] S. Burger, K. Bongs, S. Dettmer, W. Ertmer, K. Sengstock, A. Sanpera, G. V. Shlyapnikov, and M. Lewenstein, Phys. Rev. Lett. **83**, 5198 (1999).

[22] Th. Busch and J. R. Anglin, Phys. Rev. Lett. **84**, 2298 (2000).

[23] F. S. Cataliotti, S. Burger, C. Fort, P. Maddaloni, F. Minardi, A. Trombettoni, A. Smerzi, and M. Inguscio, Science **293**, 843 (2001).

[24] D. M. Ceperley, Rev. Mod. Phys. **67**, 279 (1995)

[25] Z.-B. Chen and Y.-D. Zhang, Phys. Rev. A **65**, 022318 (2002).

[26] F. Dalfovo, S. Giorgini, L. P. Pitaevskii, S. Stringari, Rev. Mod. Phys., **71**, 463 (1999).

[27] B. Damski, L. Santos, E. Tiemann, M. Lewenstein, S. Kotochigova, P. Julienne, and P. Zoller, Phys. Rev. Lett. **90**, 110401 (2003).

[28] K. B. Davis, M.-O. Mewes, M. R. Andrews, N. J. van Druten, D. S. Durfee, D. M. Kurn, and W. Ketterle, Phys. Rev. Lett. **75**, 3969 (1995).

[29] Degasperis A., Am. J. Phys., **66** 6 (1998).

[30] D. DeMille, Phys. Rev. Lett. **88**, 067901 (2002).

[31] J. Denschlag, J. E. Simsarian, D. L. Feder, Charles W. Clark, L. A. Collins, J. Cubizolles, L. Deng, E. W. Hagley, K. Helmerson, W. P. Reinhardt, S. L. Rolston, B. I. Schneider, and W. D. Phillips, Science **287**, 97 (2000).

[32] J. M. Duan and S. Yip, Phys. Rev. Lett. **70** 3647 (1993).

[33] J. M. Duan, Europhysics Lett. **29** 489 (1995).

[34] Z. Dutton, M. Budde, C. Slowe, and L.V. Hau, Science **293**, 663 (2001).

[35] Einstein, A., Sitzber. Kgl. Preuss. Akad. Wiss., 261, (1924).

[36] Einstein, A., Sitzber. Kgl. Preuss. Akad. Wiss., 3, (1925).

[37] Enz, V., Helv. Phys. Acta **37**, 245 (1964).

[38] D. L. Feder, M. S. Pindzola, L. A. Collins, B. I. Schneider, and C. W. Clark, Phys. Rev. A **62**, 053606 (2000).

[39] Feynman R.P., Phys. Rev., **91** 1291 (1953).

[40] Feynman R.P., Phys. Rev., **91** 1301 (1953).

[41] Feynman R.P., Phys. Rev., **94** 262 (1954).

[42] R. P. Feynman, *Statistical Mechanics,* (W. A. Benjamin Inc., Reading, MA, 1972)

[43] D. V. Fil and S. I. Shevchenko, Low Temp. Phys. **30**, 770 (2004) [Fiz. Nizk. Temp. **30**, 1028 (2004)].

[44] D. V. Fil and S. I. Shevchenko Phys. Rev. A **72**, 013616 (2005)

[45] Frenkel, Ya. T., and T. Kontorova, Zh. Eksp. Teor. Fiz. **8**, 1340 (1938).

[46] Gibbon, J. D., I. N. James, and I. M. Moroz, Phys. Scr. **20**, 402 (1979).

[47] Ginzburg V.L., and L.D. Landau, Zh. Eksp. Teor. Fiz. **20**, 1064 (1950).

[48] S. Giovanazzi, A. Smerzi, and S. Fantoni, Phys.Rev.Lett. **84**, 4521 (2000).

[49] Girardeau M. D., J. Math. Phys. (N.Y.) **1**, 516 (1960);

[50] Girardeau M. D., Phys. Rev. **139**, B500 (1965).

[51] Greiner M., Mandel O., Esslinger T., Hansch T. W. and Bloch I. Nature **415**, 39 (2002).

[52] Griffin, A., 1999, in *Bose-Einstein Condensation in Atomic Gases, Proceedings of the International School of Physics EnricoFermi, Course CXL*, edited by M. Inguscio, S. Stringari, and C. E. Wieman (IOS Press, Amsterdam), p. 1.

cond-mat/9901123.

[53] Gross, E. P., Nuovo Cimento **20**, 454 (1961);

[54] Gross, E. P., J. Math. Phys. **4**, 195 (1963).

[55] S. Gupta, K. W. Murch, K. L. Moore, T. P. Purdy, and D. M. Stamper-Kurn, Phys. Rev. Lett. **95**, 143201 (2005)

[56] T. L. Gustavson, A. P. Chikkatur, A. E. Leanhardt, A. Grlitz, S. Gupta, D. E. Pritchard, and W. Ketterle, Phys. Rev. Lett. **88**, 20401 (2002).

[57] P. Hommelhoff, W. Hnsel, T. Steinmetz, T. W. Hnsch, and J. Reichel, New Journal of Physics **7**, 1, (2005).

[58] A. Isacsson, M.-C. Cha, K. Sengupta, and S. M. Girvin, Phys. Rev. B **72**, 184507 (2005).

[59] D. Jaksch, C. Bruder, J. Cirac, C. Gardiner, P. Zoller, Phys. Rev. Lett. **81**, 3108 (1998).

[60] D. Jaksch and P. Zoller, Annals of Physics **315**, 52 (2005).

[61] Jiannis K. Pachos and Peter L. Knight, Phys. Rev. Lett. **91**, 107902 (2003).

[62] Josephson B.D., Phys. Lett., **1**, 251 (1962).

[63] M. Yu. Kagan and D. V. Efremov, Phys. Rev. B **65**, 195103 (2002).

[64] V. M. Kaurov and A. B. Kuklov, Phys. Rev. A **71**, 011601 (2005).

[65] V. M. Kaurov, A. B. Kuklov, and A. E. Meyerovich, Phys. Rev. Lett. **95**, 090403 (2005).

[66] V. M. Kaurov and A. B. Kuklov, Phys. Rev. A **73**, 013627 (2006).

[67] A. B. Kuklov and B. V. Svistunov, Phys. Rev. Lett. **90**, 100401 (2003).

[68] A. Kuklov, N. Prokofev, and B. Svistunov,. Phys. Rev. A **69**, 025601 (2004).

[69] A. Kuklov, N. Prokofev, and B. Svistunov, Phys. Rev. Lett. **92**, 030403 (2004).

[70] A. Kuklov, N. Prokofev, and B. Svistunov, Phys. Rev. Lett. **92**, 050402 (2004)

[71] A.B. Kuklov, N.V. Prokof'ev, B.V. Svistunov and M. Troyer, Annals of Physics, **321**, 1602 (2006).

[72] Leggett A. J., Rev. Mod. Phys. **71**, S318 (1999).

[73] Lieb E. H. and Liniger W., Phys. Rev. **130**, 1605 (1963).

[74] Lieb E. H., Phys. Rev. **130**, 1616 (1963).

[75] B. Kahn and G.E. Uhlenbeck, Physica **5**, 399 (1938).

[76] K. T. Kapale and J. P. Dowling, Phys. Rev. Lett. **95**, 173601 (2005).

[77] P.L. Kapitza, Nature **141**, 74 (1938).

[78] Kath Bonnie and Kath Bill, SIAM News, *Making Waves: Solitons and Their Optical Applications*, **31**, Number 2, (1998).

[79] W.H. Keesom and A.P. Keesom, Physica bf 3, 359 (1936).

[80] Y. Shin, M. Saba, T.A. Pasquini, W. Ketterle, D.E. Pritchard, A.E. Leanhardt, Phys. Rev. Lett. **92**, 050405 (2004).

[81] Landau L. D., J. Phys. U.S.S.R., *5*, 71 (1941).

[82] Landau L. D., J. Phys. U.S.S.R., *11*, 91 (1947).

[83] A. J. Leggett, Rev. Mod. Phys. **47**, 331 (1975).

[84] Leiden University, Einstein's historical archive URL:
http://www.lorentz.leidenuniv.nl/history/einstein/einstein.html

[85] Lin Lei, C. Shu, and G. Xu, J. Stat. Phys. **39**, 633 (1985).

[86] London F., Nature, **141**, 643 (1938).

[87] I. Marino, S. Raghavan, S. Fantoni, S. R. Shenoy, and A. Smerzi, Phys. Rev. A **60**, 487 (1999).

[88] T. Matsubara, Prog. Theor. Phys. **6**, 714 (1951).

[89] J E Mooij and C J PM Harmans, New Journal of Physics, **7**, 219 (2005).

[90] M. G. Moore and H. R. Sadeghpour, Phys. Rev. A **67**, 041603(R) (2003).

[91] W. J. Mullin, Am. J. Phys. **68**, 120 (2000).

[92] A.E. Muryshev, H.B. van Linden van den Heuvell, and G.V. Shlyapnikov, Phys. Rev. A **60**, R2665 (1999).

[93] Olshanii M., Phys. Rev. Lett. **81**, 938 (1998).

[94] H. Ott, J. Fortagh, G. Schlotterbeck, A. Grossmann, and C. Zimmermann, Phys. Rev. Lett. **87**, 230401 (2001);

[95] Dmitry E. Pelinovsky, D. J. Frantzeskakis, and P. G. Kevrekidis, Phys. Rev. E **72**, 016615 (2005).

[96] Penrose, O., Phyl. Mag. **42**, 1373 (1951).

[97] Penrose O. and Onsager L., Phys. Rev., **104**, 576 (1956).

[98] D. S. Petrov, G.V. Shlyapnikov, and J.T.M. Walraven, Phys. Rev. Lett. **85**, 3745 (2000).

[99] Pitaevskii, L. P., Zh. Eksp. Teor. Fiz. **40**, 646 (1961), [Sov. Phys. JETP **13**, 451 (1961)].

[100] A. E. Popescu and R. Ionicioiu, Phys. Rev. B **69**, 245422 (2004).

[101] S. Raghavan, A. Smerzi, S. Fantoni, and S. R. Shenoy, Phys. Rev. A **59**, 620 (1999).

[102] Remoissenet M., *Waves Called Solitons: Concepts and Experiments*, Springer, 1999.

[103] A. G. Rojo and G. D. Mahan, Phys. Rev. Lett. **68**, 2074 (1992).

[104] Scott, A. C., Am. J. Phys. **37**, 52 (1969).

[105] A.C. Scott, F.T.F. Chu, D.W. McLaughlin, The soliton: a new concept in applied science, Proc. IEEE **61**, 1443 (1973)

[106] Y. Shin, C. Sanner, G.-B. Jo, T. A. Pasquini, M. Saba, W. Ketterle, D. E. Pritchard, M. Vengalattore and M. Prentiss, Phys. Rev. A **72**, 021604(R) (2005).

[107] C. D. J. Sinclair, E. A. Curtis, I. Llorente Garcia, J. A. Retter, B. V. Hall, S. Eriksson, B. E. Sauer, and E. A. Hinds, Phys. Rev. A **72**, 031603(R) (2005).

[108] A. Smerzi, S. Fantoni, S. Giovanazzi, and S. R. Shenoy, Phys. Rev. Lett. **79**, 4950 (1997);

[109] Sols, F., 1999, in *Josephson effect between Bose-Einstein condensates , Proceedings of the International School of Physics EnricoFermi, Course CXL*, edited by M. Inguscio, S. Stringari, and C. E. Wieman (IOS Press, Amsterdam), p. 453; cond-mat/9810338

[110] B. Tanatar and A. K. Das, Phys. Rev. **B 54**, 13827 (1996).

[111] S. V. Terentjev and S. I. Shevchenko, Fiz. Nizk. Temp. **25**, 664 (1999) [Low Temp. Phys. **25** 493].

[112] Tisza L., Journal de Physique et Radium, **1**, 164, 350 (1940).

[113] G.E. Uhlenbeck, *Over statistische methoden in de theorie der quanta*, Ph.D. thesis, Universiteit Leiden, 1927.

[114] V.E.Zakharov, A.B.Shabat, Zh.Eksp.Teor.Fiz. **64**, 1627 (1973); V.E.Zakharov, A.B.Shabat, Sov.Phys.JETP **37**, 823 (1973).

[115] I. Zapata, F. Sols and A.J. Leggett, Phys. Rev. A **57**, R28 (1998).

[116] C. C. Bradley, C. A. Sackett, J. J. Tollett, and R. G. Hulet, Phys. Rev. Lett. **75**, 1687 (1995).

[117] W. Ketterle, Rev. Mod. Phys. **74**, 1131, (2002).

[118] Metcalf H. and van der Straten P. 1999 *Laser Cooling and Trapping* (Heidelberg: Springer).

[119] Grimm R., Weidemuller M. and Ovchinnikov Yu. B., Adv. At. Mol. Phys. **42**, 95 (2000).

[120] S. Sarker, S.E. Trullinger and A.R. Bishop, Phys. Lett. A **59**, 255 (1976).

[121] J. F. Currie, S. Sarker, A.R. Bishop and S.E. Trullinger, Phys. Rev. A **20**, 2213 (1979).

[122] J. Lajzerowicz and J.J. Niez, J. de Phys. **40**, L165 (1979)

[123] S. E. Trullinger and R. M. DeLeonardis, Phys. Rev. B **22**, 5522 (1980).

[124] P. Coullet, *et al*, Phys. Rev. Lett. **65**, 1352 (1990).

[125] Bruce Denardo, William Wright, Seth Putterman and Andrs Larraza, Phys. Rev. Lett. **64**, 1518 (1990).

[126] Igor S. Aranson and Lorenz Kramer, Rev. Mod. Phys. **74**, 99-143 (2002).

[127] B. Denardo, *et al*, Phys. Rev. Lett. **64**, 1518 (1990).

[128] B. Denardo, *et al*, Phys. Rev. Lett. **68**, 1730 (1992).

[129] L. Korzinov, M.I. Rabinovich, and L.S. Tsimring , Phys. Rev. A **46**, 7601 (1992).

[130] T. Frisch, S. Rica, P. Coullet, and J.M. Gilli, Phys. Rev. Lett. **72**, 1471 (1994).

[131] I.V. Barashenkov, S. R. Woodford, and E. V. Zemlyanaya, Phys. Rev. Lett. **90**, 054103 (2003)

[132] A.E. Muryshev, H.B. van Linden van den Heuvell, and G.V. Shlyapnikov, Phys. Rev. A **60**, R2665 (1999); D.L. Feder, *et al*, *ibid.* **62**, 053606 (2000); Z. Dutton, *et al*, Science **293**, 663 (2001).

[133] M. Abramowitz and I. A. Stegun, *"Handbook of Mathematical Functions with Formulas, Graphs, and Mathematical Tables"*, 9th printing, New York: Dover, pp. 567-581, 1972

[134] L. D. Carr1, Charles W. Clark, and W. P. Reinhardt, Phys. Rev. A **62**, 063610 (2000).

[135] M. P. A. Fisher, *et al.*, Phys. Rev. **B 40**, 546(1989).

[136] M. Greiner, *et al.*, Nature **415**, 39(2002)

[137] E. Demler and F. Zhou Phys. Rev. Lett. **88**, 163001(2002)

[138] A.B. Kuklov and B.V. Svistunov Phys. Rev. Lett. **90**, 100401(2003)

[139] A.E. Meyerovich, Phys. Rev. A **68**, 051602(2003)

[140] A.B. Kuklov, N.V. Prokof'ev, and B.V. Svistunov Phys. Rev. Lett. **92**, 030403(2004)

[141] A.B.Kuklov, N.V. Prokof'ev, B.V. Svistunov, Phys. Rev. Lett. **92**, 050402(2004)

[142] L.-M. Duan, E. Demler, and M.D. Lukin Phys. Rev. Lett. **91**, 090402(2003)

[143] A.E. Meyerovich, Sov.Phys. JETP, **60**, 741(1984) [Zh. Eksp. Teor. Fiz. **87**, 1293(1984)]; in: *Prog.Low Temp.Phys.,* ed. by D. F. Brewer (North-Holland, Amsterdam, *1987),* Vol. 11, pp. 1-73; *Spin-Polarized Phases of* ^3He, in: Helium Three, eds. W.P.Halperin and L.P.Pitaevski (Elsevier, Amsterdam) 1990, p.757.

[144] E. Timmermans, *et al.*, Phys. Rev. Lett.**83**, 2691(1999)

[145] E.Mueller, private communication.

[146] N.V. Prokof'ev, B.V. Svistunov, and I.S. Tupitsyn, Sov. JETP **87**, 310(1998); N.V. Prokof'ev and B.V. Svistunov, Phys. Rev. Lett. **87**, 160601(2001).

[147] M. Wallin, *et al.*, Phys.Rev.**B49**, 12115(1994)

[148] D.M. Ceperley and E.L. Pollock Phys. Rev.**B39**, 2084(1989)

[149] E.L. Bolda and D.F. Walls, Phys. Rev. Lett. **81**, 5477(1998);

S. Inouye, S. Gupta, T. Rosenband, A. P. Chikkatur, A. Grlitz, T. L. Gustavson, A. E. Leanhardt, D. E. Pritchard, and W. Ketterle, Phys. Rev. Lett. **87**, 080402(2001).

[150] P.O. Fedichev, A.E. Muryshev, and G.V. Shlyapnikov, Phys. Rev. A **60**, 3220 (1999).

[151] A. Fetter and A. Svidzinsky, J. Phys.: Condens. Matter **13**, R135 (2001).

[152] L. Pitaevskii and S. Stringari, Phys.Rev.Lett. **87**, 180402 (2000).

[153] D.S. Petrov, G.V. Shlyapnikov, and J.T.M. Walraven, Phys. Rev. Lett. **85**, 3745 (2000); *ibid.* **87**, 050404 (2001); S. Dettmer, *et al*, *ibid.* **87**, 160406 (2001).

[154] K. Bongs, *et al*, Phys. Rev. A **63**, 031602(R) (2001); A. Gorlitz, *et al.*, Phys. Rev. Lett. **87**, 130402 (2001).

[155] For a review see J. Reichel, Appl. Phys. B **74**, 469 (2002); P. Treutlein, *et al*, quant-ph/0311197.

[156] H. Ott, J. Fortagh, G. Schlotterbeck, A. Grossmann, and C. Zimmermann, Phys. Rev. Lett. **87**, 230401 (2001); E.A. Hinds, C.J. Vale, and M.G. Boshier, *ibid.* **86**, 1462 (2001); For a review see L. Feenstra, L.M. Andersson, J. Schmiedmayer, cond-mat/0302059 (2003).

[157] M.R. Andrews, *et al*, Science **275**, 637-641 (1997).

[158] Y. Shin, *et al*, Phys. Rev. Lett. **92**, 150401 (2004).

[159] B.P. Anderson, *et al*, Phys. Rev. A **67**, 033601 (2003).

[160] V.S. Shchesnovich, B.A. Malomed and R.A. Kraenkel, Physica **D188**, 213, (2004).

[161] M. Romagnoli, S. Trillo, and S. Wabnitz, Opt. Quantum Electron. **24**, S1237 (1992); A. Ankiewicz, M. Karlsson and N. Akhmediev, Optics Communications **111**, 116 (1994).

[162] M. Olshanii, Phys. Rev. Lett. **81**, 938 (1998).

[163] L.D. Landau, E.M. Lifshitz, L.P. Pitaevskii, *"Statistical Physics"*, Butterworth-Heinemann 3rd edition (1999), p.368.

[164] N.N. Carlson, Physica **D98**, 183 (1996).

[165] L. N. Bulaevski and V. L. Ginzburg, Sov. Phys. JEPT **18**, 530 (1964)]

[166] S. Sarker, S.E. Trullinger and A.R. Bishop, Phys. Lett. A **59**, 255 (1976).

[167] P. Coullet, *et al*, Phys. Rev. Lett. **65**, 1352 (1990).

[168] L. Korzinov, M.I. Rabinovich, and L.S. Tsimring , Phys. Rev. A **46**, 7601 (1992); T. Frisch, S. Rica, P. Coullet, and J.M. Gilli, Phys. Rev. Lett. **72**, 1471 (1994).

[169] B. Denardo, *et al*, Phys. Rev. Lett. **64**, 1518 (1990); B. Denardo, *et al*, *ibid.* **68**, 1730 (1992);

[170] I.V. Barashenkov, S. R. Woodford, and E. V. Zemlyanaya, Phys. Rev. Lett. **90**, 054103 (2003)

[171] I. Spitkovsky, private communication.

[172] D.T. Son and M.A. Stephanov, Phys. Rev. A, **65**, 063621 (2002).

[173] Yu. Kagan, N.V. Prokof'ev, and B.V. Svistunov, Phys.Rev. A, **61**, 045601(2000).

[174] Yu. Kagan, B.V. Svistunov, and G.V. Shlyapnikov, Sov. Phys. - JETP **66**, 314 (1987); D.S. Fisher and P.C. Hohenberg, Phys. Rev. B **37**, 4936 (1988).

[175] K. Bongs, S. Burger, D. Hellweg, M. Kottke, S. Dettmer, T. Rinkleff, L. Cacciapuoti, J. Arlt, K. Sengstock, W. Ertmer, J.Opt. B **5**, S124 (2003).

[176] S. Inouye, *et al* Phys. Rev. Lett. **87**, 080402 (2001).